Title

High Pressure Studies on Nanometer Sized Clusters: Structural, Optical, and Cooperative Properties

Author

Tolbert, S.H.

Publication Date

1995-05-01

Thesis/dissertation

LBL-37591
UC-404

Lawrence Berkeley Laboratory
UNIVERSITY OF CALIFORNIA

Materials Sciences Division

High Pressure Studies on Nanometer Sized Clusters: Structural, Optical, and Cooperative Properties

S.H. Tolbert
(Ph.D. Thesis)

May 1995

Prepared for the U.S. Department of Energy under Contract Number DE-AC03-76SF00098

DISCLAIMER

LBL-37591
UC-404

High Pressure Studies on Nanometer Sized Clusters: Structural, Optical, and Cooperative Properties

Sarah Helen Tolbert

Department of Chemistry
University of California, Berkeley

and

Materials Sciences Division
Lawrence Berkeley Laboratory
University of California
Berkeley, California 94720

May 1995

This work was supported by the Director, Office of Energy Research, Office of Basic Energy Sciences, Materials Sciences Division, of the U.S. Department of Energy under Contract No. DE-AC03-76SF00098.

High Pressure Studies of Nanometer Sized Clusters: Structural, Optical, and Cooperative Properties

by

Sarah Helen Tolbert

High Pressure Studies on Nanometer Sized Clusters: Structural, Optical, and Cooperative Properties

by

Sarah Helen Tolbert

B.S. (Yale University) 1990

A dissertation submitted in partial satisfaction of the
requirements for the degree of
Doctor of Philosophy
in
Chemistry
in the
GRADUATE DIVISION
of the
UNIVERSITY of CALIFORNIA at BERKELEY

Committee in charge:

Professor A. Paul Alivisatos, Chair

Professor Herbert L. Strauss

Professor Raymond Jeanloz

1995

Abstract

High Pressure Studies on Nanometer Sized Clusters:
Structural, Optical, and Cooperative Properties

by

Sarah Helen Tolbert

Doctor of Philosophy in Chemistry
University of California at Berkeley
Professor A. Paul Alivisatos, Chair

High pressures are employed to study the properties of nanometer sized crystallites. The results include an understanding of the factors that control phase stability in finite solids, information about the coupling between clusters in ordered arrays, and insight into the effects of finite size on the electronic properties of nanometer-scale semiconductors.

High-pressure Selenium EXAFS is used to study pressure-induced structural transformations in CdSe nanocrystals. In agreement with bulk CdSe, the nanocrystals undergo an apparent wurtzite to rock salt transformation. The transformation pressure, however, is much higher than that observed in bulk systems.

High-pressure X-ray diffraction is used to confirm the EXAFS results. Additionally, diffraction peak widths indicate that nanocrystals do not fragment upon transformation. Optical absorption is correlated with the structural transformations and used to measure transition pressures; a smooth increase in transformation pressure is

observed with decreasing nanocrystal size. The thermodynamics of the transformation are modeled using an elevated surface energy in the high-pressure phase relative to the low-pressure nanocrystals. This elevated surface energy results from symmetry-allowed motions of the nanocrystal interior during a transformation. These motions cause an overall change in the shape of a nanocrystal and move surface atoms into unfavorable bonding geometries.

Surface-energy control of phase stability is confirmed by high-pressure studies on Si nanocrystals coated with SiO_2. Because of the stable Si/SiO_2 interface, large increases in transformation pressure are seen in crystallites up to 500 Å diameter. Further, an overall change in crystallite shape upon transformation is seen from X-ray diffraction line widths.

Interactions between clusters are studied in ordered arrays. Single crystals of C_{60} clusters were examined under high pressure and low temperature using Raman scattering. The results provide information about the clusters' rotational state and allow for speculation about the coupling between intra- and inter-cluster vibrational modes.

The optical properties of high-pressure phase CdSe clusters are studied to learn about quantum confinement in well characterized indirect-gap semiconductor nanocrystals. Clear evidence for confinement of electronic transitions is presented. Comparison of wurtzite- and rock salt-phase absorption shows that rock salt nanocrystals down to 9.6 Å (radius) remain fundamentally indirect-gap systems with no appreciable dipole-allowed transitions.

To my parents

Bert and Anne Tolbert

who taught me about life and about science

And to my husband

Ben Schwartz

with whom I continue to learn about both of these things

Table of Contents

Acknowledgments

There are a number of people whose help has been very important in this research effort. In the first place, I need to thank my graduate research advisor, Paul Alivisatos. Paul provide me with a good combination of scientific advice and direction while at the same time giving me the freedom to pursue many experiments in my own way. More importantly, however, Paul was a source of endless enthusiasm about nanocrystal science in general and about the high pressure studies on nanocrystals in particular.

The other students and post-docs in the Alivisatos research group were all a very meaningful part of my graduate experience. Some people, however, need special acknowledgments. Joseph Shiang was a particularly important part of my graduate career. His endless patience and willingness to discuss scientific problems were indispensable during my first years as a graduate student. His scientific insight was appreciated throughout our time as students together. Vicki Colvin also taught me a great deal about the physics of semiconductor nanocrystals. In addition, her help, and that of Janet Bowen Katari and Andrew Guzelian in the synthesis and characterization of nanocrystal samples was greatly appreciated. Avery Goldstein and Andreas Kadavanich need a special acknowledgment for their TEM work. Their sample characterization was key to the success of the high pressure experiments.

Amy Bowen Herhold, Christopher Johnson, and Andreas Kadavenich have all, at various times, worked with me at the Stanford Synchrotron Radiation Laboratory. For putting up with long hours, a stressed lab mate, and many large insects, I am genuinely appreciative. Amy and Chris also need to be acknowledged for there work on the optical properties of high pressure phase CdSe nanocrystals (chapter 8). This work was truly a collaborative effort between the three of us.

There are a number of people outside of UC Berkeley who's help also needs to be recognized. Professor Malcolm Nicol and Suzanna Gibson taught me a great deal about the high pressure X-ray diffraction experiments at SSRL. Their time, effort, and machining skills are greatly appreciated. Hector Lorenzana introduced me to the great art of diamond anvil cell alignment and taught me many of the tricks of the trade. David Schiferl also shared his insights on high pressure diamond anvil cells, as well as lending me his piston/cylinder diffraction cell for the silicon nanocrystal diffraction experiments. Finally I would like to thank Louis Brus, who worked with me on the silicon nanocrystal experiments. He provided many useful scientific discussions as well as all the samples used in the experiment.

This work was supported by the Director, Office of Energy Research, Office of Basic Energy Sciences, Materials Sciences Division, of the U.S. Department of Energy under Contract No. DE-AC03-76SF00098.

Chapter 1: Introduction

1.1 Pressure Induced Structural Transformations:

In many systems, a phase transition can be described as the point when the length scale of fluctuations between two stable states of the system diverges. Thus, in principle, phase transitions are only defined for infinite systems. The question of just how large a system must be before it can be said to undergo a phase transition is a long-standing and timely one. The rapid advances that have occurred recently in the preparation and characterization of nanocrystals finally enable studies of transformations between stable states of finite systems. It is now possible to discover whether a given type of nanocrystal will exist in a small number of well defined structures, or whether finite systems become essentially amorphous as they reach the limit of very small size. It can be determined whether transformations between stable states in a finite system occur via single or multiple nucleation events, and with or without hysteresis. The perturbations caused by the large number of surface atoms can also be addressed: Will the surface alter the stability of different structures? Finally and perhaps most importantly, is there a size below which a nanocrystal is so small that any changes in its structure must be viewed as an isomerization, rather than a phase transition?

Previously, only one type of phase transition has been studied extensively in in the nanometer size regime, both theoretically and experimentally, and that is melting. In a wide variety of materials ranging from metals to semiconductors to insulators, a decrease in solid to liquid transition temperature has been observed with decreasing nanocrystal size.[1,2] Melting point depressions of over 50% are observed for sufficiently small sized nanocrystals. An understanding of this depression can be obtained by considering the factors that contribute to the total energy of a nanocrystal: in a system containing only a few hundred atoms, a large fraction of these atoms will be located on the surface. As surface atoms tend to be coordinatively unsaturated, there is a large energy associated

with this surface. The key to understanding this melting point depression is the fact that the surface energy is always lower in the liquid phase compared to the solid phase. In the dynamic fluid phase, surface atoms move to minimize surface area and unfavorable surface interactions. In the solid phase, rigid bonding geometries cause stepped surfaces with high energy edge and corner atoms. By melting, the total surface energy is thus reduced. This stabilizes the liquid phase over the solid phase. The smaller the nanocrystal, the larger the contribution made by the surface energy to the overall energy of the system and thus the more dramatic the melting point depression.[1] As melting is believed to start on the surface of a nanocrystal, this surface stabilization is an intrinsic and immediate part of the melting process.[3,4]

Using the known 1/radius drop off in cohesive energy/atom and the resulting depression in melting temperature as a starting point,[5] it is worthwhile to consider the different regimes of behavior that are expected in ever smaller crystals. First, one encounters the regime where only small numbers of nucleation events can occur in a given crystallite, leading to changes in the kinetics of melting. Next, the number of surface atoms becomes a large fraction of the total number of atoms, perturbing the relative stability of the liquid and the solid phases. This is the nanocrystal regime of 100 to 10,000 atoms, in which there is a well defined interior with a single, defined structure at low temperature. Finally, as the number of surface atoms exceeds the number in the interior, the quantum mechanical nature of the chemical bonding changes, and entirely new structures may emerge. This is in many ways the most interesting regime, because it is here that one might find entirely new structures with properties that are not simple extrapolations from the bulk material. We may not expect the size dependence of the melting temperature to extend into this regime, since the intrinsic bonding of the atoms can change. For example, calculations show that there may be no single well defined structure for Si clusters of 10-45 atoms.[6] More ionic semiconductors, in contrast, seem to retain unique crystalline structures down to very small sizes.[7,8] One of the most important

questions in cluster physics and chemistry is thus: are there a small number of well-defined low temperature structures in nanocrystals?

To extend our understanding of the effects of size on phase stability and to address the issues discussed above, we have chosen to study *solid-solid* phase changes in tetrahedral inorganic semiconductors as a function of the size of the crystal from 1,000,000 down to 100 atoms. In the extended solids, these materials exist in a small number of well defined crystal structures; interconversion between these structures is usually accompanied by a discontinuous change in unit cell volume. As with melting, there tends to be very different bonding in different structures: covalent versus metallic, for example. The mechanics of transformation, however, are quite different from melting. In an order/disorder transition like melting, there is diffusive motion of atoms which starts at the surface and moves inward. In a solid-solid phase transition, in contrast, atoms frequently move along a well defined transition path in a cooperative manner.

While transformations of this sort can be induced by changes in temperature in some solids, many more materials will transform between solid structures upon the application of high pressures. In particular, tetrahedral semiconductors tend to exhibit solid-solid phase changes at relatively modest pressures. Because of the directionality of the bonding, tetrahedral semiconductors have very open structures with large void volumes. Under pressure, the energy of the system can be easily lowered by a volumetrically more efficient packing of atoms. As a result, diamond, zinc blende, and wurtzite phase semiconductors undergo transformations to rock salt or β-Sn phases at pressures between 2 and 15 GPa. The rock salt phase exhibits octahedral bonding with large Madelung stabilization and can occur in ionic systems such as I-VII, II-VI and some III-V semiconductors. The β-Sn phase is a distorted octahedral structure. This metallic phase is observed at high pressures in IV-IV and less ionic III-V semiconductors. Our goal is to develop a general understanding of the effect of size on homogeneous first order

solid-solid phase transitions. Because of their large volume change and moderate transition pressures, we will use tetrahedral semiconductor nanocrystals as model systems.

A wide variety of semiconductor nanocrystals can be prepared. In particular, advances in wet chemical synthetic techniques now allows for the preparation of virtually any II-VI and some I-VII semiconductor nanocrystals in a variety of sizes with high crystallinity and narrow size distributions.[9,10] Gas pyrolysis reactions have been successfully used to produce highly crystalline IV-IV nanocrystals in a variety of sizes, although size distributions are not nearly as narrow as for the II-VI systems.[11] Finally, organometallic syntheses, similar to those used for II-VI semiconductors, are now being utilized to make III-V and IV-IV nanocrystals.[12,13] All of these methods produce crystallites with some type of surface passivation layer which prevents agglomeration of the nanocrystals, and allows the crystallites to be dissolved in various organic solvents. Here we concentrate on two different types of nanocrystals: the II-VI system, CdSe, and the IV-IV system Si. These systems are exemplary as they span the range of possible ionicities in tetrahedral systems: from dominantly ionic to completely covalent. Preparation of CdSe[9,14] and Si[11] nanocrystals is now well documented. For the experiments presented here, Si nanocrystals in the diamond structure were produced with high crystallinity and moderate size distributions in sizes ranging from 50 Å to 250 Å in radius. CdSe nanocrystals with a wurtzite structure were produced with high crystallinity and narrow size distributions in sizes ranging from 10 to 30 Å in radius. A TEM micrograph of a field of 25 Å radius CdSe nanocrystals arrayed on an amorphous carbon grid is presented in figure 1.1. The individual lattice planes visible in most crystallites indicate the highly ordered nature of each discrete cluster.

Bulk CdSe transforms from a wurtzite structure to a rock salt structure at 3.0 GPa with applied hydrostatic pressure.[15] Bulk silicon transforms from the diamond structure to the β-Sn phase at approximately 11 GPa, and then further transforms to a primitive hexagonal structure at about 16 GPa.[16] As we will show, in all cases and for all sizes

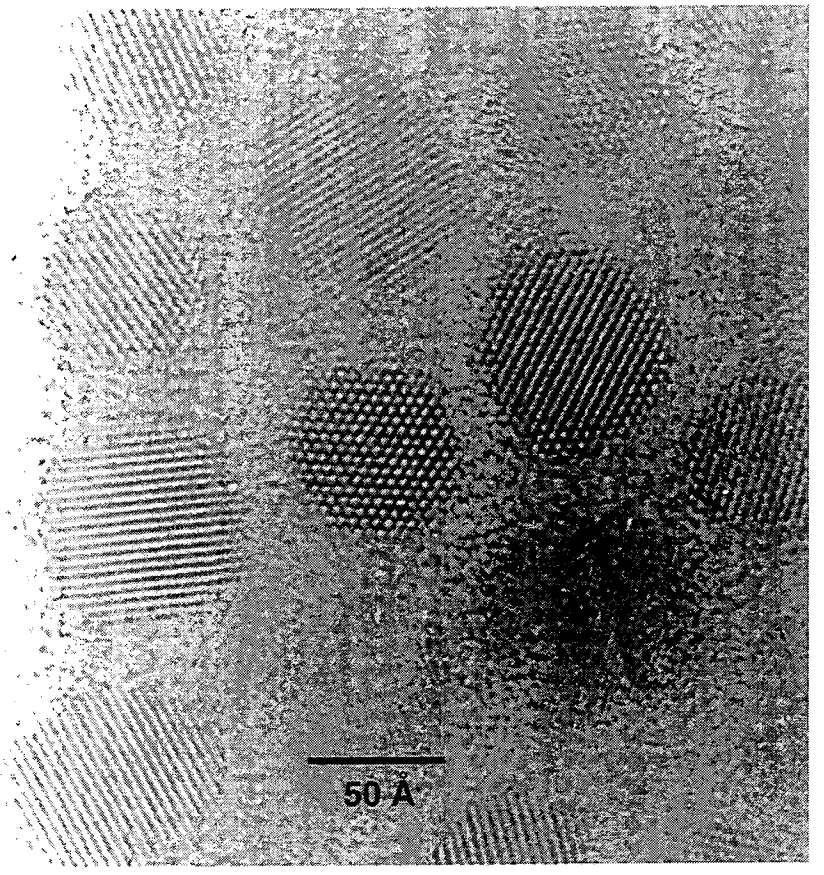

Figure 1.1: TEM micrograph of approximately 5 nm diameter CdSe nanocrystals. The nanocrystals are sitting on an amorphous carbon film. Clear faceting of the crystallites can be observed.

examined, these phase transition pressures are significantly elevated in nanocrystals compared to the bulk material.[17] Further, the elevation is a function of crystallite size with smaller diameter crystallites undergoing transitions at higher pressures. Chapters 3-5 of this thesis contain data from a variety of experiments on pressure induced phase transformations in nanocrystals. This data can be combined to produce a general understanding of the elevation in phase transition pressure and the effects of size on first order solid-solid phase transitions.

1.2 Cooperative Effects in Clusters as a Function of Pressure:

As we have discussed above, the most common use of pressure is to interconvert solid structures. In an ordered system, however, pressure can also be used to study the interactions between clusters. In particular, externally applied pressure can be used to change the spacings between clusters and thus to study the coupling between them. This general technique has been successfully applied to study the interaction between molecules in organic[18,19,20] and inorganic molecular crystals.[21] While temperature can also be used to change the spacings between clusters, interpretation of these results is complicated by the fact that both cluster-cluster spacings and the populations in various vibrational levels of the system change with temperature. The combination of temperature and pressure, however, allows these coupling and population effects to be separated.

In chapter 7 of this thesis, interactions between the icosohedral carbon clusters, C_{60}, will be discussed. Because C_{60} clusters are quite small, highly symmetric, and completely monodisperse, they can be induced to order into high quality single crystals. Cluster-cluster interactions can then be studied from Raman vibrational peak widths and peak positions. These experiments involve both the use of variable temperature and variable pressure. In particular, the effect of the cluster rotational state in the C_{60} - C_{60} vibrational dephasing is examined.

1.3 Optical Properties of Nanocrystals at High Pressure:

The study of the phase transition process has historically been one of the primary goal of high pressure research. Another potential field of study, however, is the study of the phase transition *product*. The outcome of a structural transformation is, in a very real sense, a new material with properties that can be completely different from the starting material. Thus, chapter 8 of this thesis is dedicated to the study of the optical properties of the high pressure phase, or rock salt phase, of CdSe nanocrystals.

In the bulk, the wurtzite phase of CdSe is a direct gap semiconductor. Through the study of CdSe, CdS and other related direct gap semiconductors, the effects of finite size on the optical properties of these systems have been well established. These effects include shifts in the absorption onset to higher energy,[22] the formation of discrete state in the absorption spectra,[23] and the concentration of oscillator strength into just a few allowed optical transitions.[24] The effect of finite size on indirect gap semiconductor nanocrystals is much less well established. The same phenomena observed in direct gap systems are predicted for indirect gap systems.[25] In addition, there exists the possibility that a semiconductor which has an indirect gap in the bulk can have dipole allowed (or direct) transitions in finite size due to the loss of translational symmetry.[26] Unfortunately, it is not currently possible to synthesize indirect gap semiconductor nanocrystals with sufficiently narrow size distributions to test these theories.

Bulk rock salt phase CdSe is an indirect gap semiconductor.[27] Pressure can thus be used to convert direct gap wurtzite phase nanocrystals with narrow size distributions into rock salt phase nanocrystals, also with narrow size distributions. The electronic properties of these crystallites can then be studied in an effort to understand the effect of finite size on a material which is an indirect gap semiconductor in the bulk. Furthermore, because the same crystallites can be studied in both the direct and indirect gap phases, a direct comparison between the electronic properties of these two systems can be made.

1.4 Notes and References:

1. C. J. Coombes, *J. Phys.* **2**, 441 (1972); P. Buffat and J.-P. Borel, *Phys. Rev. A* **13**, 2287 (1976).

2. A. N. Goldstein, C. M. Echer, and A. P. Alivisatos, *Science* **256**, 1425 (1992).

3. P. R. Couchman and W. A. Jesser, *Nature* **269**, 481 (1977).

4. F. Ercolessi, W. Andreoni, and E. Tosatti, *Phys. Rev. Lett.* **66**, 911 (1991).

5. K-J. Hanszen, *Z. Phys.* **157**, 523 (1960).

6. U. Röthlisberger, W. Andreoni, and M. Parrinello, *Phys. Rev. Lett.* **72**, 665 (1994).

7. N. Herron, J. C. Calabrese, W. E. Farneth, and Y. Wang, *Science* **259**, 1426 (1993).

8. R. L. Whetten, *Acc. Chem. Res.* **26**, 49 (1993).

9. C. B. Murray, D. J. Norris, and M. G. Bawendi, *J. Am. Chem. Soc.* **115**, 8706 (1993).

10. Y. Wang and N. Herron, *Research Chem. Intermediates*, **15**, 17 (1991).

11. K. A. Littau, P. J. Szajowski, A. J. Muller, A. R. Kortan, and L. E. Brus, J. Phys. Chem. **97**, 1224 (1993); W. L. Wilson, P. F. Szajowski, and L. E. Brus, Science **262**, 1242 (1993).

12. M. A. Olshavsky, A. N. Goldstein, and A. P. Alivisatos, *J. Am. Chem. Soc.* **112**, 9438 (1990); H. Uchida, C. J. Curtis, and A. J. Nozik, *J. Phys. Chem.* **95**, 5382 (1991); H. Uchida, C. J. Curtis, P. V. Kamat, K. M. Jones, and A. J. Nozik, *J. Phys. Chem.* **96**, 1156 (1992); L. Butler, G. Redmond, and D. Fitzmaurice, *J. Phys. Chem.* **97**, 10750 (1993).

13. J. R. Heath, J. J. Shiang, and A. P. Alivisatos, *J. Chem. Phys.* **101**, 1607 (1994).

14. J. E. Bowen Katari, V. L. Colvin, A. P. Alivisatos, *J. Phys. Chem.* **98**, 4109 (1994).

15. A. L. Edwards, and H. G. Drickamer, *Phys. Rev.* **122**, 1149 (1961); A. Onodera, *Rev. Phys. Chem. Japan* **39**, 65 (1969); W. C. Yu and P. J. Gielisse, *Mat. Res. Bull.* **6**, 621 (1971).

16. This is actually somewhat of a simplification. Bulk Si appears to transform from the β -Sn phase to the closely related Imma structure via a second order transformation. The

Imma phase then transforms to a primitive hexagonal structure, again via a second order transformation. A variety of references combine to explain this complicated phase behavior: R. H. Wentorf, Jr. and J. S. Kasper, *Science* **139**, 338 (1963); J. C. Jamieson, *Science* **139**, 762 (1963); J. S. Kasper and S. M. Richards, *Acta. Cryst.* **17**, 752 (1964); F. P. Bundy, *J. Chem. Phys.* **41**, 3809 (1964); J. Z. Hu and I. L. Spain, *Solid State Com.* **51**, 263 (1984); H. Olijnyk, S. K. Sikka, and W. B. Holzapfel, *Phys. Lett.* **103A**, 137 (1984); M. I. McMahon and R. J. Nelmes, *Phys. Rev. B* **47**, 8337 (1993).

17. No elevation in transition pressure was observed in one experiment performed on 100-300 Å CdS nanocrystals. This result is to be expected, given the size of these crystallites and the results presented here on CdS and CdSe: B. F. Variano, N. E. Schlotter, D. M. Hwang, and C. J. Sandroff, *J. Chem. Phys.* **88**, 2848 (1988).

18. D. Salmon, V. L. Shannon, and H. L. Strauss, *J. Chem. Phys.* **90**, 773 (1989).

19. H. Shimizu and N. Miyahara, *Chem. Phys. Lett.* **110**, 615 (1984).

20. R. Zallen, C. H. Griffiths, M. L. Slade, M. Hayek, and O. Brafman, *Chem. Phys. Lett.* **39**, 85 (1976).

21. R. Zallen and M. L. Slade, *Phys. Rev. B.* **18**, 5775 (1978).

22. R. Rossetti, R. Hull, J. M. Gibson, and L. E. Brus, J. Chem. Phys. **82**, 552 (1984); M. L. Steigerwald, A. P. Alivisatos, J. M. Gibson, T. D. Harris, R. Kortan, A. J. Muller, A. M. Thayer, T. M. Duncan, D. C. Douglass, and L. E. Brus, J. Am. Chem. Soc. **110**, 3046 (1988).

23. C. B. Murray, D. J. Norris, M. G. Bawendi, J. Am. Chem. Soc. **115**, 8706 (1993).

24. T. Vossmeyer, L. Katsikas, M. Giersig, I. G. Popovic, K. Diesner, A. Chemseddine, A. Eychmüller, and H. Weller, *J. Phys. Chem.* **98**, 7665 (1994).

25. L. E. Brus, *J. Chem. Phys.* **80**, 4403 (1984); R. Rossetti, R. Hull, J. M. Gibson, and L. E. Brus, *J. Chem. Phys.* **83**, 1406 (1985); L. E. Brus, *J. Phys. Chem.* **90**, 2555 (1986).

26. M. S. Hybertsen, *Phys. Rev. Lett.* **72**, 1514 (1994); T. Takagahara and K. Takeda, *Phys. Rev. B* **46**, 15,578 (1992).

27. A. Rubio, O. Zakharov, and M. L. Cohen, Dept. of Physics, Univ. of California, Berkeley (private communication).

Chapter 2: Experimental

2.1 Introduction:

The purpose of this chapter is to provide some additional details about the experiments presented in this thesis. While each chapter does contain an experimental section, some of the smaller details, useful for actually repeating an experiment, are not included in these sections. The reader interested only in the scientific conclusions of this work may choose to skip this chapter.

2.2 Synthesis of CdSe Nanocrystals:

The synthesis of CdSe nanocrystals in a wide range of size with narrow size distributions is now a well established art.[1,2] The general method starts with a solution of di-methyl-Cadmium and Se metal dissolved in tri-butyl-phosphine at about 0.5 M. One to 1.5 ml of this solution is then injected into hot tri-octyl-phosphine oxide (T = 330-360 °C) under argon. Samples in the 10-15 Å radius range can be produced by varying the molarity of the Cd and Se in the solution and changing the injection temperature. The relationship between nanocrystal size and the concentrations in the Cd/Se solution is not, however, a simple one. While more concentrated solutions and lower temperatures generally produce larger crystallites, it is not usually possible to determine, *a priori*, what size crystallites one will make. Larger samples are made by cooling medium sized samples to approximately 300 °C and then adding additional aliquot of Cd/Se solution. Samples can then be precipitated from the phosphine oxide solution into MeOH and filtered.

For experiments aimed at understanding the structural stability of nanocrystals, however, narrow size distributions and a range of sizes are not sufficient. To produce interpretable results, it appears to be very important that the nanocrystals are free of structural defects. These defects can, potentially, change the internal energy of a nanocrystal, provide sites for anomalous nucleation of phase transitions, or interfere with

the path driven motions of atoms during a transformation. To avoid defected nanocrystals, the temperature of the initial Cd/Se injection is quite important. Injection at temperatures lower than 330 °C was found to produce nanocrystals with poor crystallinity. Nanocrystals were considered defect free if the overall size, determined by Transmission Electron Microscopy and Small Angle X-ray Scattering, agreed with the domain size determined from the X-ray diffraction peak width using the Scherrer formula.

2.3 EXAFS and X-Ray Diffraction at High Pressure:

There are two major problems which plague high pressure EXAFS experiments. The first of these is single crystal diffraction from the diamonds of the high pressure cell. This issue is addressed in some detail in chapter 3 and thus will not be repeated here. The other problem faced in an EXAFS experiment, and also in high pressure X-ray diffraction, is one of sample size. Because the sample volume in a diamond anvil cell is on the order of 1 nano-liter, total signal is frequently a problem. Two aspect of the problem need to be addressed.

The diameter of the sample chamber is usually on the order of 0.2 mm. While this size is not a problem for experiments involving lasers that can be focused, it does present some difficulties for X-ray experiments. At most synchrotron light sources X-ray beams can be focused slightly, but in the end, the incoming beam must simply be apertured down to the diameter of the sample compartment. This is particularly true for scattering experiments where diffraction from the metal gasket of the high pressure cell interferes with the real signal when the beam diameter is larger than the size of the sample chamber. To obtain adequate signal to noise ratios with reasonable integration times in this highly apertured geometry, a very bright X-ray source is generally required. All of the experiments presented here were thus carried out on permanent magnet, multipole wiggler lines at the Stanford Synchrotron Radiation Laboratory.

The second issue for X-ray experiments at high pressure is the total cross-section of the sample. The thickness of most high diamond anvil cell samples is on the order of 30-50 μm. To prevent particle-particle interactions, samples are usually homogeneously dissolved in an organic solvent. For most solvents, nanocrystal solubility does not exceed a few percent by volume and so the total cross-section of the dissolved nanocrystals in the diamond cell tends to be very low; too low in many cases to actually make the experiments practical. There are two ways around this problem. For samples which do not need to exceed 10 GPa in pressure, gasket thicknesses can be increased to 100 μm. These gaskets do not tend to behave very well under high pressure, but up to 10 GPa, the deformation is not unacceptable.

The more important method for increasing overall cross-section is to increase the sample solubility. In appropriate solvents (most notably the coordinating solvent, 4-ethyl-pyridine), CdSe nanocrystal concentrations of up to 1 mg/μl have been obtained. This corresponds to a volume fractions of almost 50%. The solubility in coordinating solvents is a strong function of the CdSe nanocrystal surface structure, however. While the details of this dependence are not well understood, it appears that crystallites with very high coverage of tri-octyl-phosphine-oxide (TOPO) are not exceedingly soluble in coordinating solvents. Consistent with the idea that the dissolution process in pyridine is an exchange reaction between the TOPO molecules on the surface of the crystallites and the pyridine,[1] the nanocrystal solubility increases with time in solution. Samples, however, with very poor TOPO coverage are also not highly soluble in pyridine, presumably because of surface oxidation. Solubility can vary wildly from sample to sample. It is, however, one of the most important variables for making X-ray absorption and scattering experiments work on nanocrystal systems at high pressure.

2.4 Optical Absorption at High Pressure:

Because semiconductor nanocrystals can be homogeneously dissolved in organic solvents, these systems offer a unique opportunity to use optical absorption to monitor structural transformations. In bulk systems, these experiments are much more difficult: Powdered samples tend to scatter and single crystal samples must be exceedingly thin to keep the optical density in a reasonable range. In addition, the light spot (usually an incandescent source) must be focused to a size smaller than the single crystal sample to prevent light leakage through the pressure medium surrounding the sample. For nanocrystal samples, all of these problems are avoided. The beam diameter can be much larger than the sample diameter as the beam is effectively apertured by the high pressure cell gasket. Reference scans, taken with a gasket but no sample in the high pressure cell, can then be used to normalize the spectra. Reference scans taken after the sample has been pressurized and released can be used to better reflect the shape and size of the gasket hole at high pressure.

One problem does arise in these experiments, however. As the sample is pressurized, the metal gasket distorts. This results in a change in the apparent optical density of the sample which does not reflect any really change in the molar extinction coefficient. The effects can be simply corrected for using Beer's law if the gasket diameter and thickness are also determined as a function of pressure. Sample diameters can be measured using a light microscope with a reticule. Sample thicknesses are most easily measured from Fabry-Perot thin film interference patterns. These can be obtained by passing a white light source through the cell and observing the intensity oscillations in the transmitted light. The sample thickness (T) is approximated by

$$T = \frac{1}{2 \cdot n_P \cdot \omega}, \qquad (1)$$

where ω is the period of the oscillations (in cm^{-1}) and n_P is the index of refraction of the pressure medium at pressure P. Values of n_P for non-standard high pressure solvents can

be roughly estimated from the atmospheric pressure index of refraction by assuming that there is minimal volume change of the sample chamber upon release of pressure.

2.5 Notes and References:

1. C. B. Murray, D. J. Norris, and M. G. Bawendi, *J. Am. Chem. Soc.* **115**, 8706 (1993).

2. J. E. Bowen Katari, V. L. Colvin, A. P. Alivisatos, *J. Phys. Chem.* **98**, 4109 (1994).

Chapter 3: Extended X-Ray Absorption Fine Structure (EXAFS)

3.0 Abstract

High pressure Se EXAFS data have been obtained on 2.7 nm radius CdSe semiconductor nanocrystals. This system is observed to undergo a solid-solid phase transition at 6.5 GPa which is approximately twice the reported value for bulk CdSe. In combination with high pressure optical absorption experiments, EXAFS data can be used to identify the high pressure phase structure as rock salt. EXAFS data can be fit with equations of state to yield pressure volume curves. The resultant values of the bulk modulus and its derivative with respect to pressure are $B_o = 37 \pm 5$ GPa and $B_o' = 11 \pm 3$.

3.1 Introduction:

How will the phase transition from one solid structure to another be different in a nanocrystal, as compared to the bulk solid? As the domain size of a material is decreased, how will this affect the relative stability of different possible structures of the material? This question has ramifications in fields as diverse as electrical engineering, where the size of features in integrated circuits is approaching the nm regime, and geo-physics, where the phase diagram of solids with nanometer domain sizes is unknown. Changes in phase transition points with the intrinsic size of a nanocrystal may arise through the influence of the surface of the nanocrystals, which adds a large term to the internal energy of each phase, or potentially through purely dynamical or kinetic effects, since the length scale of the maximum possible fluctuation in a nanocrystal is restricted by its size. In this chapter we present a structural study of the pressure induced transformation from a dominantly covalent, four-coordinate wurtzite structure to an ionic six coordinate rocksalt structure in a sample containing nanocrystals of CdSe homogeneously dispersed in a pressure transmitting medium.

Recent developments in synthetic methods now allow for the preparation of crystalline, highly monodisperse CdSe nanocrystals in a wide range of sizes. In addition, recent high pressure studies on CdS[1,2] and CdSe[3,4] nanocrystals have shown surprising results. While both of these bulk systems undergo a high pressure phase transition from a low pressure covalent phase to a high pressure rock salt phase at about 3 GPa[5,6,7], experiments using optical absorption and resonance Raman spectroscopies show that for nanocrystals in the 2-5 nm range, the covalent phase is stable to pressures 2-3 times those observed in bulk systems. Due to the indirect nature of the high pressure phase band gap however, no information on the high pressure phase structure can be obtained from these experiments. Similar experiments on GaAs/AlAs multilayers[8] also show an elevation in phase transition pressure, though again high pressure phase structures can only be speculated on by analogy with bulk systems.

A related question to the effect of finite size on high pressure transitions is the well known reduction of the melting temperature in nanocrystals. Much progress has been made in understanding these transitions. In a wide variety of materials, ranging from metals[9,10] to semiconductors[11], changes in melting temperature with size can be almost completely accounted for by a thermodynamic model in which the surface energy of the liquid phase is less than that of the solid. For nanometer size particles, essentially no hysteresis is observed in the melting curves; that fact, coupled with the at least qualitative success of the thermodynamic surface energy model, leads to the conclusion that dynamical effects play no role in the reduction of melting temperature. The same may not hold true for solid-solid phase transitions at room temperature, where substantial barriers must be overcome, and large hysteresis effects are sometimes observed even in the bulk material. A detailed knowledge of the structural changes with pressure in a nanocrystal system are needed to see whether thermodynamic or kinetic effects predominate.

The goal of this experiment is thus to obtain direct structural data on nanocrystal systems at high pressure. The two direct structural techniques that can be applied to

characterize the system are X-ray diffraction and EXAFS. We have chosen to start with Se EXAFS because of the intrinsic lack of long range order in nanocrystals. Figure 3.1 demonstraits that high quality Se EXAFS data can be obtained on our nanocrystal samples. The quality of the nanocrystal data is, in fact, almost identical to that obtained on bulk CdSe. While we have subsequently shown that it is possible to obtain complementary diffraction data on the nanocrystals at high pressure, Se EXAFS provides a direct measure of the Cd-Se bond length and as such is ideally suited for our purpose. In order to apply thermodynamics to these systems (Chapter 4), we require the pressure-volume curves.

It should be noted that the goal of this experiment is only to obtain data on the Cd-Se bond length. While EXAFS is frequently reported to accurately measure both the coordination number and the bond length, the coordination number data is generally not as certain, and this is even more so for EXAFS measurements performed on samples in a diamond anvil cell. The period of the EXAFS oscillations arises from the size of the reflecting cavity that surrounds the absorbing atom, and is unaffected by the cell. Changes in the coordination number will result in a change in the total amplitude of the oscillation relative to the absorption edge. This amplitude can be perturbed by background from the high pressure cell. In addition, the amplitude of the oscillations is a function of both the coordination number and the Debye-Waller factor in the material, and these two effects are very hard to separate. As the pressure of the system is increased the Debye-Waller factor is constantly changing, and these changes tend to manifest themselves as anomalous change in coordination number. Because of all of these effects, we will only report bond length data for high pressure samples. This is sufficient information, however, to calculate a variety of useful thermodynamic constants for CdSe nanocrystals under high pressure. In addition, bond length data, while not proof of structure, can be used to learn about the structure of high pressure phase CdSe nanocrystals.

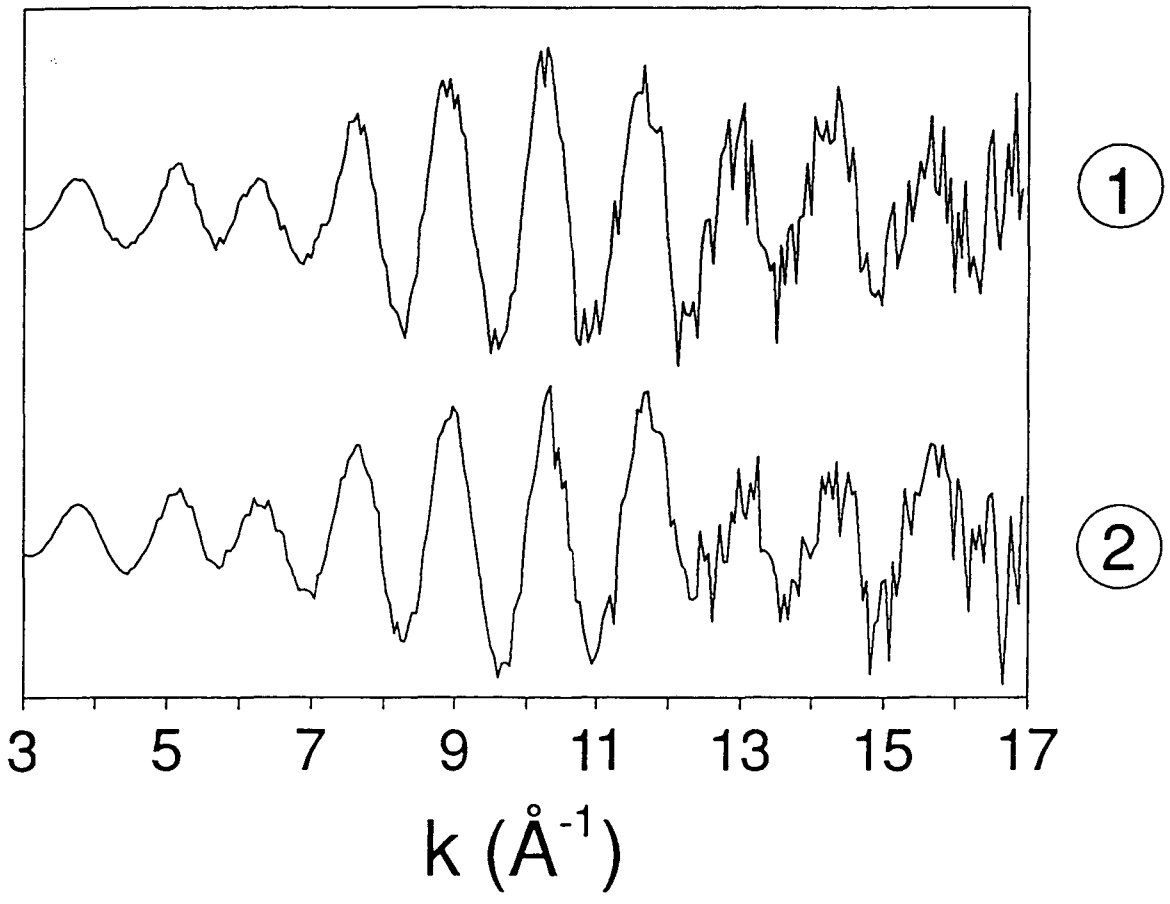

Figure 3.1: Background corrected atmospheric pressure Se EXAFS data obtained on bulk CdSe ① and 11 Å radius CdSe nanocrystals ② [presented as $k^3\chi(k)$]. The quality of the data is quite high and is essentially identical for bulk and nanocrystal systems.

3.2 Experimental:

The CdSe nanocrystals used in this experiment were prepared chemically using a modification of the method of Murray and Bawendi[12]. Crystallites were characterized using X-ray powder diffraction, TEM, optical absorption, and Raman scattering. Crystallite size and size distribution were determined using TEM and Small Angle X-ray Scattering (SAXS). The sample used in this experiment was found to be wurtzite in structure with an average size of 2.7 nm radius with a s of 18%. Imperfect agreement between SAXS/TEM sizes and X-ray domain size indicates the presence of some stacking faults or grain boundaries in the sample.

High pressure optical absorption data was obtained using a scanning Cary model 118 UV/visible spectrometer in combination with a Mao-Bell type diamond anvil cell with spring steel gaskets and 0.2 mm diameter sample chambers. Nanocrystals were dissolved in 4-ethyl-pyridine, a solvent which has been shown to be a reasonable quasi-hydrostatic pressure medium to pressures in excess of 10 GPa.[13] Pressure was determined using ruby fluorescence. In all cases, multiple fluorescence measurements were taken at various locations in the cell and pressure gradients were shown not to exceed 8%.

Se EXAFS data was obtained at the Stanford Synchrotron Radiation Laboratory on focused wiggler beam lines 6-2 and 10-2. Atmospheric pressure data were obtained using X-ray fluorescence and a Lytel detector. High pressure data were obtained in an absorption geometry using ion chamber detectors.

A significant problem with high pressure EXAFS experiments is interference due to Bragg diffraction from the single crystal diamonds of the high pressure cell. This diffraction can cause a forest of peaks that completely obscure the structure in the EXAFS region. Some improvement can be made by rotating the cell around its azimuthal angle (along the X-ray beam path). As a result of small imperfections in the cut and alignment of the diamonds and of the diamond cell, the X-ray beam is rarely exactly parallel to a crystallographic axis of the diamonds. By rotation around the azimuthal angle, the Bragg

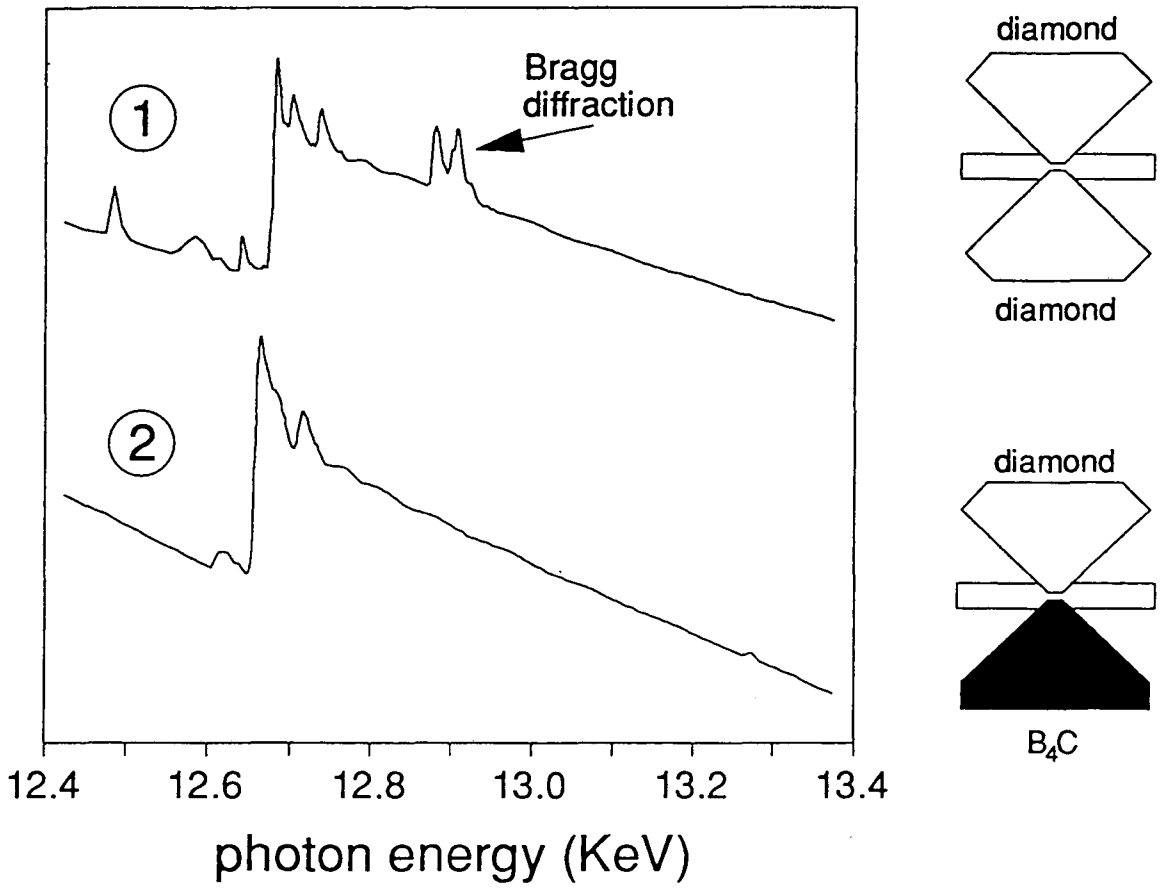

Figure 3.2: Raw high pressure Se EXAFS data obtained ① in a high pressure cell with two diamond anvils, and ② in a high pressure cell with one diamond anvil and one boron carbide anvil. The spikes in the first spectra are the result of diffraction from the single crystals diamonds of the high pressure cell. While some spikes are still present in the second spectra, they have all been moved to the near edge region and so do not interfere with the analysis of the EXAFS data.

condition can thus be altered and diffraction peaks can be moved away from the energy region of interest. This empirical optimization technique is limited however, by the fact that the orientation of the two diamonds with respect to each other is fixed in the process of aligning and loading the cell, and thus complete optimization is not possible. Other methods of dealing with interfering bragg diffractions include replacement of the diamond anvils with Boron Carbide (B_4C) anvils[14]. Boron Carbide is polycrystalline, and thus produces no interfering diffraction peaks. It has the limitation that it is not optically transparent and thus precludes the use of ruby fluorescence to determine pressure. We have thus chosen to conduct our experiments using a modified Merrill-Bassett type diamond anvil cell with one diamond anvil, and one B_4C anvil. This allows for complete rotational optimization of the single diamond as well as providing an optical window for ruby fluorescence measurements. Figure 3.2 shows the reduction in interfearing bragg diffraction in the mixed diamond/B_4C anvil cell in comparison to the pure diamond cell.

EXAFS data were analyzed using standard procedures[15]. Data was background corrected, Fourier filtered, and fit to a standard EXAFS equation:

$$\chi(k) = \frac{N}{k \cdot r^2} e^{-2\sigma^2 k^2} \cdot F(k) \cdot \sin[2kr + \phi(k)] \qquad (1)$$

where k is the photoelectron wavevector, N is the number of nearest neighbors, r is the real space bond length, s is the Debye-Waller factor, F(k) is the backscattering amplitude, and I(k) is the total phase shift experienced by the photoelectron. Scattering phase and amplitude factors were calculated theoretically using bulk CdSe lattice geometry in combination with the program Feff 5, version 5.04.

3.3 Results:

Optical absorption spectra of these direct gap semiconductors nanocrystals show a discrete absorption feature at energies above the bulk band gap due to quantum confinement of the initial electronic excited state. This feature is seen to move smoothly

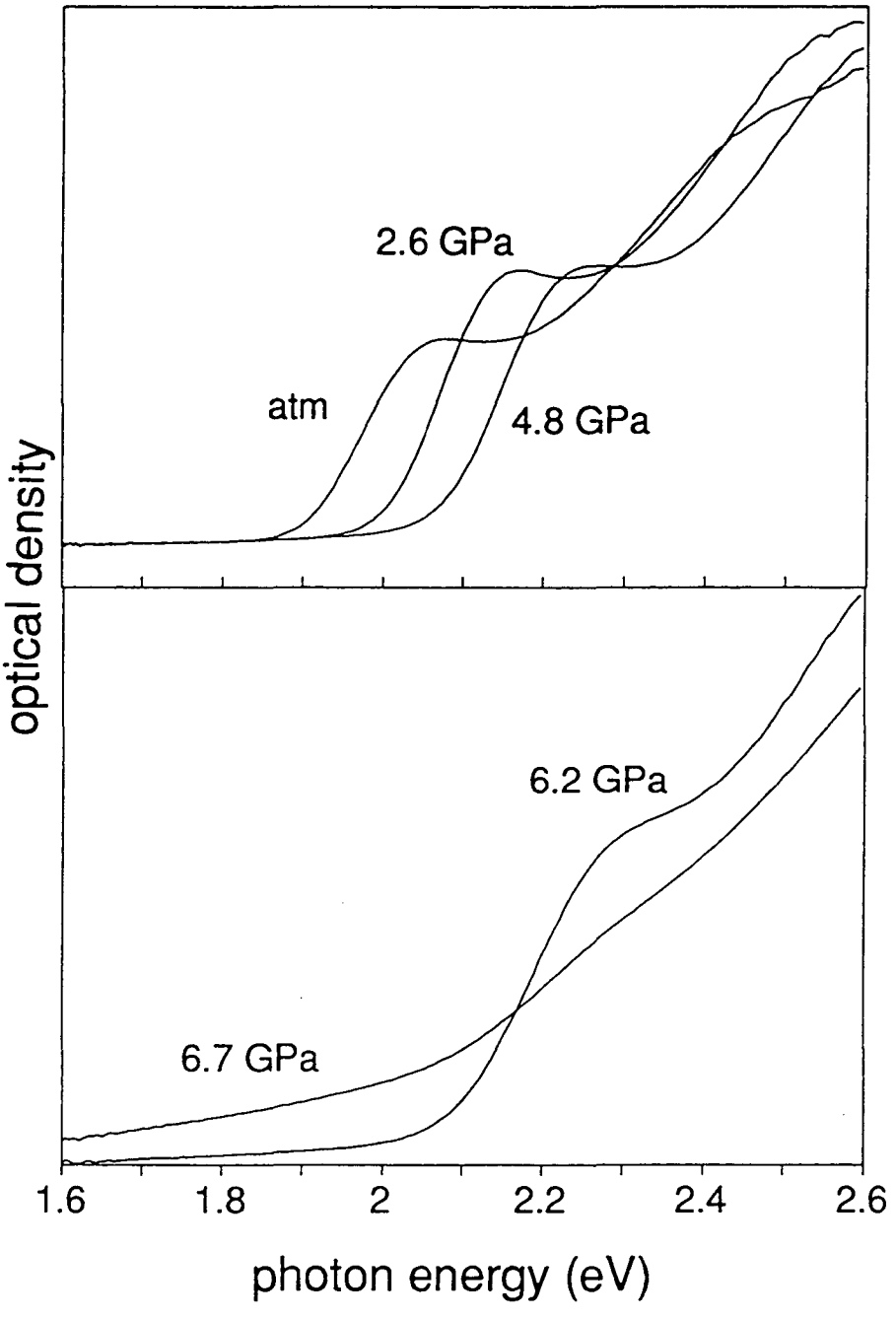

Figure 3.3: High pressure optical absorption data obtained on 2.7 nm radius CdSe nanocrystals. (a) Shift of the confined optical absorption feature with pressure. (b) Disappearance of the confined feature at the structural transition pressure.

to higher energy upon the application of pressure. At pressures between 6.2 and 6.7 GPa, approximately 2 times the reported bulk transition pressure, the discrete feature disappears and is replaced by a weak featureless absorption, shifted to the red of the direct gap feature (figure 3.3). Upon release of pressure, the discrete absorption is recovered, though the reverse transition is marked by 4-5 GPa of hysteresis.

Se EXAFS data on atmospheric pressure nanocrystal samples produce a bond length of 2.61 Å and a coordination number of 3.5, in good agreement with bulk CdSe values of 2.62 Å and 4. Background corrected EXAFS data obtained on our nanocrystal samples at a variety of pressures is presented in figure 3.4. The data shifts monotonically upon the application of pressure up to 6.4 GPa, at which point a discontinuous change is observed, followed by another smooth shift. Cadmium-Selenium bond length changes obtained form fitting these data are presented in figure 3.5. Upto approximately 4 GPa, the data are in good agreement with the bulk CdSe linear compressibility. Data obtained upon the gradual release of pressure (5.5, 2.5 and 0.7 GPa) appears to show a mixed phase with a very low coordination number and a poorly defined bond length, though the 5.5 GPa data does appear to be dominantly rock salt in character. Upon full release of pressure, the bond length is observed to return to 2.63 (Å) and the coordination number to 3.4.

3.4 Discussion:

3.4.1. Interpretation of Structural Data

Optical absorption data suggests that 27 Å radius CdSe nanocrystals undergo a reversible solid-solid phase transition at pressures between 6.2 and 6.7 GPa (upstroke). Roughly parabolic energy dependence in the high pressure phase absorption spectra further suggests that this new phase has an indirect band gap[16]. By analogy with the bulk, a reasonable structural candidate is rock salt, though other distorted octahedral structures with multiple first shell bond lengths are possible[17]. Other possibilities include amorphous

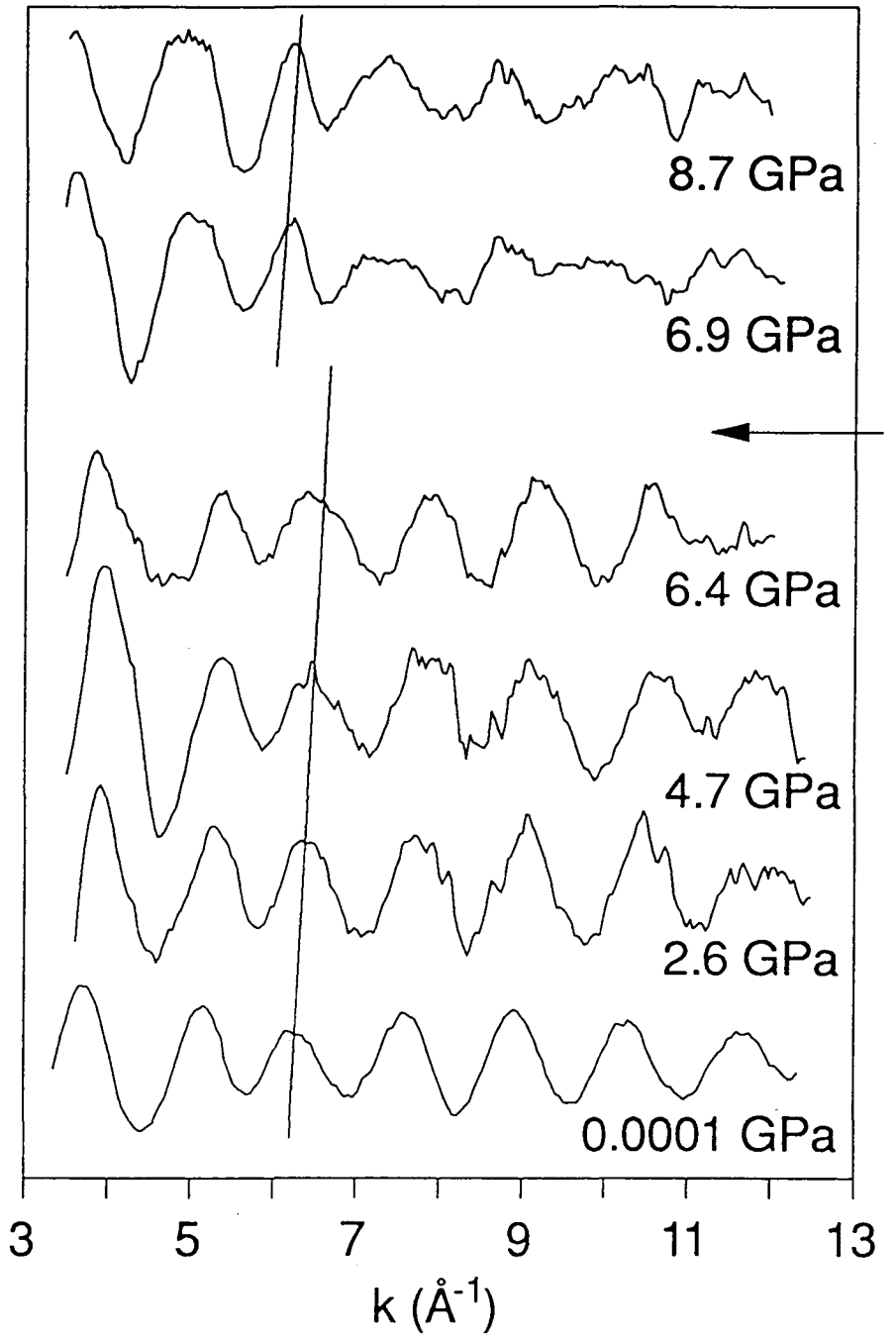

Figure 3.4: Back ground corrected Se EXAFS data, presented as $k \cdot \chi(k)$, obtained on 2.7 nm radius CdSe nanocrystals as a function of pressure. The arrow corresponds to the optically detected phase transition pressure. A shift in the EXAFS oscillations is observed at this pressure.

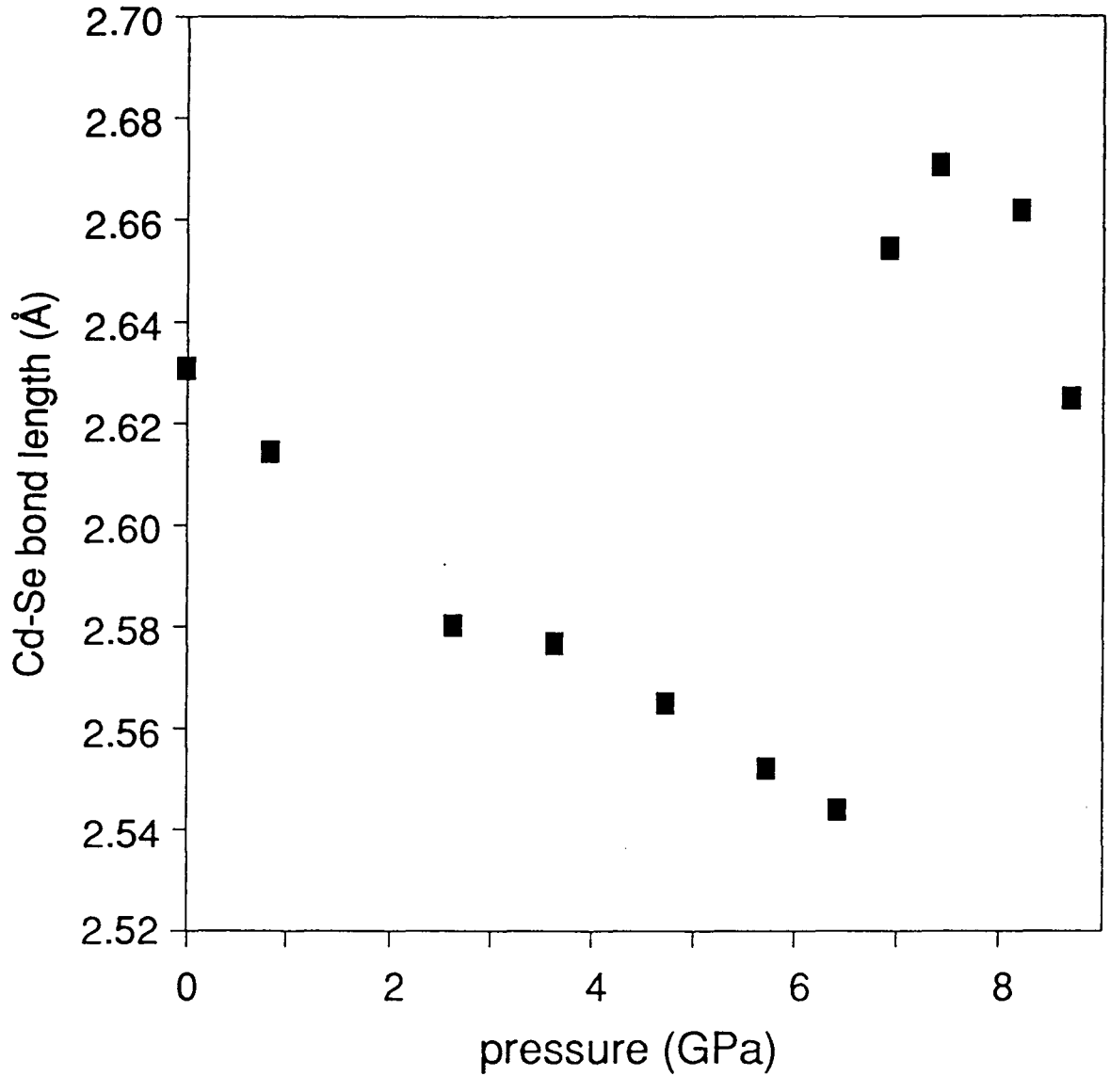

Figure 3.5: Change in the Cd-Se bond length with pressure for 2.7 nm radius CdSe nanocrystals obtained from Se EXAFS. A large change in Cd-Se bond length can be seen at the structural transformation pressure (about 6.5 GPa).

or disordered states. Although it is not possible to distinguish between these possibilities using optical absorption, EXAFS can clearly separate them. Amorphous material should show a distribution of bond lengths and a low average coordination number. In contrast, rock salt material should show a single peak first shell peak and a second shell when the background subtracted data is Fourier transformed into real space. Other six coordinate structures would show multiple prominent bond lengths.

Figure 3.6 shows that quality EXAFS data can be obtained on high pressure phase nanocrystals, and that the EXAFS spectrum is dominated by a single bond length. These data suggest that the high pressure phase is not amorphous, and that the structure has only one dominant bond length. A small Se-Se second shell peak further suggests that the high pressure phase material has some degree of long range order. Although this is not sufficient information to positively identify the high pressure phase structure as rock salt, additional information can be gained by considering bond lengths. Figure 3.5 shows the change in bond length with pressure. At the optically detected phase transition point, the bond length is observed to become suddenly longer. This is indicative of a transition to a structure with a higher coordination number and packing fraction. The only reasonable structure that fills all of these requirements is rock salt. In addition, high pressure X-ray powder diffraction just obtained on these systems positively confirms the structural identity of the high pressure phase as rock salt.[18]

With a knowledge of the high and low pressure phase structure, it becomes possible to calculate the volume change upon transition. Studies on a wide variety of materials show that wurtzite or zinc blende to rock salt transitions are usually accompanied by about a 20% decrease in unit cell volume[19,20]. Figure 3.7 shows the actual data for our 27 Å clusters. A 24% volume contraction is observed.

Complete recovery of the four coordinate structure by atmospheric pressure is supported by both optical absorption and EXAFS data. Optical absorption shows a return of the discrete, allowed band gap transition in atmospheric pressure recovered samples,

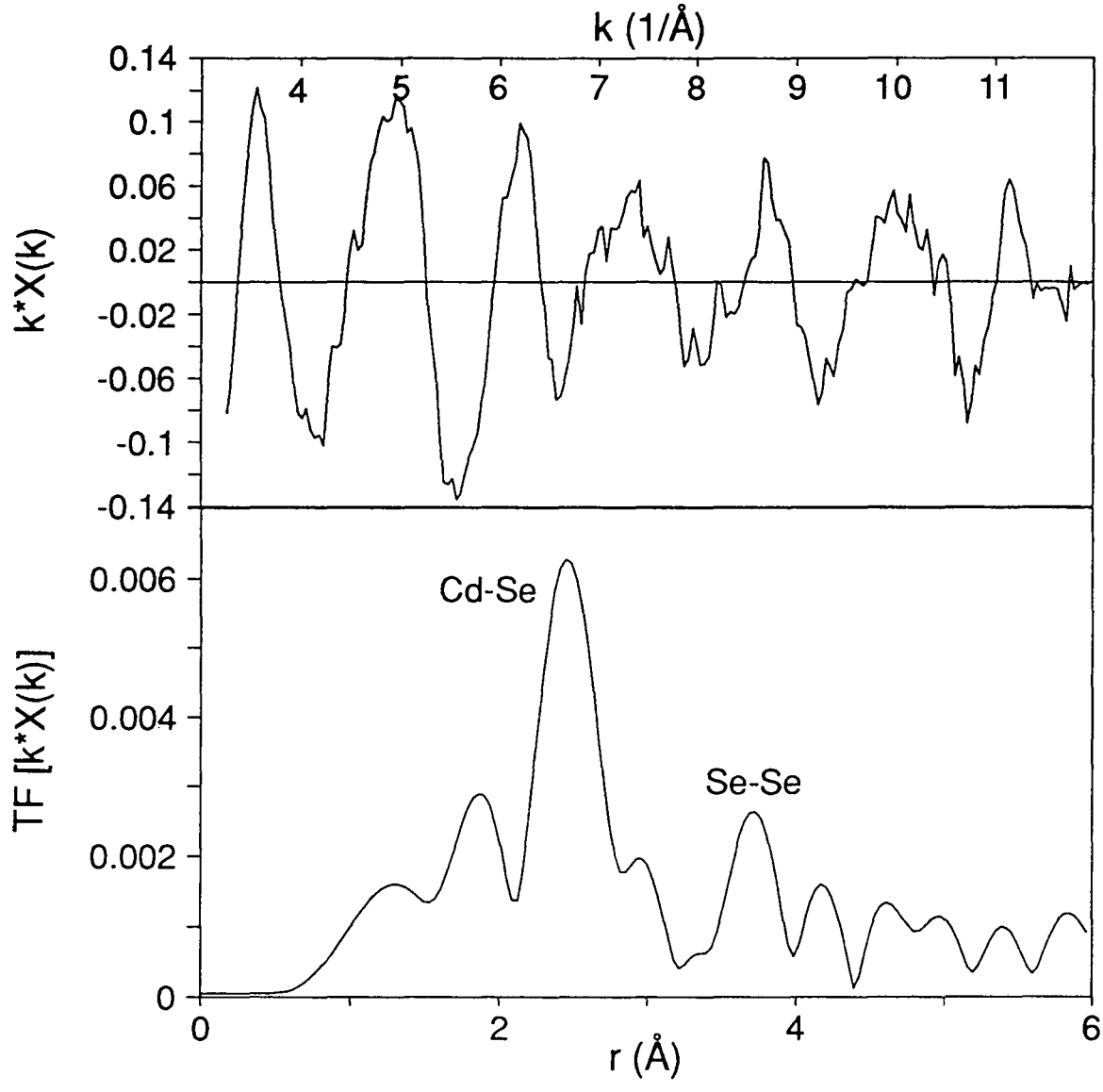

Figure 3.6: Se EXAFS data obtained on 2.7 nm radius CdSe nanocrystals at 8.2 GPa in the high pressure phase: Top - Back ground correct raw data presented as $k \cdot \chi(k)$. Bottom - Fourier transformed data. Cd-Se first shell and Se-Se second shell peaks are indicated in the transformed spectra.

and EXAFS shows a bond length and coordination number in atmospheric pressure recovered samples that is in good agreement with unpressurized samples. At pressures, however, only slightly above atmospheric (less than 1 GPa), both EXAFS and optical absorption show incomplete recovery of the wurtzite phase. Although this type of solid-solid transition usually exhibits large hysteresis, our nanocrystals appear to show significantly more hysteresis than bulk CdSe[5]. This is a subject of current investigation.

3.4.2. Calculation of Thermodynamic Parameters

The data presented in figure 3.7 can be fit with the Murnaghan equations of state[21,22]

$$V = \frac{V_o}{\left(1 + \frac{B_o'}{B_o} \cdot P\right)^{\frac{1}{B_o'}}} \qquad (2)$$

to yield values of B_0 (the bulk modulus) and its derivative with respect to pressure (B_0'). B_0 is the reciprocal of the linear volume compressibility. Most B_0 values for covalent semiconductors are in the range of 50-100 GPa, with B_0' small. The values obtained for our CdSe nanocrystals show $B_0 = 37 \pm 5$ GPa and $B_0' = 11 \pm 3$. This can be understood by noting that the compressibility of the CdSe nanocrystals seems to decrease at extremely high pressure. In bulk systems where this part of P-V space is not accessible, compressibility data can only be fit to the region between atmospheric pressure and 3 GPa. The nanocrystal data in that low pressure region is quite linear and can be accurately fit using bulk values of B_0. As the system is compressed beyond the bulk stability limit, we begin to sample the anharmonic parts of the Cd-Se potential and the compressibility deviates from the bulk value. The anomalous high pressure stability of these systems thus allows us to better determine the anharmonic terms in the potential of both the nanocrystals and the bulk.[22]

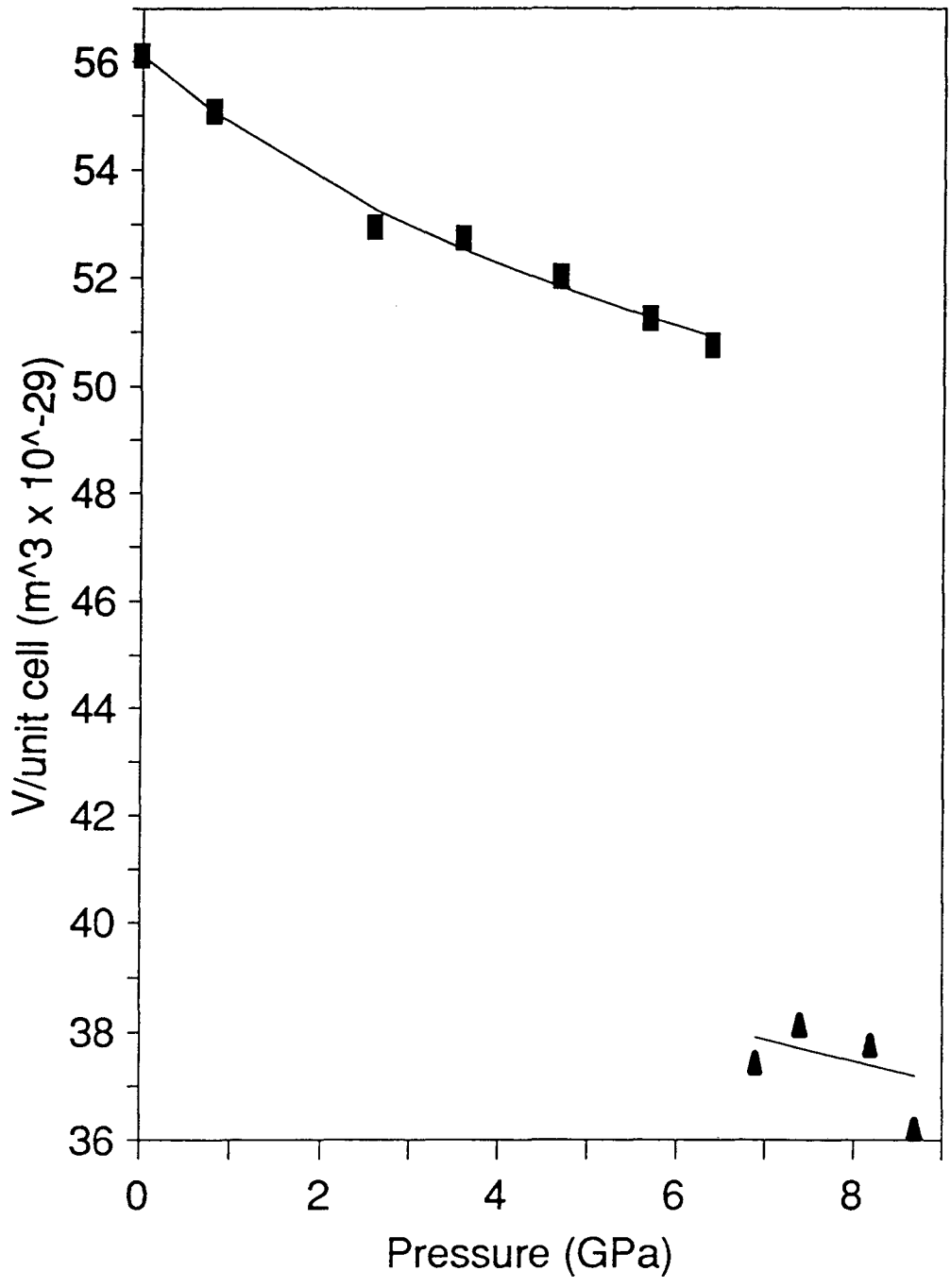

Figure 3.7: Change in unit cell volume with pressure for 2.7 nm radius CdSe nanocrystals. The points are calculated from the data in figure 3.4 and assume a rock salt structure for the high pressure phase nanocrystals. The line represents a fit to the Murnaghan equations of state (equation 2).

While the rock salt phase data presented here is not sufficient to fit with a compressibility value, it can be used in combination with bulk rock salt phase diffraction data to obtain a reasonable value for the high pressure phase linear compressibility. It should be noted, though, that it is not strictly legitimate to use bulk and nanocrystal data together in this way, as the nanocrystal bond lengths should be shifted to slightly smaller bond lengths due to the effects of surface tension. These lattice contraction effects, however, are small in comparison to pressure induced bond length changes and so the error introduced by this method of calculation is not unreasonable. From our rock salt phase EXAFS data and the data of Mariano and Warekois[23], we calculate a B_o value of 66.3 GPa with an atmospheric pressure unit cell volume of 4.40×10^{-29} m^3. These values are useful for a thermodynamic analysis of the elevation in phase transition pressure in finite size. While the quality of the data is not sufficient to obtain a B_o' value, it can be assumed that this value will be small as the pressures reached in this experiment are much lower than any reported second phase transitions observed in bulk CdSe. In the rock salt phase, the system is probably still in the harmonic part of the Cd-Se potential.

3.4.3 EXAFS on Nanocrystals as a Function of Size

In order to apply the concepts of thermodynamics to understanding phase transformations in nanocrystals, some measure of the surface energy associated with a nanocrystal is required. This surface energy can be estimated through direct means, such as calorimetry, by comparing bulk and nanocrystal systems. A simpler way to estimate the surface energy, however, involves the use of the Laplace Law. This equation, derived for homogeneous systems like a liquid droplet, relates the surface energy of a sphere to an effective pressure on the droplet. This pressure can then be related to a lattice contraction through the volume compressibility. The formalism has been successfully used to measure the surface energies in small crystallites from shifts in the X-ray or electron diffraction patterns with size.[11] As the surface energy is an important thermodynamic parameter for

understanding the observed elevation in solid-solid phase transition pressure, one goal of this EXAFS experiment is to obtain a measure of the Cd-Se bond length as a function of nanocrystal size. Previous EXAFS experiments on CdS nanocrystal, however, have shown no evidence for a lattice contraction,[24] despite the fact that a contraction could be seen in X-ray diffraction experiments.

In an effort to obtain a measure of the surface energy in our CdSe nanocrystals and to understand these earlier results, atmospheric pressure EXAFS data was collected on a variety of different size nanocrystals. The results are presented in figure 3.8, plotted as fractional changed in Cd-Se bond length as a function of inverse nanocrystal radius. Similar results obtained from X-ray diffraction experiments are included for comparison. The lattice contraction observed from EXAFS is clearly much smaller than that seen in a diffraction experiment. An explanation for this behavior lies in the nature of these two measurements. A diffraction experiment intrinsically relies on long range order to generate a signal. Diffraction, thus, measures only the bond lengths in the ordered, or interior, part of the nanocrystals. EXAFS, in contrast is sensitive to only first shell, or short range order. EXAFS thus samples the interior and the surface of the nanocrystal equally. As the surface of the nanocrystal should be somewhat disordered (in order to optimize for surface reconstruction and bonding of the surface atoms to the organic capping ligands), the Cd-Se bond lengths on the surface should be slightly longer than in the interior of the crystallites. The lattice contraction in a nanocrystal will increase with decreasing particle radius and thus increasing surface area to volume ratio. At the same time, however, the fraction of atoms on the nanocrystal surface (with slightly longer bond lengths) should increase. If these two effects cancel, very little overall lattice contraction will be observed in EXAFS.

The more relevant question, however, is which technique is best suited to estimate the surface energy in the crystallites? In deriving the Laplace law,[25] an infinitesimally thin surface or interface region is assumed. The nature of the bonding in a realistic interface

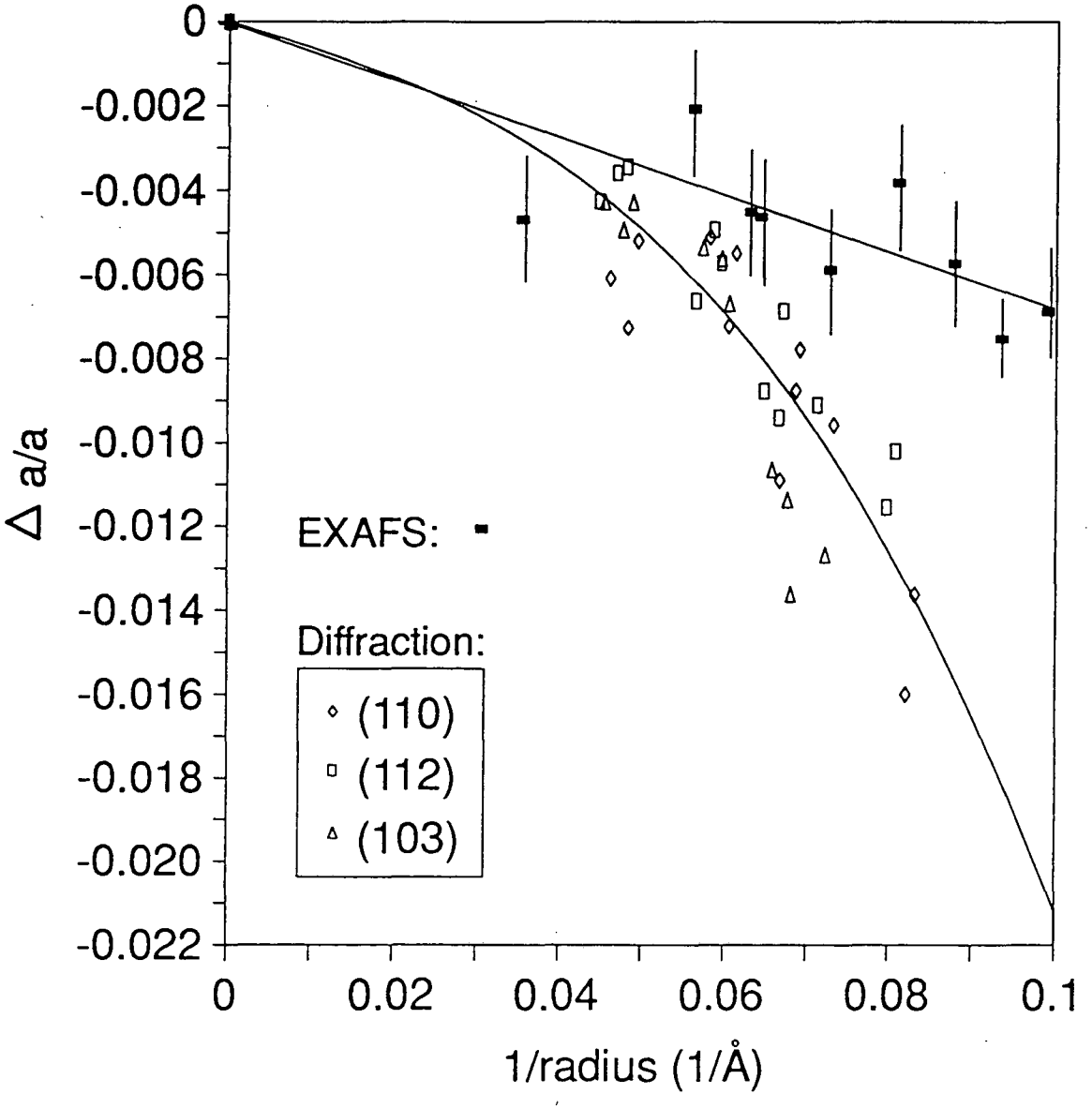

Figure 3.8: Fractional change in lattice constant as a function of inverse nanocrystal radius. Filled symbols are calculated from Se EXAFS data. Open symbols derive from X-ray diffraction. The lattice contraction observed in diffraction experiments is significantly larger than that seen in EXAFS.

region is not considered, only the energetics of these bonds. Applying this concept to a solid made up of atoms (particularly when the total dimensions of the solid are on the atom length scale) is not strictly legitimate. If the formalism is to be used, it is best to average over the structural parameters only from the interior region of the crystallites and approximate the interface as an infinitely thin surface. In Chapter 4, the Laplace law will thus be used in combination with X-ray diffraction data on many sizes of nanocrystals to determine the surface tension in the wurtzite phase. The results will be used in a thermodynamic model of the wurtzite to rock salt transformation in CdSe nanocrystals.

3.5 Conclusions:

In this chapter we have presented Se EXAFS data obtained on 2.7 nm radius CdSe nanocrystals above and below the observed solid-solid phase transition. The low pressure wurtzite phase data can be fit with the Murnaghan equations of state to yield a value of B_o = 37 ± 6 GPa and B_o' = 11 ± 3. The high pressure phase EXAFS data is in good agreement with a bulk rock salt structure. The data can be used to generate a B_o value in the rock salt phase of 66.3 GPa. Despite the agreement with bulk CdSe compressibiliteis and structures, the phase transition does not occur until the system has been pressurized to 3.5 GPa above the bulk limit of stability.

The implications of this work to fields outside of solid state physics and chemistry are interesting and merit some speculation. Although these experiments were performed on isolated nanocrystals homogeneously dissolved in solution, it is reasonable to assume that as long as there is a high energy interface, this type of effect should be observed in fused nanocrystal systems as well. That would suggest that accurate modeling of systems as diverse as geological structures and the high pressure stability of materials would require a knowledge not only of the types of compounds involved, but of their domain size, provided the domains are not greater than nanometer dimensions.

3.6 Notes and References

1. Haase, M. and Alivisatos, A.P.: J. Phys. Chem. **96**, 6756 (1992).

2. Zhao, X.S., Schroeder, J., Persans, P.D., and Bilodeau, T.G.: Phys. Rev. B. **43**, 12580 (1991).

3. Tolbert, S.H. and Alivisatos, A.P: Zeitschrift fur Physik D - Atoms, Molecules, and Clusters. **26**, 56 (1993).

4. Alivisatos, A.P., Harris, T.D., Brus, L.E., and Jayaraman, A.: J. Chem. Phys. **89**, 5979 (1988).

5. See chapter 4, reference 7 for more detail on the CdSe wurtzite to rock salt transition and hysteresis: Edwards, A.L. and Drickamer, H.G.: Phys. Rev. **122**, 3196 (1962).

6. Zhao, X.-S., Schroeder, J., Bilodeau, T.G., Hwa, L.-G.: Phs. Rev. B. **40**, 1257 (1989).

7. Onodera, A.: Rev. Phys. Chem. Japan **39**, 65 (1969).

8. Cui, L.J., Venkateswaran, U.D., and Weinstein, B.A.: Phys. Rev. B. **45**, 9248 (1992).

9. Coombes, C.J.: J. Phys. **2**, 441 (1972).

10. Buffat, P. and Borel, J.-P.: Phys. Rev. A **13**, 2287 (1976).

11. Goldstein, A.N., Echer, C.M., and Alivisatos, A.P.: Science **256**, 1425 (1992).

12. Murray,C.B., Norris,D.J., and Bawendi,M.G.: J. Am. Chem. Soc., **115**, 8706 (1993).

13. Tolbert, S.H. and Alivisatos, A.P.: unpublished results

14. Ingalls, R., Crozier, E.D., Whitmore, J.E., Seary, A.J. and Tranquada, J.M.: J. Appl. Phys. **51**, 6 (1980).

15. Teo, B.K. *EXAFS: Basic Principles and Data Analysis*, Springer-Verlag, Berlin, 1986, pp. 21-52.

16. Pankove, J.I. *Optical Processes in Semiconductors*, Dover Publications Inc., New York, 1971, pp. 1-21.

17. Froyen, S. and Cohen, M.L.: Phys. Rev. B **28**, 3258 (1983).

18. Tolbert, S.H. and Alivisatos, A.P.: *Science*, **265**, 373 (1994); Tolbert, S.H. and Alivisatos, A.P.: *J. Chem. Phys.* **102**, 4642 (1995).

19. Cline, C.F. and Douglas, R.S.: J. Appl. Phys. **36**, 2869 (1965).

20. Hanneman, R.E., Danus, M.D., and Gatos, H.C.: J. Phys. Chem. Solids **25**, 293 (1964).

21. Murnaghan, F.D.: Proc. Natl. Acad. Sci. USA **30**, 224, (1944).

22. It has recently been brought to our attention that the Murnaghan equations of state can over-estimate the value of B_o'. A better approximation of this value can be obtained using the Birch-Murnaghan Equations of State.

23. Mariano, A.N. and Warekois, E.P.: Science **142**, 672 (1963).

24. Marcus, M.A., *et al.*: Nanostructured Materials **1**, 323 (1992).

25. Levine, I. A, *Physical Chemistry*, McGraw Hill, New York, 1988, pp.361-364.

Chapter 4: High Pressure X-Ray Diffraction and Optical Absortption

4.0 Abstract

Structural transformations in CdSe nanocrystals are studied using high pressure X-ray diffraction and high pressure optical absorption at room temperature. The nanocrystals undergo a wurtzite to rock salt transition analogous to that observed in bulk CdSe. Both the thermodynamics and the kinetics of the transformation, however, are significantly different in finite size. The nanocrystal phase transition pressures vary from 3.6 to 4.9 GPa for crystallites ranging from 21 to 10 Å in radius, respectively, in comparison to a value of 2.0 GPa for bulk CdSe. The size dependent data can be modeled using thermodynamics when surface energies are accounted for. Surface energies calculated in this way can be used to understand the dynamic microscopic path followed by atoms during the phase transition. X-ray diffraction data also shows that unlike bulk CdSe, crystalline domain size is conserved upon multiple transition in the nanocrystals, indicating that the transition only nucleates once in each nanocrystal.

4.1 Introduction:

Recent studies of clusters in both the gas and condensed phases show multiple examples of novel bonding geometries, many of which differ from those observed in bulk systems.[1] The existence of these unique structures opens up the general question of the effects of physical size on structural stability in nanometer size solids. As the total extent of a material is decreased from the bulk limit to systems containing only a few hundred atoms, how will the relative stability of different possible solid structures change?

One way to answer this question is to use pressure to force finite size materials to convert from one solid structure to another, a technique frequently used in bulk solids to assess the relative stability of various crystal structures. In extending these experiments to finite systems, a number of factors are potentially important. Three questions in particular

will be addressed in this chapter: (1) To what extent can pressure induced solid-solid structural transformations be used to understand the relative stability of various solid structures in finite size? (2) How will the transition kinetics differ in finite size, as compared to bulk solids? (3) What can be learned about the basic nature of solid-solid phase transitions by studying finite systems?

The surface energy of a nanocrystal can play a dominant role in determining the stable phases. In melting studies on a wide variety of nanocrystal materials, a depression in melting temperature is observed with decreasing size. The data can be quantitatively explained by the notion that the liquid phase is stabilized relative to the solid because the cluster surface energy is lower in the liquid phase.[2,3] In an attempt to answer question (1) above, we will apply these surface tension ideas to solid-solid phase transitions. The results, combined with a general understanding of surface structure and surface energy, will be used to address questions (2) and (3).

The system that we have chosen for these experiments is CdSe semiconductor nanocrystals. In this chapter we extend our previous work[4] on high pressure transformations in CdSe nanocrystals. These crystallites can be synthesized with very narrow size distributions and high crystallinity in sizes ranging from 10 - 30 Å in radius.[5,6] The high quality of these samples makes them ideal for studying the effect of size on structural stability.

Bulk CdSe is known to undergo a wurtzite to rock salt transition at 2.0 ± 0.2 GPa.[7] The transition is accompanied by a 20% decrease in unit cell volume and a change in coordination number from 4 to 6. In CdSe[8,9] and CdS[10,11] nanocrystals, however, it has been observed that the low pressure wurtzite structure is stable to pressures much higher than the bulk transition pressure. In GaAs/AlAs superlattices[12] an elevation of the AlAs phase transition pressure has also been observed. Neither the CdS/Se nanocrystal nor the superlattice experiments, based on either Raman or optical absorption, determined the high pressure phase structure, or the degree of crystallinity in the high pressure phase.

Also, due to limits in the ability to chemically synthesize II-VI nanocrystals, earlier experiments investigated only one size nanocrystal, and samples contained a broad size distribution. Advances in synthetic methods have now removed these constraints.[5,6]

Recently, we have applied high pressure Se EXAFS to the question of understanding the transformed structure in these crystallites.[13] Unlike X-ray diffraction where large Debye-Scherrer broadening makes experiments on small samples very difficult, EXAFS probes short range order and so quality EXAFS data can be collected on very small nanocrystal samples. These experiments were limited, however, in that they could not assess the degree of crystallinity in transformed samples, and they could only suggest that, by analogy with bulk CdSe, a rock salt structure was reasonable for the high pressure phase.

In this chapter we have thus chosen to apply a combination of high pressure X-ray diffraction and high pressure optical absorption to the study of solid-solid structural transformations in CdSe semiconductor nanocrystals. These techniques allow us to determine both the structure and degree of crystallinity of the nanocrystals in every phase, as well as the dependence of the transformation pressure on nanocrystal size. The experiments show that the phase transition pressure is elevated in finite size, but that the nanocrystal domain size is conserved upon transition. These results have important implications for theories of solid-solid phase transitions in both nanocrystalline and bulk systems. More importantly, this combination of experiments allows us to separate thermodynamic from kinetic effects and thus gain some real understanding of the factors that control stability in finite size.

4.2 Experimental:

Bulk CdSe samples, which had been annealed to reduce structural faults, were obtained from Cleveland Crystals. The CdSe nanocrystals used in this experiment were prepared chemically using a modification of the method of Murray and Bawendi.[5,6]

Crystallites were characterized using X-ray powder diffraction, Transmission Electron Microscopy (TEM), X-ray Photoelectron Spectroscopy (XPS), optical absorption, and Raman scattering. TEM shows that these nanocrystals are nearly spherical, although facets can be observed in crystallites over 30 Å in diameter.[14] Detailed surface characterization was performed using XPS[6] and NMR[15]: CdSe nanocrystals dissolved in pyridine appear to have surface Cd atoms which are coordinated to solvent nitrogen atoms. Some small fraction of the surface Se atoms are bonded as tri-alkyl-phosphine-selenide. In addition, some small fraction of the surface Cd and Se atoms could be present as oxides. The total number of bound ligands appears to be limited by steric effects between ligands and not by the availability of unbound surface sites.

Crystallite size and size distributions were determined using TEM, X-ray diffraction, and Small Angle X-ray Scattering (SAXS). The samples used in this experiment were found to be wurtzite in structure with an average size dispersion of σ = 5%. Only samples which were shown to be free of stacking faults by comparison of X-ray diffraction Debye-Scherrer peak widths and TEM/SAXS sizes were used in these experiments. A sample diffraction pattern for 2.2 nm radius CdSe nanocrystals is shown in figure 4.1. The symbols indicate the experimental data. The solid line is a calculated pattern based on the size determined by TEM/SAXS and the assumption of spherical nanocrystals. Residuals are included to emphasize the agreement.

High pressure optical absorption data was obtained using a scanning Cary model 118 UV/visible spectrometer in combination with a Mao-Bell type diamond anvil cell (DAC) with spring steel gaskets and 0.2 mm diameter sample chambers. Nanocrystals were dissolved in 4-ethyl-pyridine, a solvent which has been shown to be a reasonable quasi-hydrostatic pressure medium to pressures in excess of 10 GPa,[16] and in which the nanocrystals are extremely soluble. Pressure was determined using ruby fluorescence. In all cases, multiple fluorescence measurements were taken at various locations in the cell and pressure gradients were shown not to exceed 10%.

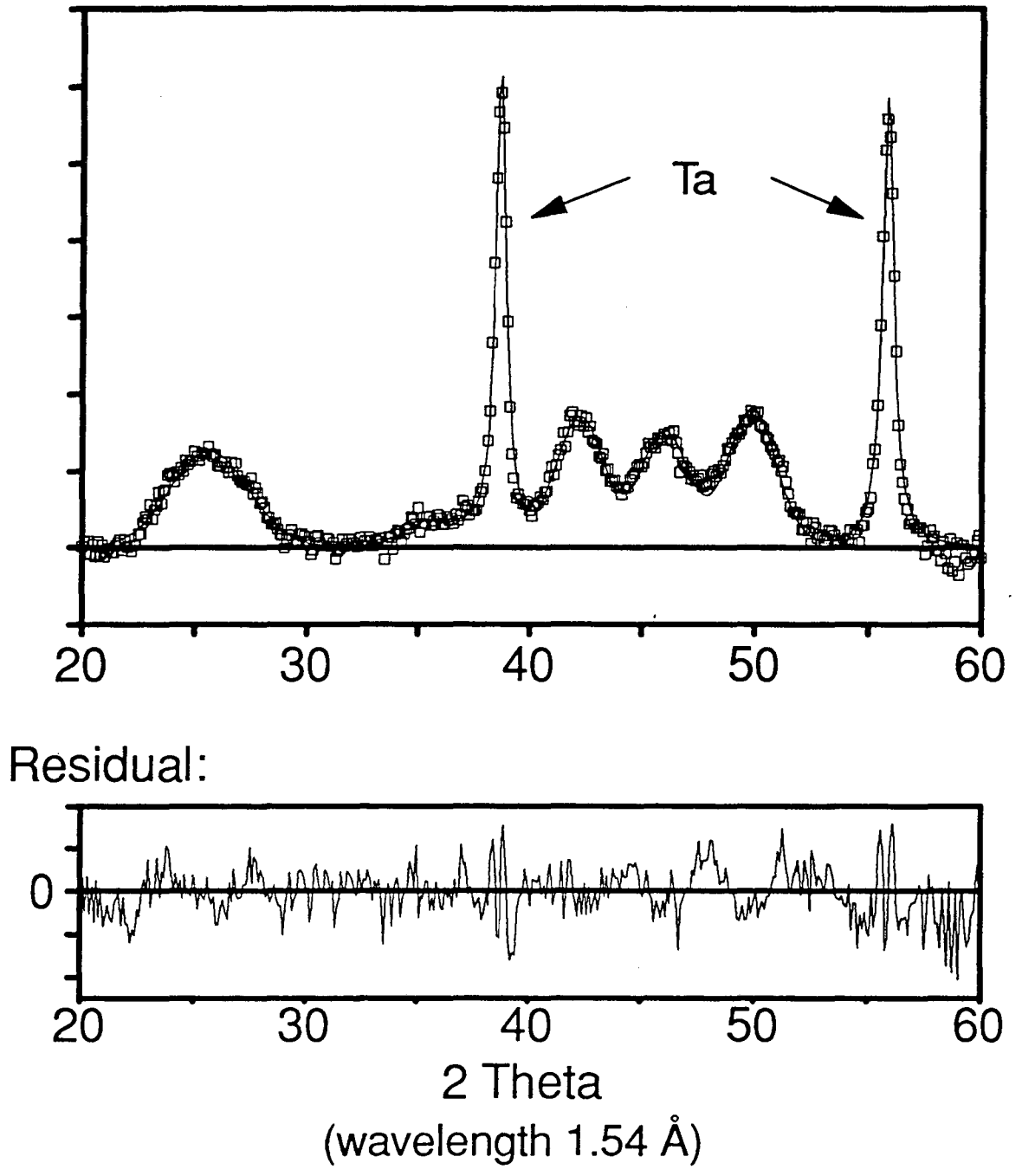

Figure 4.1: Atmospheric pressure X-ray diffraction pattern from 4.2 nm diameter CdSe nanocrystals. Open squares represent data. The solid line is calculated based on the assumption of spherical nanocrystals and the nanocrystal size determined by TEM/SAXS. Residuals are included to emphases the agreement. Tantalum diffraction peaks are from the sample holder.

High pressure X-ray diffraction experiments were carried out on wiggler beam line 10-2 at the Stanford Synchrotron Radiation Laboratory (SSRL). Focused monochromatic 12.5 KeV X-rays were collimated and apertured to a 0.1 mm beam through a series of 3 slits and pin holes. The X-ray energy was chosen to be below the Se absorption edge (12.6 KeV), thus minimizing Se absorption and K-α fluorescence. A Merrill-Bassett style diamond cell with Be rockers was used in combination with inconel gaskets. The cell was positioned at the center of a Huber 6 circle diffractometer which provided precise positioning of the cell with respect to the X-ray beam. Diffracted X-rays were collected on Fuji image plates and read with 0.1 mm resolution. Typical integration times ranged from 30 min to 1 hour, with diffraction intensities being a strong function of sample alignment. Debye-Scherrer rings were angle integrated to produce the data presented here. Like the optical absorption experiments, nanocrystal samples were dissolved in 4-ethyl-pyridine and standard ruby fluorescence techniques were used to determine pressure.

4.3 Results:

4.3.1 High Pressure X-Ray Diffraction.

High pressure X-ray diffraction data collected on bulk CdSe is presented in figure 4.2a. The system is observed to be completely transformed from a low pressure wurtzite[17] structure to a high pressure rock salt[18] structure by 3.5 GPa. This is in good agreement with values of 3.0 GPa upstroke for the bulk CdSe wurtzite to rock salt phase transition pressure presented in the literature.[7,19] Upon release of pressure, a tetrahedral structure is recovered, though it appears to be a mix of zinc blende[20] and wurtzite. This is also in agreement with previous observations.[7b,c] Intensity anomalies in the untransformed wurtzite peaks (figure 4.2a) are due to single crystal diffraction effects from the finite number of grains in the sample. Using the Scherrer formula, the diffraction peak widths can be used to calculate that the crystalline domain size decreases as the system undergoes subsequent transition (figure 4.2a), starting with an instrument limited domain size greater

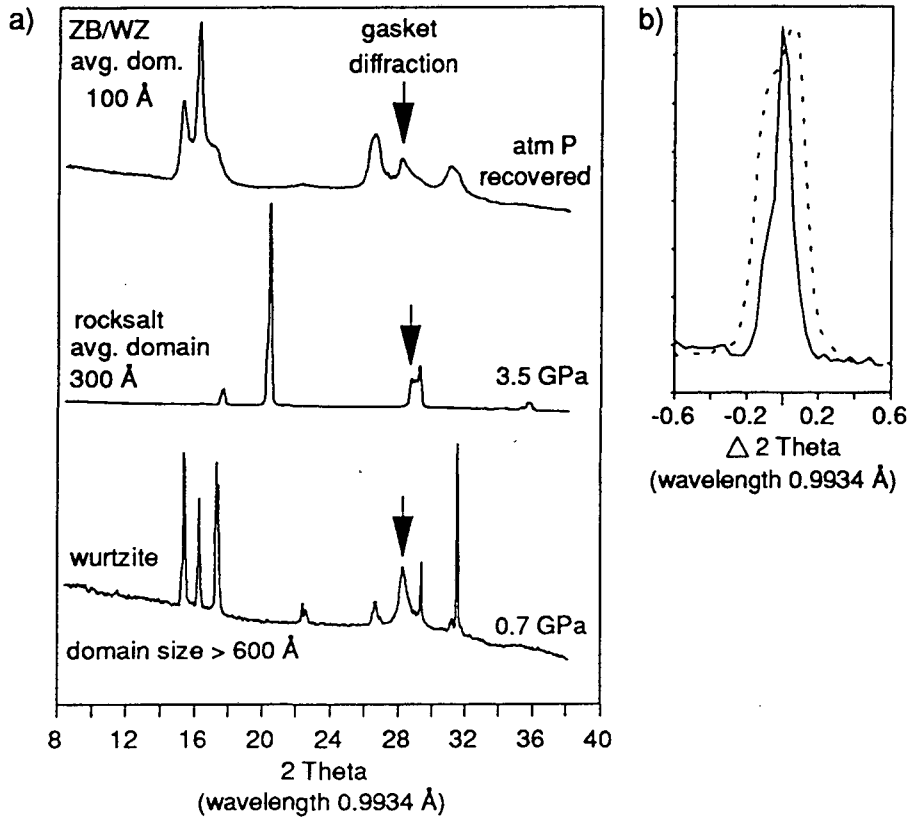

Figure 4.2: (a) High pressure X-ray diffraction data obtained on bulk CdSe. The sample is initially in the wurtzite phase. By 3.5 GPa, the sample has transformed to the rock salt phase. Upon release of pressure, a wurtzite/zinc blende mixed phase is recovered. Intensity anomalies in the original wurtzite pattern are due to single crystal effects caused by the finite number of grains in the sample. The arrow indicates diffraction from the metal gasket of the diamond cell. Domain size labels indicate the average domain size in each phase, and show a decrease in domain size with each transition. (b) Blowup of the original wurtzite (002) peak [solid line], and the rock salt (111) peak [dashed line]. See figure 4.4 for indexing. The data is plotted as $\Delta 2\theta$ with respect to the wurtzite and rock salt peak centers of 16.42 and 17.76 2θ, respectively. The marked broadening of the rock salt peak compared to the wurtzite is cause by a decrease in domain size upon phase transition.

than 600 Å (actual size = ~1 μm); decreasing to about 300 ± 40 Å in the rock salt phase, and then further decreasing to approximately 100 ± 30 Å in the recovered tetrahedral phase. Diffraction peaks from the original wurtzite phase and the transformed rock salt phase have been expanded in figure 4.2b to emphasize this change in peak width. The broadening in the recovered zinc blende/wurtzite phase is clearly seen in figure 4.2a. This observation will be discussed further in the next section.

Raw diffraction data obtained on 21 Å radius CdSe nanocrystals in the wurtzite and rock salt phases are shown in figure 4.3. Debye-Scherrer rings were angle integrated to produce the patterns presented in figures 2, 4-6, and 8. The angle integration increases the relatively poor signal to noise observed in the raw data by over an order of magnitude. Averaged data obtained on the same 21 Å radius nanocrystals is presented in figure 4.4. In contrast to bulk CdSe, the sample is observed to retain the wurtzite structure well above the bulk phase transition pressure of 3 GPa upstroke. At pressures above 6 GPa, the sample begins to convert to the rock salt structure. The co-existence of both phases is observed in the 6.3 GPa scan. The two phase stability is in part due to small pressure gradients in the DAC. Additionally, some inhomogeneity in sample size and surface structure could contribute to the observed two phase co-existence. Upon further application of pressure a clean rock salt pattern is observed. There is excellent agreement in terms of rock salt peak positions and relative intensities between the nanocrystal and bulk CdSe spectra. Upon release of pressure (figure 4.5), the transition is found to be highly hysteretic. The rock salt structure remains stable to pressures significantly below the observed upstroke transition pressure. By 1 GPa, however, the sample does begin to recover, and by atmospheric pressure, a mixed zinc blende/wurtzite pattern is recovered, again in good agreement with bulk CdSe.

Significantly different from the bulk, however, is the observation presented in figure 4.6 that the diffraction peak widths do not significantly increase upon transition from the wurtzite structure to the rock salt and back to wurtzite/zinc blende: The domain

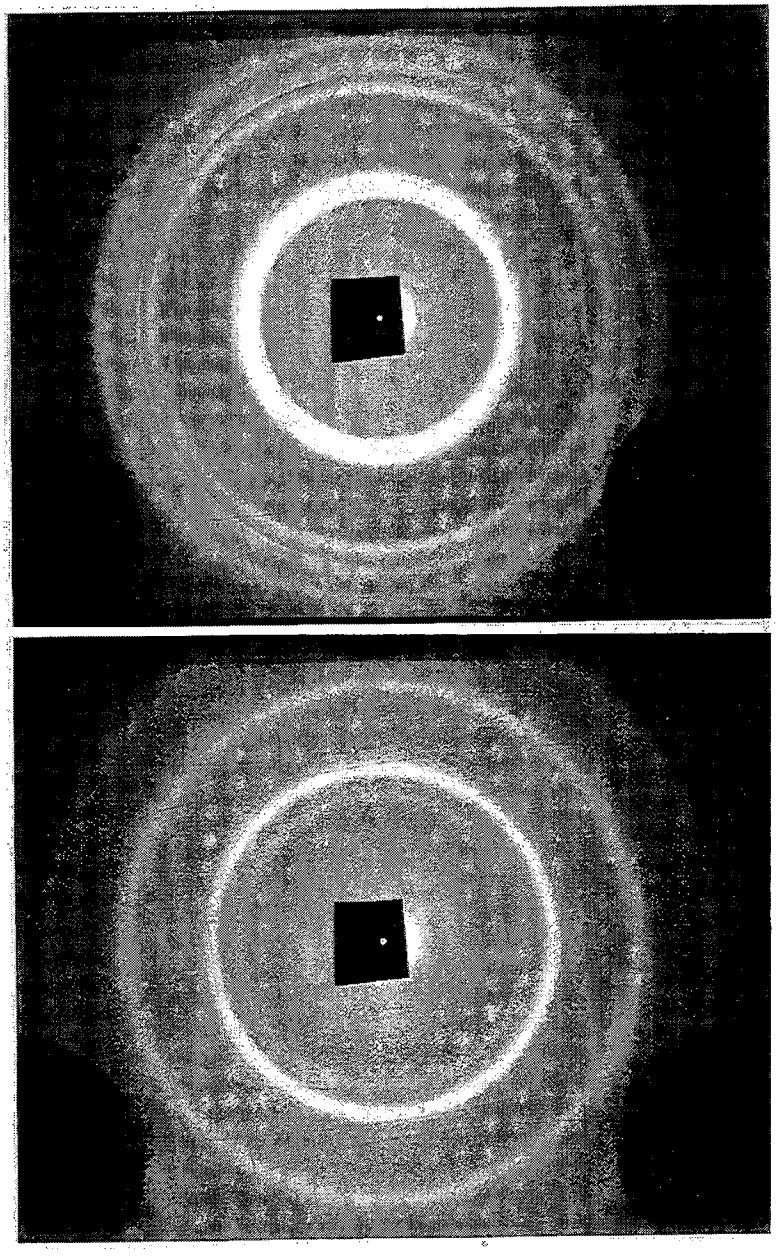

Figure 4.3: Raw diffraction data obtained on 4.2 nm diameter CdSe nanocrystals in the (top) wurtzite [1 GPa] and (bottom) rock salt [10 GPa] phases. Debye-Scherrer rings of this type are angle integrated to produce the data presented in figures 2, 4-6, and 8.

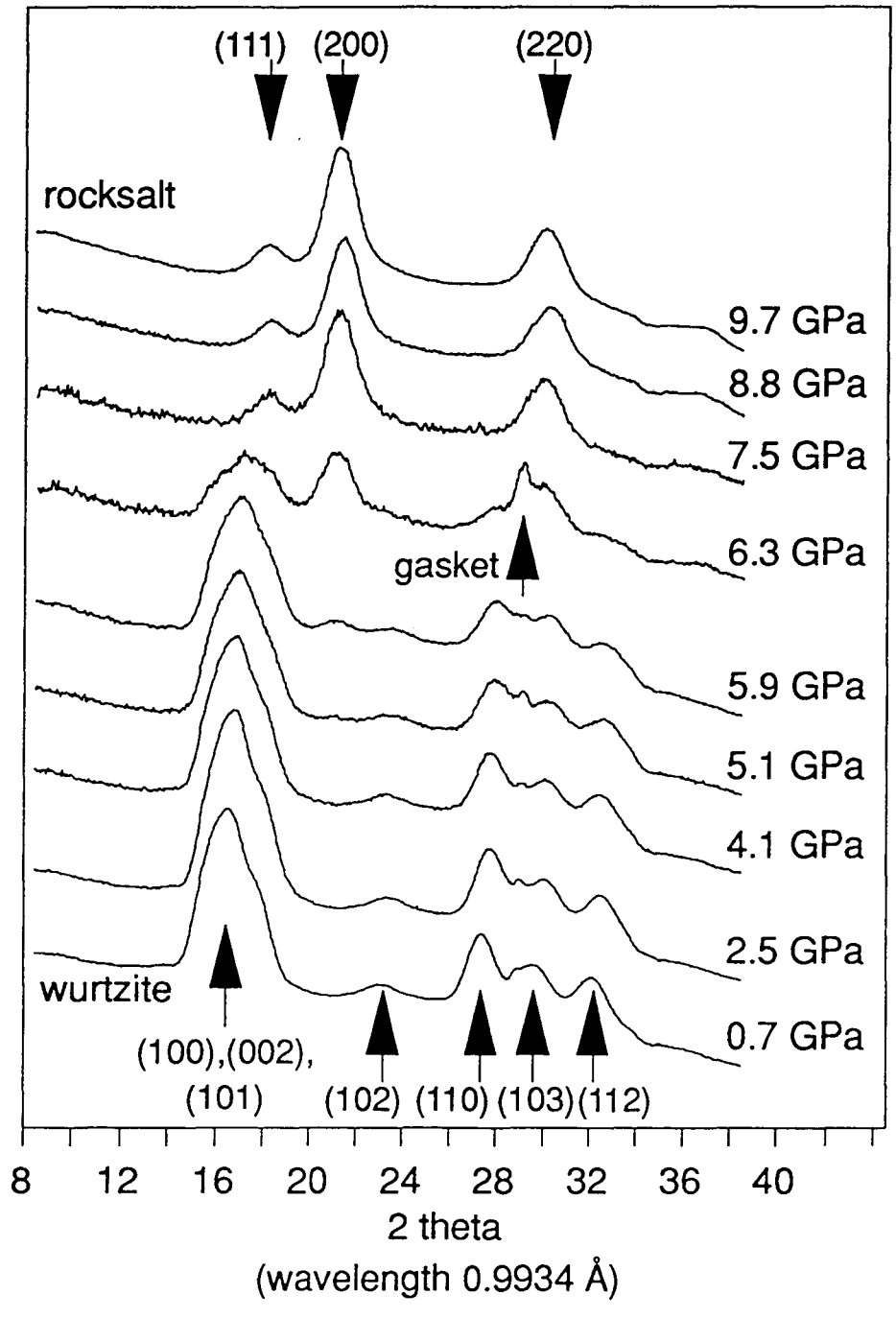

Figure 4.4: High pressure X-ray diffraction data obtained on 4.2 nm diameter CdSe nanocrystals with increasing pressure. Pressures and indexing for both the wurtzite and rock salt phases are indicated on the figure. The nanocrystals are observed to transform to the rock salt phase at approximately 6 GPa, which is twice the bulk upstroke transition pressure. The arrow indicates diffraction from the metal gasket of the diamond cell.

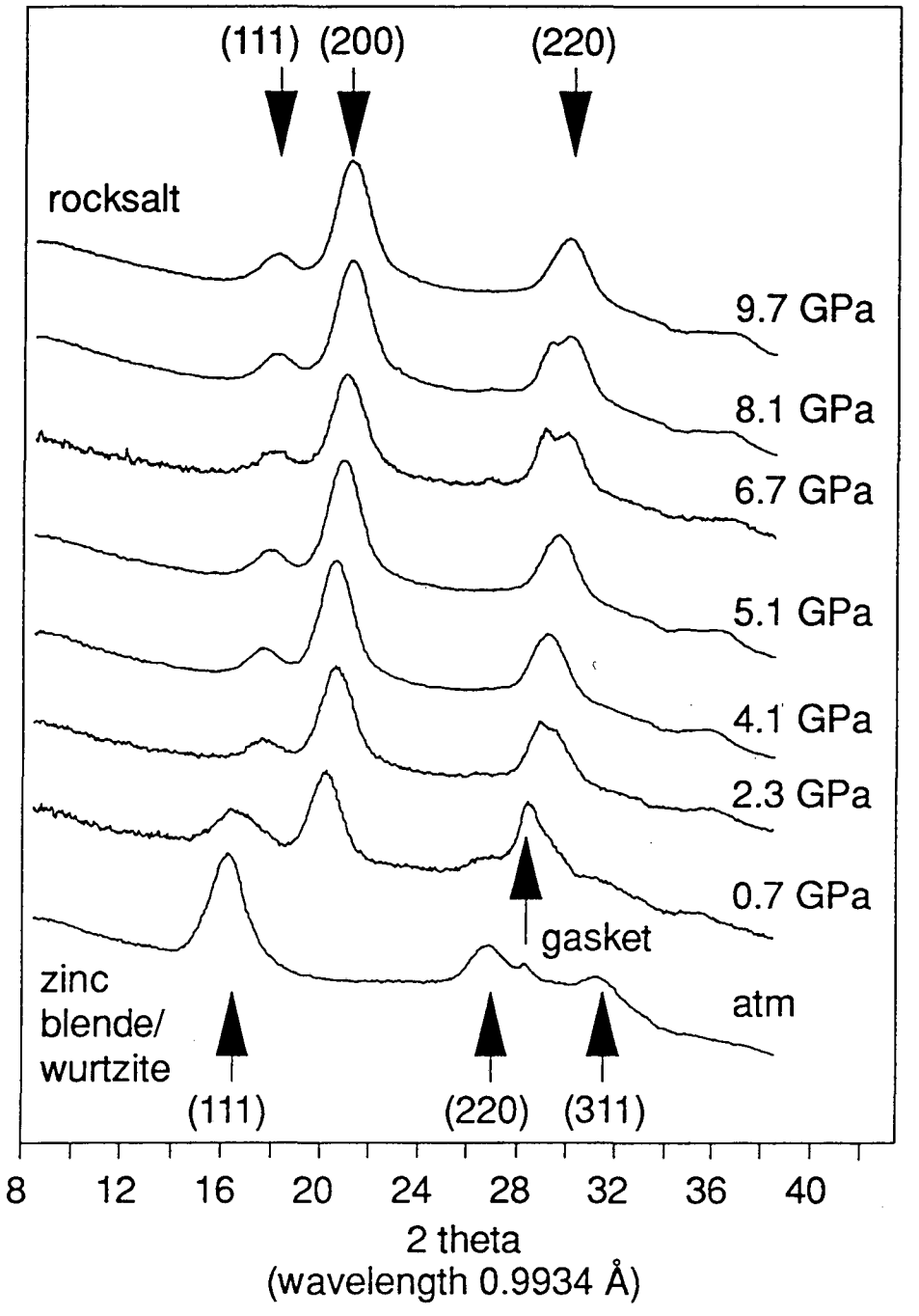

Figure 4.5: High pressure X-ray diffraction data obtained on 4.2 nm diameter CdSe nanocrystals with decreasing pressure. Pressures and indexing for both the rock salt and zinc blende phases are indicated on the figure. The nanocrystals are observed to transform from the rock salt phase to a mixed zinc blende/wurtzite phase at approximately 1 GPa. An arrow indicates diffraction from the metal gasket of the diamond cell.

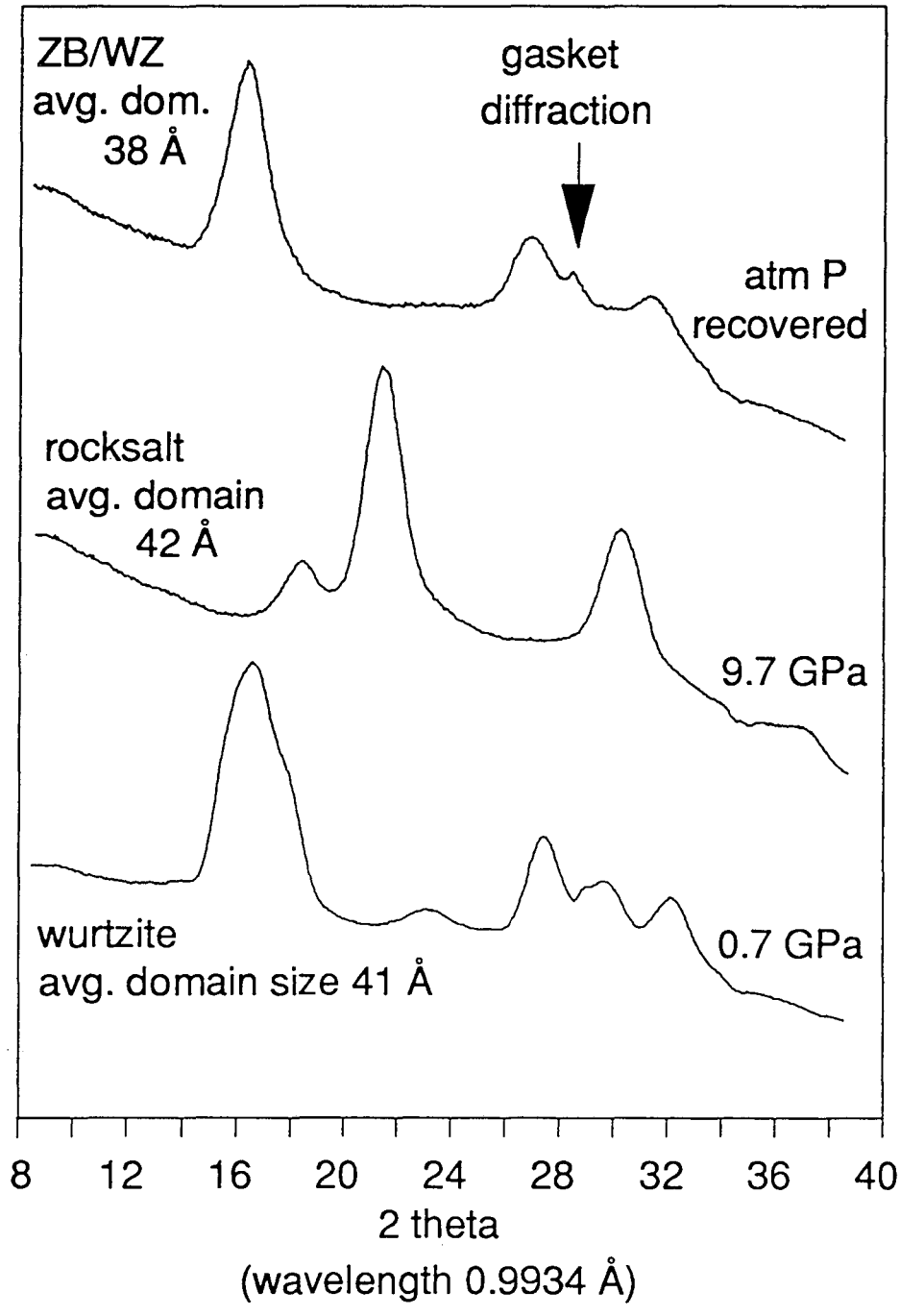

Figure 4.6: High pressure X-ray diffraction data obtained on 4.2 nm diameter CdSe nanocrystals in the untransformed wurtzite phase, the high pressure rock salt phase, and the recovered zinc blende/wurtzite mixed phase. In contrast to bulk CdSe (figure 4.2), domain size labels show that there is essentially no change in domain size after multiple transitions.

size is unchanged upon transition from wurtzite (average size = 41 ± 1 Å) to rock salt (average size = 42 ± 4 Å), and only slightly decreases on the reverse transition (average size = 38 ± 2 Å). These data suggest that nanocrystals are coherently transforming from one solid structure to another. The significance of this observation will be addressed in the discussion.

The data presented in figures 4 and 5 can be fit to obtain peak positions as a function of pressure (figure 4.7). This data can then be used to determine the bulk modulus (B_o) in the rock salt phase. B_o is defined as the reciprocal of the volume compressibility. The experimentally determined value for the rock salt phase nanocrystals of B_o = 74 +/- 2 GPa is in reasonable agreement (± 10%) with other reported values for bulk and nanocrystalline CdSe.[13,21] Unfortunately, due to the overlap of the many wurtzite diffraction peaks, it was not possible to obtain an accurate value of B_o for the wurtzite phase. The wurtzite data are, however, consistent with our previous values obtained from high pressure Se EXAFS experiments on CdSe nanocrystals.[13]

To insure that conclusions based on data obtained on 21 Å radius nanocrystals were generalizable to smaller sized crystallites, a limited data set was collected on 10 Å radius nanocrystals as well (figure 4.8). In good agreement with the results for larger crystallites, these nanocrystals were observed to transform from a wurtzite phase to a rock salt phase by 8.6 GPa, and back to a tetrahedral structure. Due to the extreme Debye-Scherrer broadening in these clusters, it is not possible to distinguish between possible tetrahedral structures in the recovered sample. Within the limits of the data, however, there does not appear to be any significant broadening of the diffraction peaks upon multiple transitions.

4.3.2 High Pressure Optical Absorption.

While the effect of pressure on optical absorption in these systems is an interesting question, it is not the focus of this chapter, and thus will not be discussed in detail.[22]

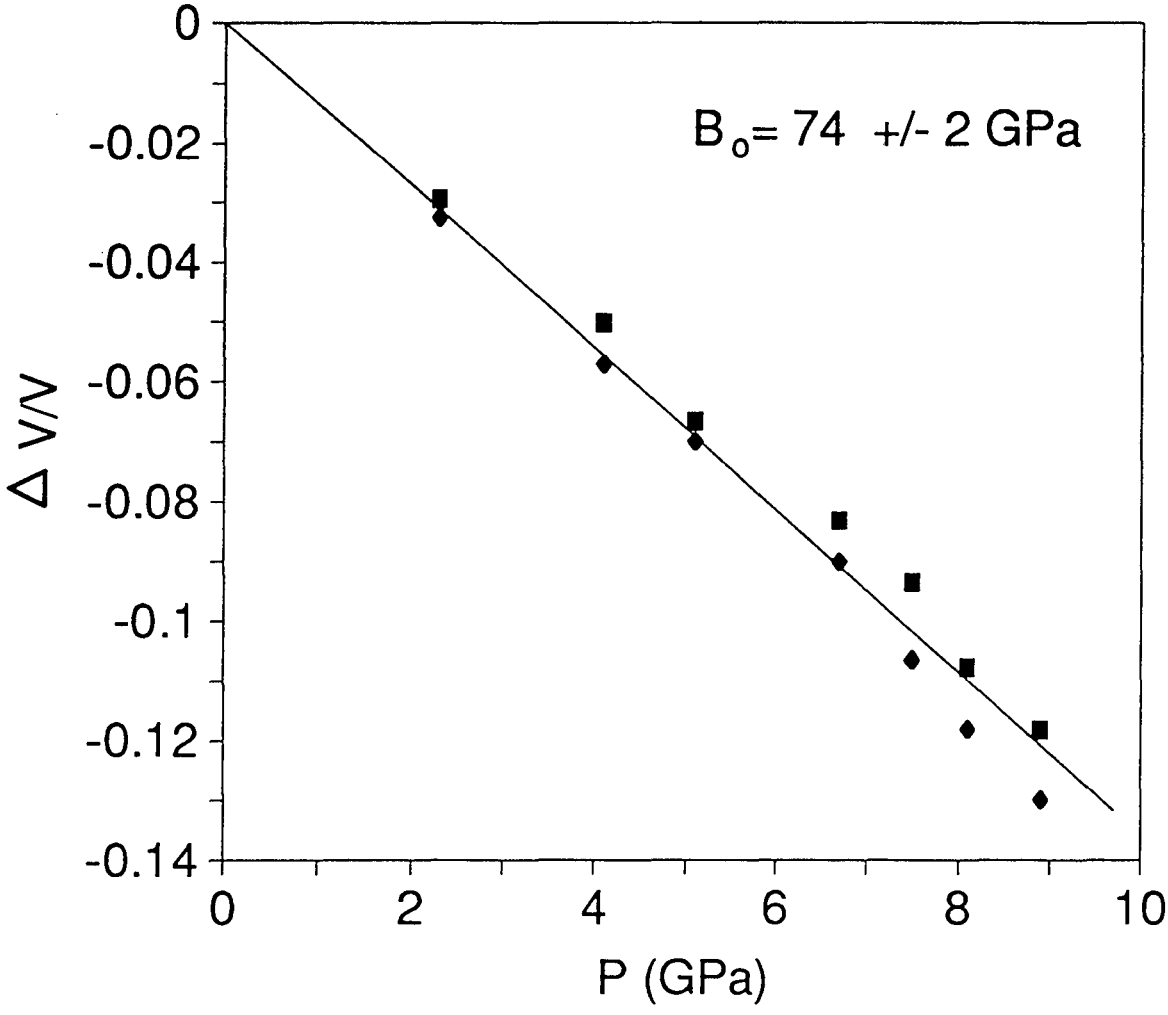

Figure 4.7: Fractional shift in unit cell volume with pressure for the rock salt phase of 4.2 nm diameter CdSe nanocrystals. Square and diamond markers correspond to data obtained using the (220) and (200) diffraction peaks respectively. The data can be fit with a volume compressibility of B_o = 74 +/- 2 GPa.

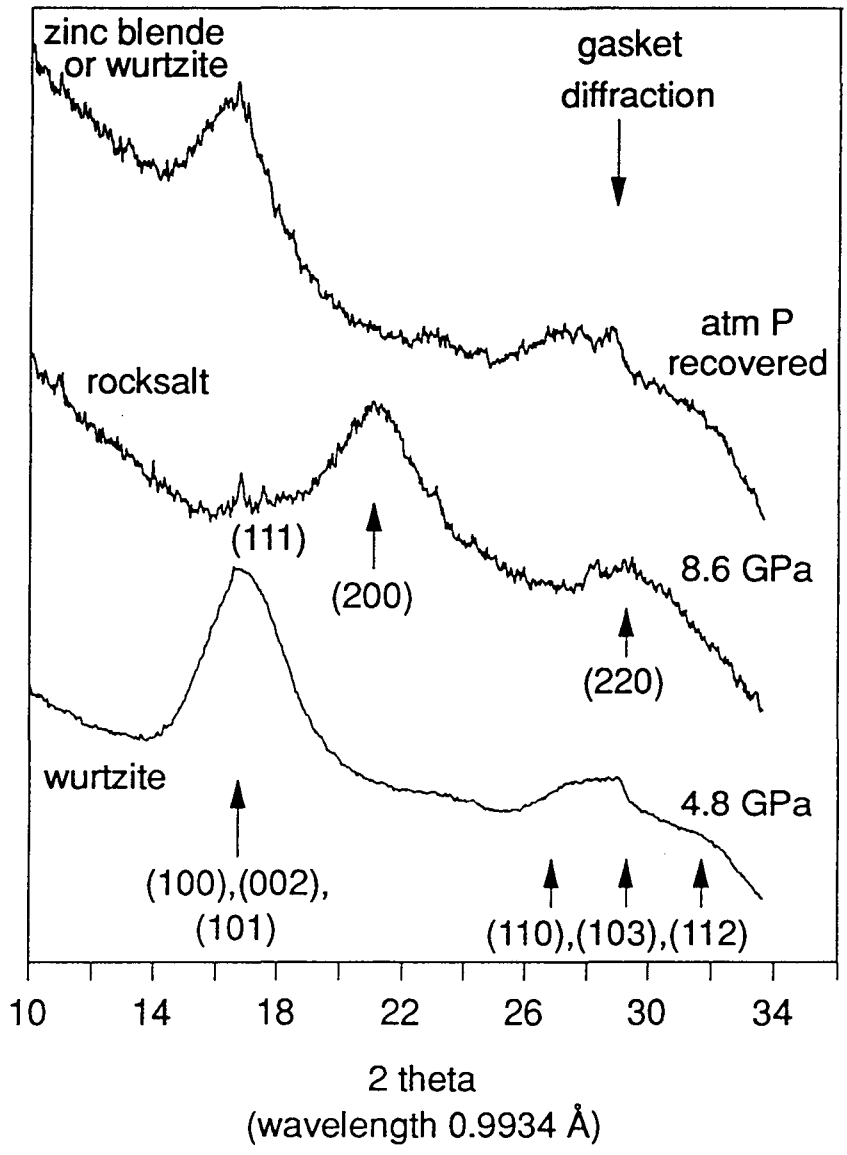

Figure 4.8: High pressure X-ray diffraction data obtained on 1.9 nm diameter CdSe nanocrystals in the untransformed wurtzite phase, the high pressure rock salt phase, and the recovered tetrahedral phase. Pressures and indexing for both the wurtzite and rock salt phases are indicated on the figure. The arrow pointing down indicates diffraction from the metal gasket of the diamond cell. The data shows no increase in domain size upon multiple transitions, and indicates that results obtained on 4.2 nm diameter nanocrystals are generalizable to smaller crystallites.

Optical absorption is used here simply to identify the extent of transformation with varying pressure. High pressure optical absorption data obtained on 14 Å radius CdSe clusters are presented in figure 4.9. The data presented here have been corrected for intensity changes due to deformation of the DAC gasket. These corrections are determined by observing the changes in diameter and thickness of the gasket hole for a typical gasket using an optical microscope and the thin film interference between the diamond surfaces. Volume and thickness changes were related to variations in concentration and path length, and these effects were corrected for using Beer's law. The resulting uncertainty in the correct data was approximately ± 15%. Part (a) shows the shift in the first confined wurtzite phase exciton transition with increasing pressure. The magnitude of this shift is observed to be fairly constant over a wide range of nanocrystal sizes.

Figure 4.9(b) shows the disappearance of the confined absorption peak at the phase transition pressure. The featureless absorption spectrum in the high pressure phase is consistent with a high pressure rock salt structure, which is predicted to be an indirect, narrow gap semiconductor. The optically determined phase transition pressure is observed to correlate well with the structural phase transition pressure determined by high pressure X-ray powder diffraction (better than ± 0.3 GPa). This correlation allows for the routine assessment of phase transition pressures on multiple sizes of nanocrystals using simple optical techniques in our own laboratory. In figure 4.9(c), the confined direct gap absorption is shown to return upon release of pressure. This result is in good agreement with the complete recovery of the tetrahedral phase observed in X-ray diffraction and the observation that the domain size, and thus the confinement size, is not altered. (The zinc blende and wurtzite phases are not distinguishable by their optical absorption spectra.) No significant loss of oscillator strength is observed in the optical spectra upon reverse transition, though some broadening of the peak has occurred. The increased tail to the red in the recovered peak could be due to an elevated number of surface states, formed through the rearrangement of the surface with multiple transitions at room temperature.

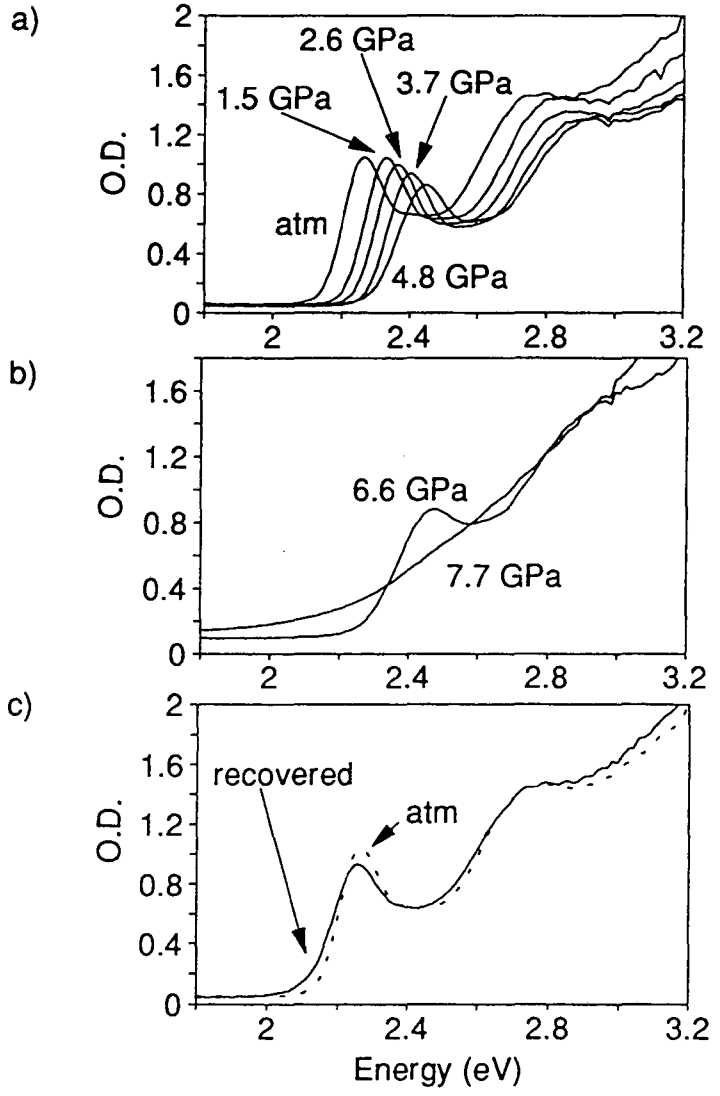

Figure 4.9: High pressure optical absorption obtained on 2.8 nm diameter CdSe nanocrystals at high pressure. Part (a) shows the shift in the wurtzite phase absorption with pressure. Part (b) demonstrates that optical absorption can be used to determine the phase transition pressure. The direct gap wurtzite feature disappears and is replaced by a featureless absorption which can be assigned to the indirect gap of the rock salt phase. Part (c) shows that upon release of pressure, the direct gap features are recovered. All spectra have been normalized for changes in optical density (O.D.) due to deformation in the diamond cell gasket.

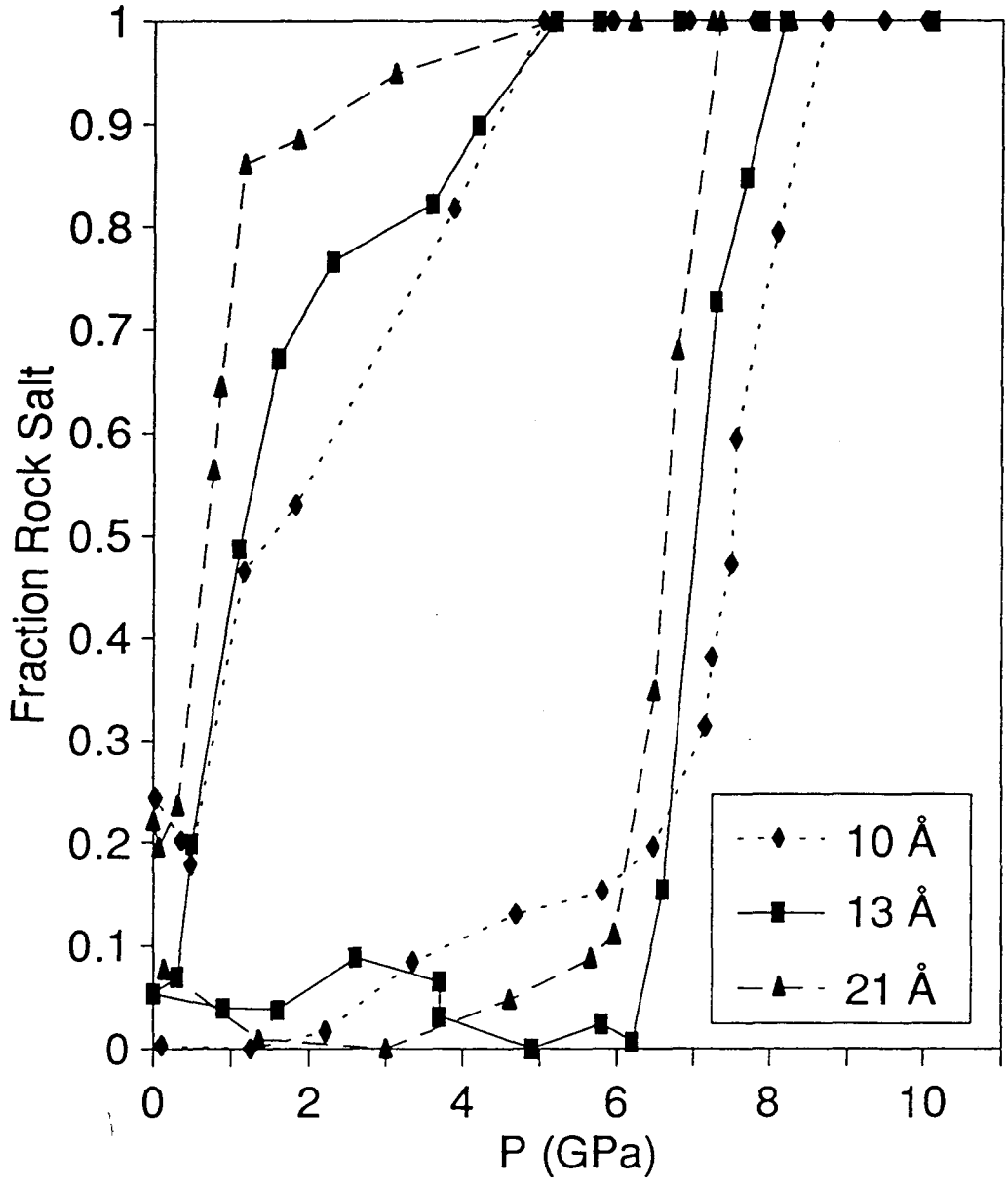

Figure 4.10: Hysteresis curves for 3 sizes of CdSe nanocrystals. Data were obtained by integration of the low pressure phase absorption features shown in figure 4.9. "Fraction Rock Salt" is defined as 1 - (fractional wurtzite phase absorption). Up-stroke and down-stroke phase transition pressures are assigned to the 50% transformed points on these hysteresis curves. "Thermodynamic" transition points are assigned to the midpoints of the curves (average of up-stroke and down-stroke pressures).

The hysteresis observed in figures 4 and 5 can be quantified using optical absorption. Hysteresis curves for 3 sizes of CdSe nanocrystals are presented in figure 4.10. These data are obtained by integrating the lowest energy direct gap transition in both upstroke and recovered samples. As in figure 4.9, these data have also been corrected for changes in O.D. due to deformation of the DAC cell gasket. The "fraction rock salt" value is calculated from the integrated direct gap peak area assuming 100% wurtzite at low pressures and 100% rock salt at very high pressure. The apparent incomplete recovery of some of the samples is probably due to variations in the way gaskets deform with each experimental run. The up and down stroke phase transition pressures are assigned to the 50% transformed point for both increasing and decreasing pressure. A smooth trend with size is observed with smaller clusters transforming to, and recovering from, the rock salt phase at higher pressures than larger clusters. The widths of all of these hysteresis curves are, however, significantly broader than those observed for bulk CdSe in high pressure resistivity measurements. Bulk CdSe shows an upstroke transition near 3 GPa, and a reverse transition at 1 GPa.[7] Some size dependence is observed in the sharpness of the hysteresis curves, particularly for the downstroke transitions: smaller sizes appear to recover more gradually.

The nanocrystal size dependence of the wurtzite to rock salt phase transition pressure can be obtained by assigning the phase transition pressures to the midpoints of the hysteresis curves (average of up-stroke and down-stroke transition pressures). The validity of this assignment is discussed in section 4.4.1.2. The data are presented in figure 4.11. Pressure error bars are a measure of the uncertainty in determining the up-stroke and down-stroke transition pressures; they do not reflect any errors introduced by the choice of the midpoint of the hysteresis curves. The monotonic increase in phase transition pressure with decreasing nanocrystal size suggests a systematic mechanism for this high pressure behavior. The exploration of possible mechanisms for this increase will be the focus of the remainder of this chapter.

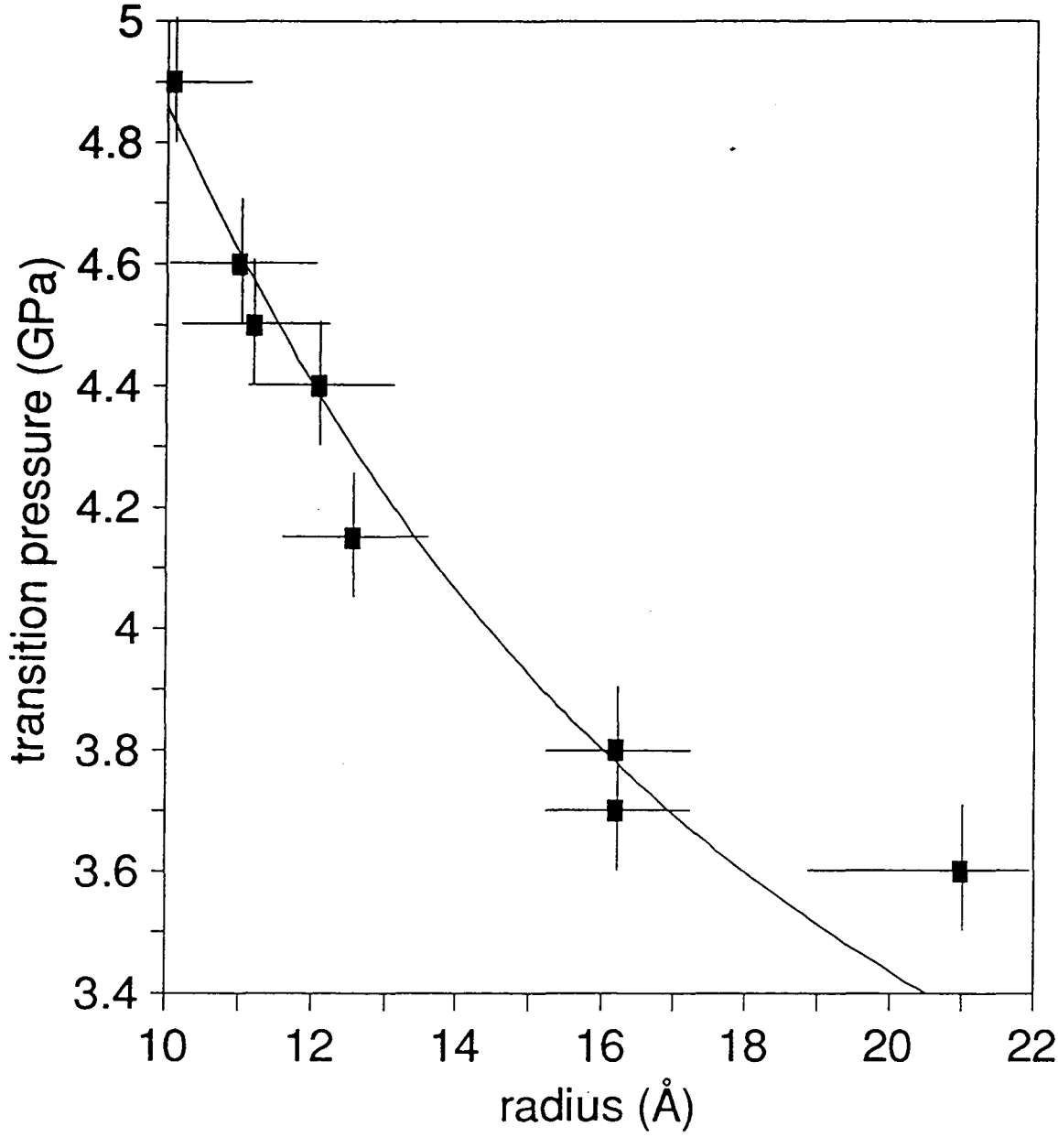

Figure 4.11: Wurtzite to rock salt transformation pressure as a function of CdSe nanocrystal radius. The transition pressures are defined according to figure 4.10. The solid line is a fit to the thermodynamic model explained in parts 1(a) and (b) of the discussion section and the appendix.

4.4 Discussion:

Can pressure induced solid-solid phase transitions be used to understand the relative stability of various solid structures in finite size? We attempt to answer this question in the first section of the discussion (Thermodynamics), where the ideas of surface thermodynamics are used to calculate surface energies in wurtzite and rock salt phase nanocrystals. In the next section (Kinetics), these surface energies are used to postulate the dynamic path followed by atoms during the phase transition. Here we attempt to answer two questions. How do transition kinetics differ in finite size, as compared to the bulk? And what can we learn about the effect of kinetics on solid-solid phase transitions by studying finite systems?

4.4.1 Thermodynamics

4.4.1.1 Thermodynamic arguments

Much understanding of the elevated phase transition pressures observed in these systems can be gained by using thermodynamics to model the transformation.[10,13] The observation that nanocrystal compressibilities, in both the wurtzite and rock salt phases, are almost identical to bulk compressibilities,[10,13] argues that the finite nature of our samples does not result in bonding that is fundamentally different from bulk systems. It is thus permissible to use bulk-like thermodynamic arguments to describe the observed solid-solid phase transitions in these nanocrystals. Bulk thermodynamic expressions, however, need to be modified by surface energy terms to describe our nanophase materials.

In this nanocrystalline system, as in bulk CdSe, we will assume that the wurtzite and zinc blende structures are approximately isoenergetic, and so the recovered wurtzite/zinc blende mixed phase will be treated as thermodynamically equivalent to the original pure wurtzite structure. This assumption is justified by the fact that in CdSe and CdS, zinc blende to rock salt and wurtzite to rock salt phase transitions are observed to occur at close to the same pressures.[7b,23] The thermodynamic arguments, presented in

some detail for a single size of nanocrystal in previous publications,[10,13] are summarized in the appendix and generalized to predict the nanocrystal size dependence of the phase transition pressure.

The internal energies for the high and low pressure phases of the nanocrystals are given by:

$$\begin{aligned} U_{WZ}(S,V) &= TS_{WZ} - PV_{WZ} + \mu_{WZ}N_{WZ} - \gamma_{WZ}A_{WZ} \\ U_{RS}(S,V) &= TS_{RS} - PV_{RS} + \mu_{RS}N_{RS} - \gamma_{RS}A_{RS} \end{aligned} \tag{1}$$

where U, S, and μ are the bulk-like internal energy, entropy, and chemical potential terms, respectively, for each phase, and γ and A are the nanocrystal surface tensions[24] and surface areas for each phase.

The exact form of γ is an important, although not well established issue. However, recent observations of faceted nanocrystals suggest that it may be possible in the future to exactly determine γ_{WZ}.[14] For these experiments, the surface energy in each phase is assumed to vary as

$$\gamma_i = c_{1,i} + \frac{c_{2,i}}{r(\text{Å})^2}. \tag{2}$$

Here the c_1 term corresponds to the bulk surface energy of some hypothetical average low index surface. In the limit of large size, only the c_1 term remains. The c_2 term corresponds to the increase in surface energy due to the curvature of the cluster. For spherical systems (which are a reasonable approximation of our nanocrystals), this term varies at 1/radius^2. The c_2 term can be thought of as the increase in γ caused by steps and edges which must be induced in a low index surface in order to make it curve into a sphere. An analogous formalism with a similar radius dependence is used to describe the effect of curvature on the surface energy of micelles.[25]

Assuming wurtzite/rock salt equilibrium, the expressions for U_{WZ} and U_{RS} in equation 1 can be combined. Thermodynamic relations can then be used to re-express equation 1 in terms of phase transition pressures, compressibilities, and surface energies,

Physical Constants	wurtzite	rock salt
B_o (GPa)	37 ± 5	74 ± 2
B_o'	11 ± 3	
V_o (m^3)	$(5.62 \pm 0.01) \times 10^{-29}$	$(4.36 \pm 0.04) \times 10^{-29}$
c_1 (N/m)	0.34 ± 0.07	0.63 ± 0.16
c_2 (N/m)($Å^2$)	84 ± 16	83 ± 20

Table 4.1: Physical constants used in thermodynamic calculations. Here B_o is the Bulk Modulus, B_o' is the derivative with the Bulk Modulus with respect to pressure, and V_o is the primitive unit cell volume at atmospheric pressure. The c_1 and c_2 terms are used to calculate the surface energy in a nanocrystal, as defined in equation 2. They are the flat surface and curvature terms, respectively. All of the constants are determined independently, except for $c_{1,RS}$ and $c_{2,RS}$, which are obtained by a fit to the size dependent phase transition data.

most of which are experimentally determinable (table 4.1). The details of this process are presented in the appendix. The goal is to compare phase transition data, collected on a variety of nanocrystal sizes, with this thermodynamic model. This process can be used to understand the nanocrystal size dependence of the phase transition pressure, and to calculate nanocrystal surface energies in the rock salt phase.

This thermodynamic model can, however, be explained on a more intuitive level by considering the energy-volume plane[26,10] (figure 4.12). In the formalism of the appendix, an energy-volume curve can be drawn for each phase of CdSe. Theoretically, one should plot the Helmholtz energy, A, versus volume. Because we have chosen to ignore entropy effects, however (see appendix), we are actually plotting the internal energy, U, versus volume. On this plane, pressures are represented by straight lines of a given slope ($-dU/dV = P$). The bulk rock salt curve is observed to be offset from the bulk wurtzite curve to higher energy and smaller volume. A line which corresponds to the bulk phase transition pressure of 2.0 GPa can be drawn tangent to these two curves. The wurtzite phase curve for any single size of nanocrystal is offset from the bulk wurtzite curve to higher energy because of the surface energy, and to slightly smaller volume because of a lattice contraction caused by this surface energy. Figure 4.12 shows these curves for bulk CdSe and 3 sizes of nanocrystals. The surface energy offset and the lattice contraction vary with crystallite size, with the smallest nanocrystals offset to the highest energy and smallest volume. The experimentally observed elevation in phase transition pressure with decreasing nanocrystal size can be simply understood by realizing that the surface energy in the rock salt phase must be higher than in the wurtzite phase. As the nanocrystal size decreases, the slope of the line needed to connect the rock salt and wurtzite curves increases, and thus the phase transition pressure increases. The fact that the nanocrystal curves in the wurtzite and rock salt phases are offset to both higher energy and smaller size, however, complicates the mathematical description of this relatively simple effect,

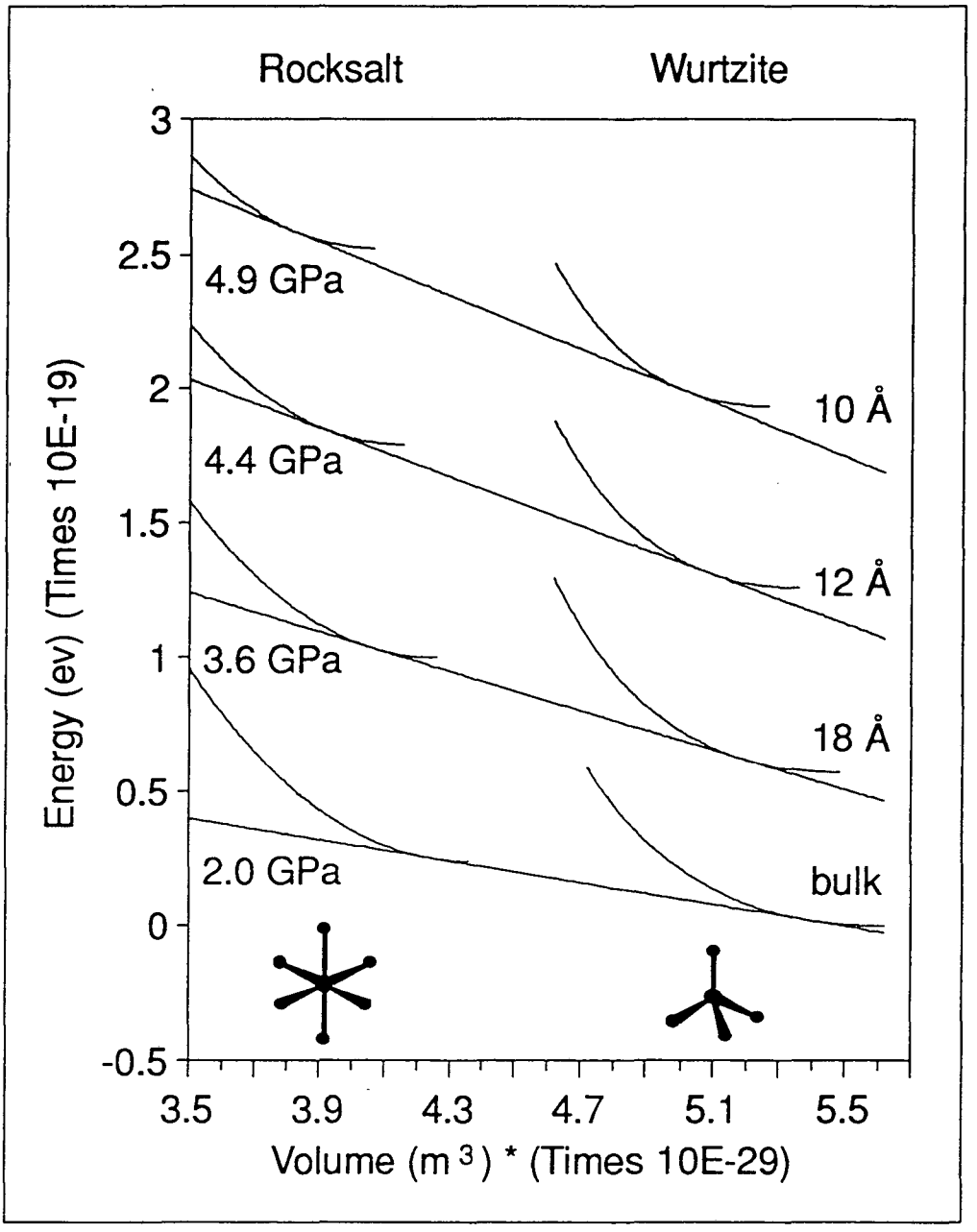

Figure 4.12: Energy volume curves for bulk CdSe and three sizes of CdSe nanocrystals in both the wurtzite and the rock salt phases. Nanocrystal curves are offset with respect to the bulk due to the surface energy in the nanocrystals. The offset of the rock salt curves with respect to the wurtzite curves determines the phase transition pressure. Transition pressures and nanocrystal sizes are indicated on the figure.

and requires the more complex description presented in the appendix to actually compare theory and experimental data.

4.4.1.2 Comparison to data

The equations presented in the appendix can be combined to define an equilibrium equation that is a function of P_T, r_{WZ}, $c_{1,WZ}$, $c_{2,WZ}$, $c_{1,RS}$, and $c_{2,RS}$. Here P_T is the measured phase transition pressure, r_{WZ} is the wurtzite nanocrystal radius, and the c_1 and c_2 terms are the flat surface and curvature terms, respectively, used to define the nanocrystal surface energy in equation 2. The values of $c_{1,WZ}$ and $c_{2,WZ}$ can be determined experimentally from the size dependence of the lattice contraction at atmospheric pressure (figure 4.13) using the Laplace Law (equation 3). This equation relates the observed lattice contraction for a spherical cluster to the surface tension (γ) through the concept of a surface pressure (P_S).[27]

$$P_S = \frac{2 \cdot \gamma(r)}{r} = \frac{\Delta a}{a} \cdot 3B_o. \qquad (3)$$

Here r is the nanocrystal radius, a is the lattice constant, and B_O is the bulk modulus. Equation 3 is only rigorously correct for a completely homogeneous, spherical system with no surface structure, like a liquid droplet. The equation has been applied to nanocrystalline solids in the past, however, with some success.[28] With some hesitation, we will use this formalism to calculate a wurtzite phase surface energy. The data in figure 4.13 are fit with a $1/r + (1/r)^3$ dependence, obtained by substitution of equation 2 into equation 3. Good agreement is observed between the lattice contraction calculated from the wurtzite (112), (110), and (103) diffraction peaks. The resulting values are $c_{1,WZ} = 0.34 \pm 0.07$ and $c_{2,WZ} = 84 \pm 16$. The value of 0.34 N/m for the bulk surface energy term is close to the value for a zinc blende CdSe (111) single crystal surface of 0.55 N/m.[29] The difference could be a function of surface passivation by bound organic ligands and any reconstruction that may occur on the nanocrystal surface.

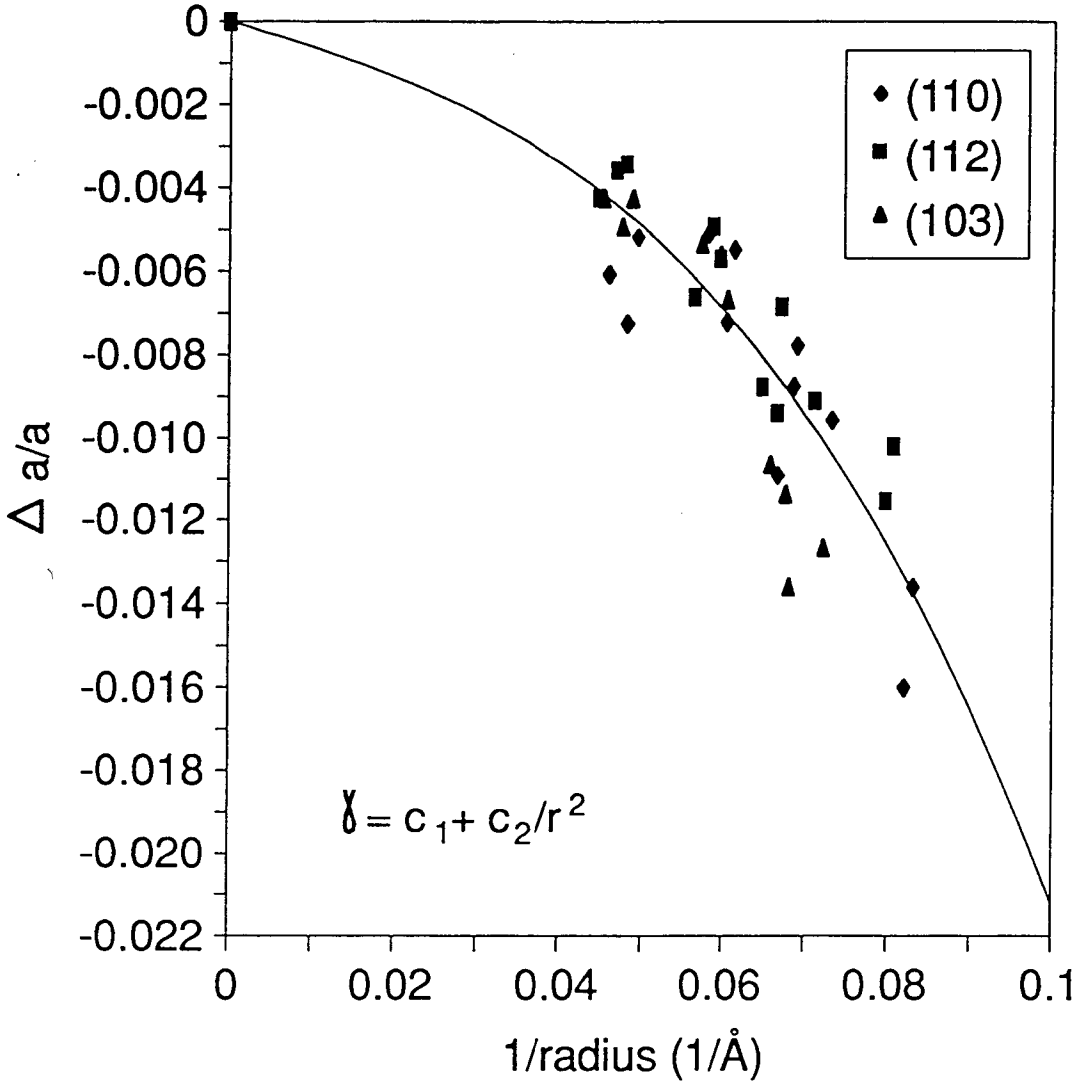

Figure 4.13: Fractional change in CdSe lattice constant at atmospheric pressure, plotted against inverse nanocrystal radius. The data is fit with an $a_1/r + a_2/r^3$ dependence, which can be used in combination with the Laplace Law to calculate an average surface tension for the wurtzite phase nanocrystals (see text). The functional form for the surface tension is shown on the figure, and is numerically equal to $\gamma_{WZ} = 0.34 + 84/r(\text{Å})^2$ (N/m), where the first term can be related to a bulk surface energy, and the second term is the elevation in γ due to the curvature of the nanocrystal. Square, diamond, and triangle markers represent data obtained using the (112), (110), and (103) diffraction peaks, respectively.

This type of model for the nanocrystal surface has consequences for our picture of thermodynamics in nanocrystals. By assuming an infinitely thin interface layer (frequently termed a 'Gibbs dividing surface') we are not allowing for strain equilibrium between the nanocrystal, a macroscopically thick interface layer, and the pressure medium. This strain equilibrium can, in principle, modify the applied pressure on the nanocrystal so that the pressure measured in the diamond cell chamber differs from that experienced by the interior of a nanocrystal. While these effects are likely present in our experiment to some degree, good agreement between bulk CdSe and nanocrystal compressibilities[13] and between bulk CdS and nanocrystal pressure Raman shifts[10] argues that the interface layer is not significantly perturbing the applied pressure. At the structural transition, the role of the interface is likely to be more significant. Section 4.4.2.4 includes a discussion of how surface strain dissipation can contribute to the observed nanocrystal hysteresis.

While the thermodynamic expressions presented in the appendix still can not be solved analytically for either $c_{1,RS}$ or $c_{2,RS}$ as a function of P_T and r_{WZ}, the equations can be compared to experimental data on $P_T(r_{WZ})$ and the values of $c_{1,RS}$ and $c_{2,RS}$ varied to maximize the agreement between the experiment and the model. Experimental values for the phase transition pressure in both bulk CdSe and CdSe nanocrystals are obtained by averaging the upstroke and downstroke transition pressures. Assigning the thermodynamic transition pressure in this way assumes symmetric contributions (over- versus under-pressing) to the thermodynamic driving force for transition ($\Delta V_{trans} \cdot [P_{trans,thermo} - P_{trans,exp}]$). For transitions which may involve mechanical instability, like this one, the assumption of symmetry in the driving force is not rigorously correct. Additionally, the assumption of symmetric hysteresis curves does not allow for the possibility of different transformation mechanisms on the forward and reverse transitions (homogeneous versus heterogeneous nucleation, for example). Lacking further information, it is the only reasonable approximation.[30] We note, however, that the errors

cited for the rock salt phase surface energy calculated from the size dependent phase transition data reflect only the scatter in the data and not any systematic error introduced by our choice of the midpoints of the hysteresis curves.

The best fit to this thermodynamic model is presented in figure 4.11, with the symbols corresponding to the data and the line representing a numerical solution to the equation presented in the appendix. The rock salt phase surface energy which produced this line is given by

$$\gamma_{RS} = (0.63 \pm 0.16) + \frac{(83 \pm 20)}{r(\text{Å})^2} (\text{N/m}) \qquad (4)$$

The observation that the c_2 terms are approximately equal in both the rock salt and wurtzite phases ($c_{2,RS}$ = 83, $c_{2,WZ}$ = 84) is consistent with our assignment that this terms stems from the nanocrystal curvature. The increase in the c_1, or the bulk surface energy term in the rock salt phase is, however, less intuitive. Simple calculations performed by B.N. Oshcherin[31] based only on the number of dangling bonds, the bond length, and the compressibility, predict the opposite trend. A value of γ_{ZB}(calc) = 0.805 N/m is reported for the lowest index, (111), bulk CdSe zinc blende surface, while the analogous value for the lowest index (100) bulk CdSe rock salt surface is γ_{RS}(calc) = 0.69 N/m. While experimental studies on bulk zinc blende surfaces suggest that these calculations overestimate the real value [($\gamma_{ZB,(111)}$ = 0.55 N/m (Ref. 29)], the trend with structure is probably meaningful, and our observed deviation from it needs to be explained. This topic will be addressed in the next section on kinetic effects in phase transitions.

4.4.2 Kinetics

Thermodynamics has proven to be useful in understanding the elevation in structural transformation pressure observed in CdSe nanocrystals. The anomalously high value calculated for γ_{RS} suggests that equilibrium thermodynamics are not, however,

painting a complete picture of this transformation. Kinetic, or path related effects need to be considered as well.

4.4.2.1 The barrier to transition in bulk CdSe

In the laboratory, first order solid-solid transformations are usually observed to occur over a range of pressures. In addition, large differences are often observed between upstroke and downstroke transition pressures. These observations all point to the existence of a barrier to transition and to the fact that the temperature at which these experiments are performed is low in comparison to the height of this transition barrier. An understanding of the kinetics is thus required to correctly apply thermodynamics to this study.

In high pressure studies on bulk semiconductors, the barrier to transition is usually explained in terms of nucleation dynamics.[32,33] Within this premise, the limiting step to transition is the formation of a stable nucleus of the rock salt phase within the extended wurtzite lattice (figure 4.14). This nucleus is destabilized by the rock salt/wurtzite interface energy and thus is unstable right at the thermodynamic transition pressure. At higher pressures, the rock salt nucleus is stabilized by its internal energy, and at some pressure it overcomes the interface energy and the transition occurs. On the reverse transition, the wurtzite phase nucleus is destabilized by the same rock salt/wurtzite interface energy, and so the pressure must be lowered an equivalent amount beyond the equilibrium transition pressure before the reverse transition is observed. This formalism thus predicts that the thermodynamic transition pressure will be near the average of the upstroke and downstroke transition pressure. The broadening of the diffraction peaks with successive phase transitions observed in figure 4.2 for bulk CdSe is indicative of this type of mechanism where multiple nucleation sites cause a decrease in crystalline domain size upon transition.

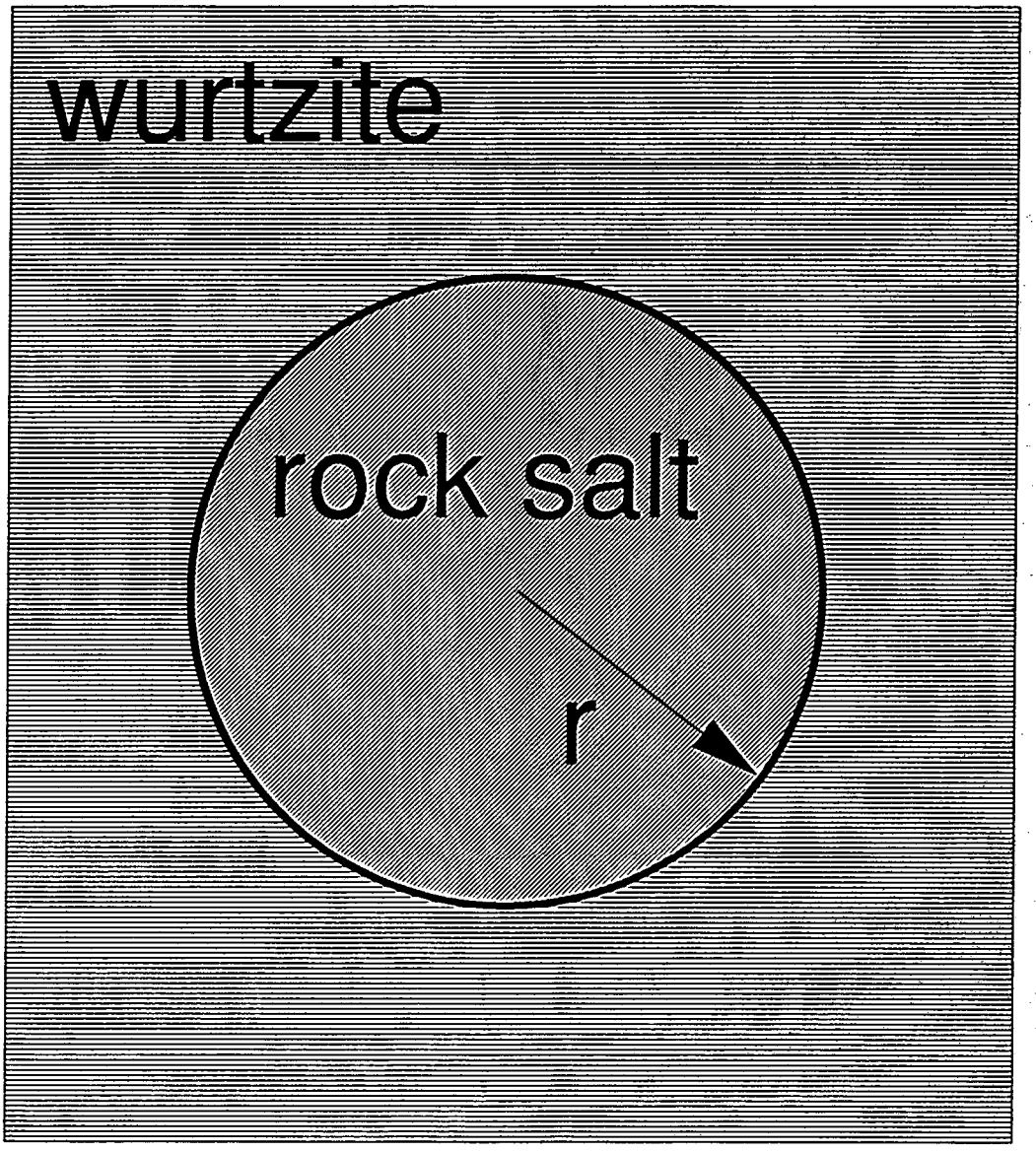

Figure 4.14: Schematic representation of a rock salt nucleation domain in a bulk wurtzite lattice. The rock salt domain is destabilized by the rock salt/wurtzite interface energy. The system must be over-pressurized (upstroke) or under pressurized (downstroke) to overcome this destabilization.

For the case of nanocrystals however, the observation that the domain size does not significantly decrease after multiple transitions argues that this type of behavior is not occurring. From the data, we can make the conclusion that multiple stable nuclei do not coexist in the same nanocrystal. As the sizes of critical nuclei and the interactions between them are not generally known in bulk systems, these results help to place a lower limit on the bulk CdSe stable nucleus size. Further experiments, related to this one, could be used to gain a more accurate idea of the forces between critical nuclei: The nanocrystal size could be increased and the experiment repeated until the domain size was no longer preserved upon transition. Work is currently underway to study phase transitions in this intermediate size range.

4.4.2.2 Path effects

The existence of broad hysteresis curves, (figure 4.10) suggest that in our nanocrystals, and possibly in bulk systems as well, there are barriers to transition other than those associated with nucleation. In order to understand these barriers, though, we must first understand the microscopic process which leads to the transformation. In bulk systems, these atomic details are usually ignored. In a nanocrystal containing only 200 atoms, however, the motions of individual atoms must affect the dynamics of the total transformation.

While the exact nature of these motions is not well understood, Burdett has shown that much insight can be gained by using symmetry and modeling the rock salt to wurtzite transition as a Peierl's distortion.[34] In the undistorted rock salt structure, every atom is bonded to 6 other symmetry identical atoms. The system is a narrow gap semiconductor with a high electronic energy. By lengthening (i.e. breaking) two of the six bonds, and shortening the other 4, it is possible to open the band gap and decrease the electronic energy. The motion is analogous to the one-dimensional Peierl's bond alternation observed in poly-acetylene.[35] The rock salt to wurtzite transition in CdSe consists of this

type of bond alternation in two orthogonal directions, and no distortion in the third direction. In both CdSe and poly-acetylene, bond alternation opens up the band gap and reduces the overall electronic energy of the system. Under pressure, however, the total volume of the system can be reduced by reversing the Peierl's distortion. Consistent with the observation in poly-acetylene,[36] the effect of pressure is to move the system toward its higher symmetry state.

This leads to the following possibility for the rock salt to wurtzite transition path: The motion can be pictured as the three-dimensional analogue of the square net to graphite transition.[37] Given a repeating pattern of 2 x 3 rectangles, the system can distort by moving the central atoms apart to form a hexagon. In three dimensions, this distortion would be accompanied by appropriate motions in the z-direction to create cyclo-hexane type boats or chairs. If the final structure is zinc blende, only chair structures will form. If the final structure is wurtzite, both chairs and boats will form. The barrier to this motion is a function of the loss of octahedral bonding as the central atoms move apart, balanced against the gain in covalent sp^3 bonds as the system approaches a tetrahedral geometry. Another way to picture this motion is presented in figure 4.15 for the rock salt to wurtzite transition. Shown in part (a) are the 2 x 3 rectangles that will become 6 membered ring chairs in (001) planes of the wurtzite structure. The rectangles are highlighted in the rock salt cube, and the transition motions are shown for the conversion of one rectangle to a chair structure. Shown in part (b) are right angle segments of the rock salt structure that can open to form boat structures in the wurtzite phase. Finally, shown in part (c) are 2 x 3 rectangles that open and fold to form more wurtzite boat structures. Note that a consistent set of motions is required for all of these distortions.

Although there is no direct experimental evidence for this path, it is consistent with Burdett's theories on Peierl's distortions. Additional support is found in the observation that the acoustic shear modes in these tetrahedral semiconductors soften, that is their frequency decreases, with increasing pressure.[38] These shear modes involve atomic

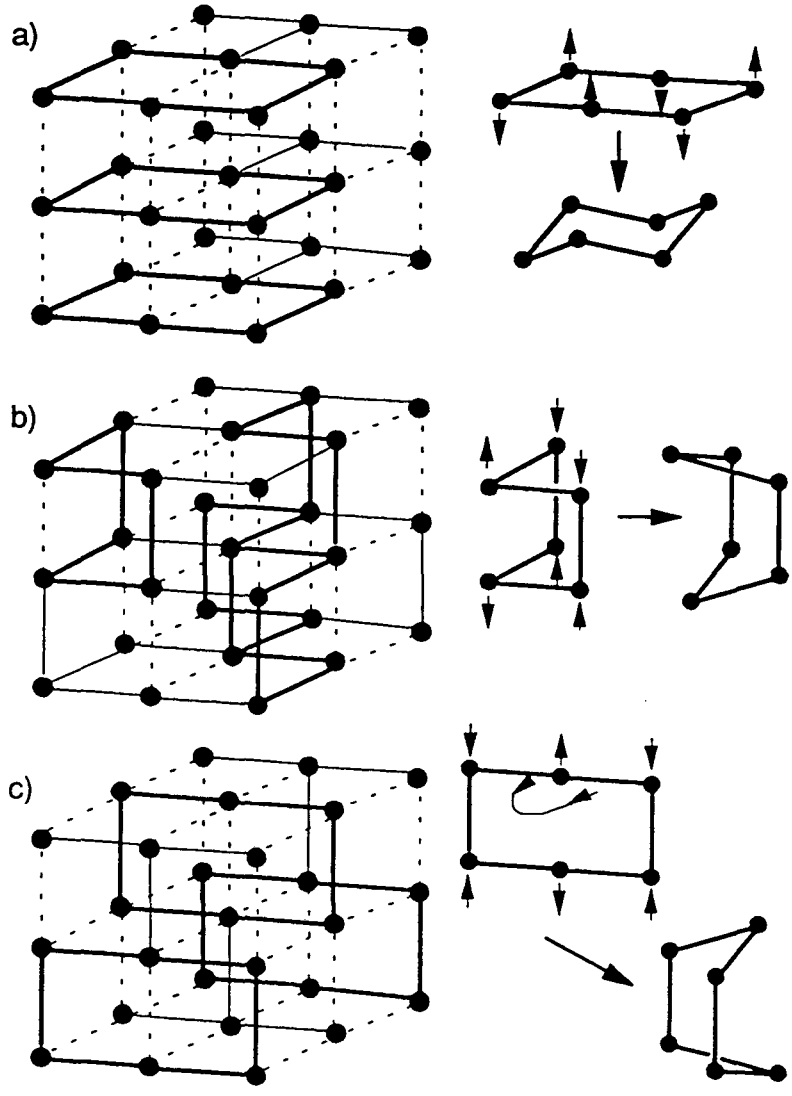

Figure 4.15: Schematic representation of a possible mode for the rock salt to wurtzite transformation. (a) The middle two atoms of a 2 x 3 rectangle move apart and the plane puckers to produce a six membered ring "chair" type structure in a wurtzite (001) plane. (b) In dimensions orthogonal to (a), right angle pieces of the wurtzite structure form six membered ring "boat" type structure. (c) Also orthogonal to (a), 2 x 3 rectangles distort into wurtzite "boat" type structures. In all cases, 6 membered ring structures are highlighted in the rock salt lattice. These rings are then redrawn with the transition motions and final structures indicated.

motions related to those described above (mostly bond angle changes[39]). The mode softening is caused by stabilization of the rock salt structure with increasing pressure. This lowers the barrier to transition and produces a broadening of the transition mode potential. It is important to note, however, that while these shear modes do soften with pressure, they do not appear to extrapolate to near zero frequency at the phase transition pressure,[40] as has been observed in second order phase transitions.[41] This implies that in moving along the transition path, there is still some finite barrier to transition, even at the phase transition pressure.

4.4.2.3 Effect on the surface

The concept of a transition mode or path is equivalent to the statement that the connectivity of the atoms does not completely change during a transition. As the shape of the unit cell changes upon transition, this connectivity necessitates a change in the overall shape of the crystallite. This effect is not easily observed in the bulk because the fragmentation of large crystals due to nucleation in multiple spots masks any local shape change. In nanocrystals, however, where entire crystallites should transform coherently, a path driven macroscopic shape change would produce detectable results. If we assume that, as synthesized at high temperature, nanocrystals have dominantly low index surfaces, the effect of the path presented in section 4.4.2.2 would be to convert a spherical wurtzite nanocrystal with a low surface energy into a prolate ellipsoid in the rock salt phase with a much higher surface energy.

An example of this is illustrated in figure 4.16. A two-dimensional cartoon of a wurtzite (001) plane is presented in part (a). The real (001) plane has alternate atoms displaced above and below the plane of the page. The "surfaces" of the plane are all low index, either the degenerate (100) or $(1\bar{1}0)$, and have only one dangling bond per atom. As described above, this structure can convert to a rock salt phase when atoms from across a ring come together to form a bond. This process produces a rock salt phase

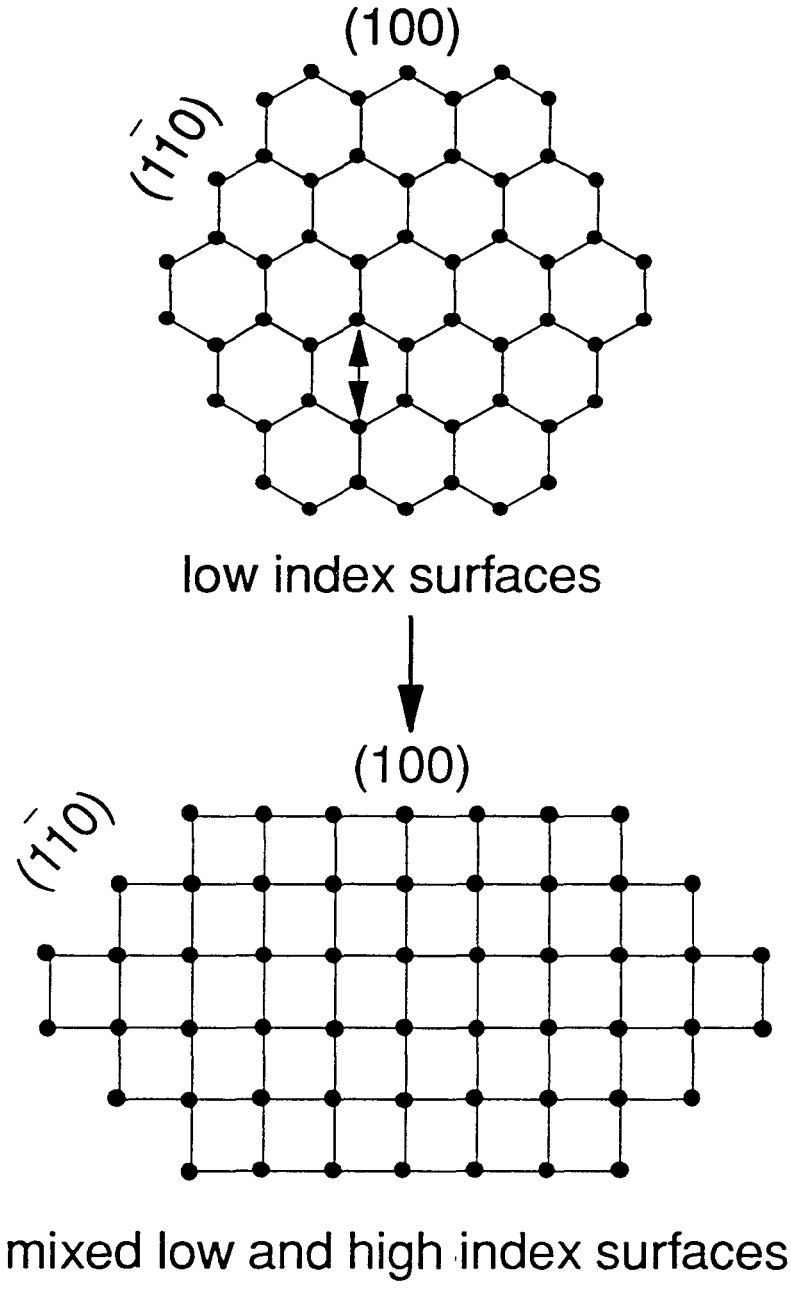

Figure 4.16: Transformation of a wurtzite phase nanocrystal to a rock salt phase nanocrystal following a 2-dimensional analogy to the mode presented in figure 4.15a. The wurtzite nanocrystal contains only low index "surfaces", while the rock salt crystallite formed by motion along the transition path contains a large fraction of high index "surfaces".

crystallite with (100) and (110) surfaces. In the rock salt structure, these surfaces are not degenerate. The (100) surface has only one dangling bond per atom and is thus low energy. The (110) surface, in contrast, has two dangling bonds per atom and constitutes a much higher energy surface.

Figure 4.17 shows an example of this transition path applied to a 3-dimensional nanocrystal. The starting wurtzite shape is the one believed to be a typical equilibrium structure, based on TEM and Raman depolarization measurements.[14] The most striking feature of the transformation is the distinctive macroscopic shape change: The crystallite has gone from spherical to oblate. Energetically more important, however, is the fact that the newly formed rock salt crystallite has a greater number of coordinatively unsaturated surface bonds. These unsaturated bonds significantly increase the surface energy in the rock salt phase, relative to the wurtzite phase. This results in the measured elevation in phase transition pressure observed in our nanocrystals.

The change in surface energy upon transformation can be emphasized numerically by considering a very small nanocrystal, containing only 90 atoms. In the wurtzite phase of such a nanocrystal, the whole system averages 80% coordinated. That is, assuming the ideal coordination is 4, the average coordination is 3.2. This is made up of a combination of 4, 3, and 2 coordinate atoms which lie both in the interior and on the surface of the nanocrystal. When the system is moved along the proposed transition path to the rock salt structure, however, the average coordination decreases to 72%, based on an ideal coordination of 6. These changes in coordination arise because the surface structure is determined by the symmetry allowed motions of interior atoms.

Because the wurtzite structure has low symmetry in comparison to the rock salt structure, it is likely that the transformation depicted in figure 4.17 is unique: bond alternation (alternate bonds coming together from across a six membered ring) will always take place along the c axis and one of the degenerate a or b axes. Because of the high symmetry of the rock salt structure, however, this is not true on the reverse transition.

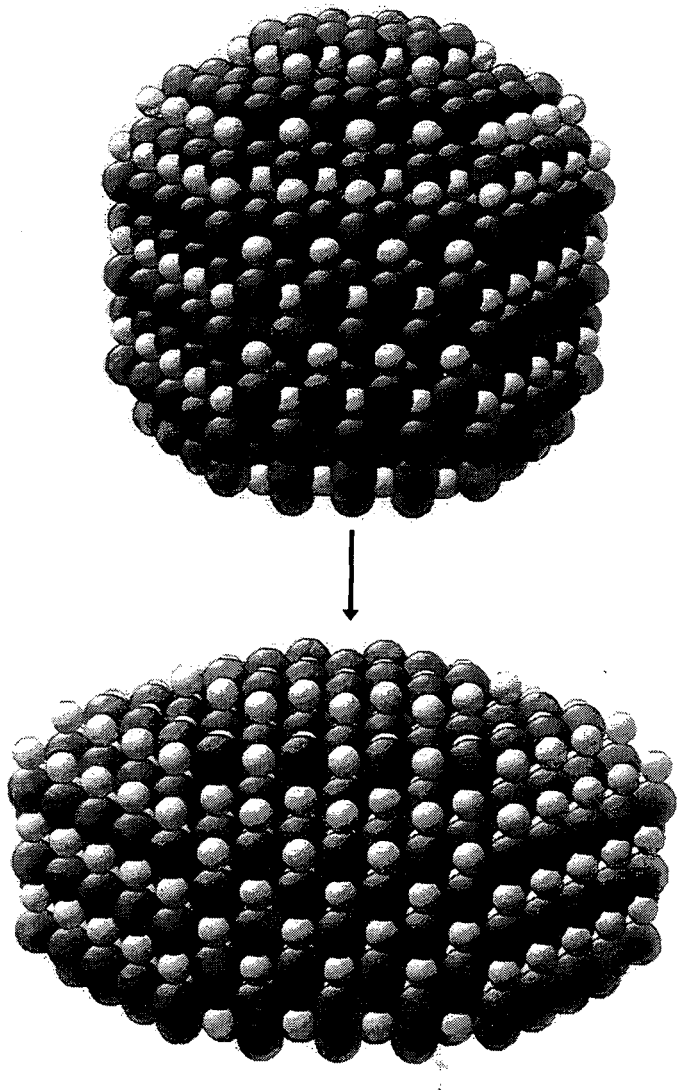

Figure 4.17: The same transformation as figure 4.16, presented in 3 dimensions. The nanocrystal transforms from spherical to prolate. The transformation is accompanied by the formation of many high index surfaces in the rock salt phase. For the wurtzite phase nanocrystal, the c axis is vertical and in the plane of the page. The a and b axes form a 120° angle in the horizontal plane perpendicular to the page. In the rock salt phase, the a, b, and c axes are orthogonal and degenerate.

The rock salt structure is three-fold degenerate and thus bond alternation (alternate bonds breaking to form six membered rings) can occur in any two of the three directions in going from rock salt to either zinc blende or wurtzite. The inhomogeneity introduced on this reverse transition is, however, reduced by the fact that transitions to tetrahedral structures with low surface energies should be accessible at higher pressures and thus should dominate.

The anomalously high rock salt phase surface energy required to fit the size dependent phase transition data is thus a real experimental consequence of the macroscopic shape change upon transformation. While this effect can not be observed in bulk CdSe, it is probably occurring. In this way, size dependent studies of phase transitions in the nanometer regime provide information about both nanocrystal and bulk transformation kinetics. Because the surface energy in a nanocrystal makes a major contribution to the total free energy of the system, the transition path can actually determine the final state of the system. In a true equilibrium experiment, where path effects would not be important, the rock salt surface energy would probably lie below the wurtzite, and a depression of the phase transition pressure would be observed. Instead, path effects lead to higher surface energies in the rock salt phase and cause the experimentally observed elevation in phase transition pressure.

4.4.2.4 Hysteresis

The large hysteresis observed in figure 4.10 indicates the existence of a barrier to transition. Forward and reverse transitions do not occur at the thermodynamic transition point because extra energy must be supplied to get the system over the transition barrier. In this section we discuss the nature of this barrier and the effect of changing temperature on these transitions.

A first question is: What is the origin of this barrier? While the actual microscopic motions of interior atoms surely play a role, the hysteresis observed in CdSe nanocrystals is much greater than that observed in bulk CdSe.[7] This suggests an additional nanocrystal specific barrier to transition. A useful body of literature to help in answering this question concerns martensitic transformations. These are temperature or pressure induced solid-solid phase transitions that can be described in terms of a soft mode picture, and which are marked by hysteresis.[42] One key feature of these transitions is that the extent of transformation can be described in terms of state variables.[43] That is, at a given T and P beyond the equilibrium transition point, the extent of transformation will be a function of T and P, and not of the time spent at those conditions. This allows the application of quasi-equilibrium thermodynamics to describe the under- or over-pressurized system. In this formalism, the width of the hysteresis curve (i.e., the difference between $P_{trans,up}$ and $P_{trans,down}$) is assigned to non-reversible, non-PV work. Microscopically, this hysteresis in Martensitic transformations can be related to inelastic atomic rearrangements.[43] The motions of interior atoms in our nanocrystals should be dominantly elastic and the energy stored in the rock salt lattice should be recoverable upon release of pressure. This leaves the non-reversible, inelastic rearrangement of surface atoms to explain the extra width of the nanocrystal hysteresis. The rearrangements could include surface reconstruction, or the breaking of surface Cd-pyridine, CdO_x, or SeO_x bonds to accommodate the new interior structure.

For clarity, it should be emphasized that there are two separate concepts in surface energy being presented here. The notion of a path driven increase in surface energy (section 4.4.2.3) is a thermodynamic idea, and corresponds to a reversible storage of energy in the lattice. This value is thus calculated from the midpoint of the hysteresis curves. The notion of non-reversible surface atom rearrangements is a non-equilibrium idea, and relates only to the width of the hysteresis curves, not the center point.

One experimental difficulty with this picture is that the recovered tetrahedral phase surface energy is not required to be exactly the same as the original wurtzite surface energy. If this recovered surface energy were higher than the original wurtzite phase surface energy (a physically reasonable assumption), some of the driving force for the reverse transition would be removed. In this case, the apparent width of the hysteresis curves would be an overestimate of the real situation. The additional width could be caused by the fact that the upstroke "thermodynamic" transition point differed from the downstroke "thermodynamic" transition point. While this idea is not unreasonable or inconsistent with the data, there is no practical way to incorporate it into the analysis of the data. Absent surface-structure specific high pressure data, we will continue to use the simplifying assumption that the surface energy in the recovered phase is the same as in the untransformed nanocrystals.

Another potential explanation for the broad width of the hysteresis curves observed in our nanocrystal transformations can be found in the work of David Turnbull.[44] Turnbull was extensively involved in developing nucleation theories of phase changes of all kinds. The work of most relevance centers around crystallization (from pure liquids[45] and from solution[46]) in "small" (5-50 μm) droplets. These studies showed that the transition hysteresis could be dramatically increased by finely dividing the solution into droplets. The "isolation theory" developed from these experiments states that foreign material is usually involved in catalysis of phase changes. When the material is finely divided, however, most droplets become free of foreign material, and so homogeneous (as opposed to heterogeneous or catalyzed) nucleation temperatures can be measured.

In applying this theory to transformations in nanocrystals, however, one key point needs to be considered. Nanocrystals have extensive surfaces with surface to volume ratios approximately eight orders of magnitude large than those present in the Turnbull droplet experiments. Will this surface serve as a nucleation site for solid-solid phase

changes? It has been observed in a variety of studies[44] that grain boundaries and impurities can act as nucleation sites for solid-solid phase transitions. A grain boundary will act as a nucleation size if

$$\gamma_{I-II} > \gamma_{II-g} - \gamma_{I-g} \tag{5}$$

where $\gamma_{I\text{-}II}$ is the phase I - phase II homogeneous interfacial tension (section 4.4.2.1), $\gamma_{II\text{-}g}$ is the phase II - grain boundary interfacial tension, and $\gamma_{I\text{-}g}$ is the phase I - grain boundary interfacial tension. By analogy, for the case of wurtzite phase nanocrystals transforming to the rock salt phase, the nanocrystal surface will act as a nucleation site if

$$\gamma_{WZ-RS} > \gamma_{RS} - \gamma_{WZ} \tag{6}$$

where $\gamma_{WZ\text{-}RS}$ is the homogeneous wurtzite/rock salt interface tension, and γ_{WZ} and γ_{RS} are the nanocrystal wurtzite and rock salt phase surface tensions.

Tetrahedral/octahedral interface energies in semiconductors are generally estimated to be on the same order as the nanocrystal surface energies we have calculated.[33] As the difference in the wurtzite and rock salt phase surface energies that we have calculated is quite large and no exact measure of $\gamma_{WZ\text{-}RS}$ is available, the possibility that the nanocrystal surface does not serve as an up-stroke nucleation site can not be ruled out. In this situation, the broad hysteresis widths could be ascribed to super-pressing of the crystallites caused by a lack of heterogeneous nucleation sites. Supporting this idea, these nanocrystal have been shown to be free of interior defects both by direct TEM observation and by comparison of TEM/SAXS sizes with X-ray diffraction line widths. Within this hypothesis, the hysteresis widths should thus reflect the homogeneous nucleation energies of CdSe, and all nanocrystals should exhibit the same homogeneous hysteresis width (in reasonable agreement with the results presented in figure 4.10). This width should also be significantly broader than that observed in bulk transformations (also in agreement with previous data[7]).

In applying equation equations 5 and 6 to the reverse transition (rock salt to wurtzite), one must conclude (assuming $\gamma_{WZ\text{-}RS} = \gamma_{RS\text{-}WZ} > 0$) that if the up-stroke

transition goes by homogeneous nucleation, the down-stroke transition must be surface catalyzed or heterogeneous nucleation. This result has significant implications for interpretation of the hysteresis curves (figure 4.10): If super-pressing effects are seen only in the upstroke transition pressure, the "thermodynamic" transition pressure should not be located at the middle of the hysteresis curves (where we have assigned it). Instead, it should be much closer to the down-stroke transition pressure. While this result would not effect the existence of a nanocrystal size dependence to the phase transition pressure (seen in figure 4.10 as a shift of the entire hysteresis curve to higher pressure with decreasing nanocrystal size) it would reduce the absolute magnitude of the elevation with size. This reduced elevation would in turn result in a lower calculated value of γ_{RS}. We note, however, that if too much asymmetry in the hysteresis curves is postulated, the resulting value of γ_{RS} will be so close to the value of γ_{WZ} that the condition for homogeneous nucleation on the up-stroke transition (stated in equation 6) will no longer be met. In the limit of heterogeneous nucleation in both the up-stroke and down-stoke transitions, the mid-point remains the most reasonable point to assign to the phase transition pressure.

Another point of interest is to consider the effect of temperature on the hysteresis. At room temperature, the barrier to transition appears be large in comparison to kT. It should be possible, however, to raise the temperature to the point that the barrier height is on the order of kT. In this situation, if the temperature is low enough that diffusion of surface atoms is still slow, little hysteresis would be expected and the observed upstroke transition pressures should correlate well with our measured thermodynamic transition pressure. If, however, the temperature is high enough that the diffusion of surface atoms becomes fast on the time scale of the phase transition, high pressure phase nanocrystals with a true equilibrium, low energy surface could be formed. In this case, the phase transition pressure should decrease to the point determined by the difference in the equilibrium rock salt and wurtzite surface energies. This reasoning suggests that the

experiments presented here should not, in fact, even be called quasi-equilibrium: not only are the nanocrystallites themselves kinetically trapped high energy structures, but the phase transition pressures we have determined are path, and thus temperature dependent quantities.

This result has implications not only for nanocrystals, but also for phase transitions in bulk materials at room temperature. In the first place, the path driven surface and shape effects described above should play an important role in bulk nucleation. As previously discussed, the hysteresis in bulk transitions is believed to stem from an interface energy associated with a nucleus of phase I in bulk phase II (figure 4.14). This interface energy should be strongly affected by the surface structure of the transformed phase I nucleus, and by the shape mismatch between the phase I nucleus and the phase II cavity. These effects are traditionally ignored in nucleation theories of phase transitions.[32,33] A knowledge of these surface and shape effects is required for a full understanding of the role of nucleation in hysteresis. Perhaps more important, however, is the concept that path driven changes in surface energy can affect measured phase transition pressures. In bulk systems which have undergone more than one solid-solid phase transition, the domains can reach the size where surface energies make a significant contribution to the total free energy of the system. In this situation, experimentally determined phase transition pressures at room temperature are not necessarily a good measure of the relative stability of various bulk phases.

The path dependence and hysteresis of the phase transition pressure could, however, be exploited for potential applications. In the high temperature high pressure experiment described previously, the temperature could be slowly reduced while the nanocrystals were still in the high pressure rock salt phase. The result would be the formation of a low energy equilibrium surface in the rock salt phase. In contrast to the present experiment, the effect of this surface would be to stabilize the high pressure phase with respect to the low pressure phase upon release of pressure. Under the right

conditions, it should even be possible to trap CdSe nanocrystals in the rock salt structure at atmospheric pressure and room temperature. Alternatively, surface capping groups and pressure media could be chosen to stabilize the rock salt phase nanocrystals. If wurtzite phase nanocrystals could be dissolved in such a medium, the possibility again exists for recovery of rock salt phase nanocrystals at atmospheric pressure and room temperature after pressurization. This idea is supported by recent results by J.Lin *et al.*[47] who have stabilized cube shaped rock salt phase CdS nanocrystals of 100 nm diameter by growing them in a highly ionic polymer matrix. In this way, surface energies and transition barriers can be used to tune the stable states of matter in the nanometer size regime.

4.5 Conclusions:

In this chapter we have examined the effect of finite size on the high pressure stability of CdSe semiconductor nanocrystals. While the nanocrystals do undergo a wurtzite to rock salt transition that is analogous to that observed in bulk CdSe, it is found that the limited extent of the crystallites affects both the thermodynamics and kinetics of the transition. The basic nature of the transition, determined using high pressure X-ray powder diffraction, shows a clean transition from a wurtzite phase to a rock salt phase, and back to a mixed wurtzite/zinc blende phase with no significant loss of crystalline domain size. The transition in the nanocrystals, however, takes place at pressures much higher than those observed for bulk CdSe.

A thermodynamic analysis of the phase transition pressure allows for the determination of the surface energy in the high pressure phase. This value is found to be $\gamma_{RS} = (0.63 \pm 0.16) + (83 \pm 20)/r(Å)^2$ (N/m), in comparison with a value of $\gamma_{WZ} = (0.34 \pm 0.07) + (84 \pm 16)/r(Å)^2$ (N/m) obtained using the Laplace Law for the low pressure phase. This large rock salt surface energy can be attributed in part to high index surfaces formed at the transition because of the dynamic path atoms must travel to move from one structure to the other. This result suggests that nanocrystal surfaces formed

during solid-solid phase transitions are non-equilibrium, and thus phase transformations of this sort are not well suited for the determination of stable *equilibrium* structures in finite size. As bulk systems approach this size regime, where surface energy terms become an important part of the total free energy, these effects need to be considered.

The transition kinetics are also affected by finite size. Broad hysteresis curves suggest significant barriers to transition in nanocrystals. It appears, however, that nanocrystals may be smaller than the critical nuclei hypothesized to provide the barrier to transition in bulk semiconductors. This result can be used to further understanding of the effect of nucleation in bulk CdSe.

The nanocrystal surface is shown to be important to both the thermodynamics and kinetics of the transformation. The surface energy, whether thermodynamic or the result of a kinetic process, appears to be the dominant factor in determining stable states in finite sized systems. Despite this fact, the basic nature of the transition remains bulk-like. The differences between transformations in finite systems and those in the bulk can be used to understand the evolution of solid-solid phase transitions from the bulk limit into a coherent molecular isomerization. This information can add both to our basic understanding of phase transitions in solids, and to our comprehension of the role of physical size in the stability of a crystallite.

4.6 Appendix:

For the bulk system, the internal energy in the high and low pressure phases is given by:

$$\begin{aligned} U_{WZ}(S,V) &= TS_{WZ} - PV_{WZ} + \mu_{WZ}N_{WZ} \\ U_{RS}(S,V) &= TS_{RS} - PV_{RS} + \mu_{RS}N_{RS} \end{aligned} \qquad \text{(A1)}$$

where U, S, and μ are the internal energy, entropy, and chemical potential, respectively, for each phase. In the case of nanocrystals, equation A1 must be modified by a surface energy term:

$$U_{WZ}(S,V) = TS_{WZ} - PV_{WZ} + \mu_{WZ}N_{WZ} - \gamma_{WZ}A_{WZ}$$
$$U_{RS}(S,V) = TS_{RS} - PV_{RS} + \mu_{RS}N_{RS} - \gamma_{RS}A_{RS} \quad \text{(A2)}$$

where γ_i and A_i are the surface tension and surface area, respectively, in phase i. Experimentally,[48] it has been observed that the entropy change upon transition is small (~1.7 e.u.), so the TS_i terms in equations A1 and A2 are frequently dropped in actual calculations of thermodynamic parameters. Given that the condition for a phase transition to occur is $\mu_{WZ} = \mu_{RS}$, the necessary condition for a phase transition in a nanocrystal system is given by

$$P_T(V_{WZ} - V_{RS}) + U_{WZ}(V_T) - U_{RS}(V_T) = \gamma_{RS}A_{RS} - \gamma_{WZ}A_{WZ} \quad \text{(A3)}$$

where V_T is the unit cell volume at the nanocrystal phase transition pressure (P_T). Equation A3 can be used in combination with a knowledge of the volume compressibility in both phases to generate the energy volume curves (figure 4.12). This allows for experimental determination of the surface energy (γ).

The first term in equation A3 can be calculated using the Murnaghan equations of state[49,50] in combination with measured CdSe nanocrystal compressibility constants. For the wurtzite phase, compressibility constants were obtained from high pressure EXAFS experiments carried out on 2.7 nm radius CdSe nanocrystals.[13] The resultant values for the bulk modulus and its derivative with respect to pressure are B_o = 37 +/- 5 GPa and B_o' = 11 +/- 3. The compressibility constant for the rock salt phase is obtained from this work: B_o = 74 +/- 2 GPa. As the data is observed to vary quite linearly with pressure, the rock salt data was not fit with a B_o' value. Note that the size dependence in equation A3 arises both from the variation of P_T with nanocrystal size, and from the nanocrystal surface energy, which is size dependent and gives rise to an effective pressure which in turn modifies the applied pressure. The relevant volume equations needed to calculate the first term in equation A3 for each phase are[50]

$$V_{WZ}(P_T, r_{WZ}) = \frac{V_{0,WZ}}{\left[1 + \frac{B_0'}{B_{0,WZ}} \cdot \left(P + \frac{2 \cdot \gamma_{WZ}}{r_{WZ}}\right)\right]^{1/B_0'}}, \tag{A4}$$

$$V_{RS}(P_T, r_{RS}) = \frac{V_{0,RS}}{\left[1 + \frac{1}{B_{0,RS}} \cdot \left(P + \frac{2 \cdot \gamma_{RS}}{r_{RS}}\right)\right]}, \tag{A5}$$

where the V_0 term for equation A4 is obtained from bulk CdSe at atmospheric pressure. In equation A5, the V_0 term is obtained by extrapolation of bond length versus pressure data from this chapter for a large size nanocrystal sample to atmospheric pressure. While this value will deviate slightly from the bulk value because of the surface pressure on the clusters, the large size of the sample makes the error introduced by this approximation small. The nanocrystal radius in the high pressure phase (r_{RS}) is calculated from the volume contraction assuming spherical nanocrystals. This, however, leads to a recursive formula for the high pressure phase volume. Thus, after one level of recursion, r_{RS} is fixed at $0.75^{1/3}$ times the wurtzite phase radius, which is the value observed experimentally for 2.7 nm crystallites from high pressure EXAFS.[15]

The second term in equation A3 must be broken into two parts to obtain numerical values:

$$\begin{aligned} U_{WZ}(V_T) - U_{RS}(V_T) = [U_{WZ}(V_T) - U_{WZ}(V_B)] - [U_{RS}(V_T) - U_{RS}(V_B)] \\ + U_{WZ}(V_B) - U_{RS}(V_B), \end{aligned} \tag{A6}$$

where V_B is the bulk unit cell volume at bulk phase transition pressure. By setting the chemical potentials equal in equation A1, it is shown that

$$U_{WZ}(V_B) - U_{RS}(V_B) = -P_B[V_{WZ}(P_B) - V_{RS}(P_B)] \tag{A7}$$

and thus the last two terms in equation A6 can be calculated from the bulk CdSe phase transition pressure and the volume change at transition in the bulk system. The middle two terms in equation A6 (square brackets) can be calculated by integrating the Murnaghan equations of state (equations A4 and A5) to generate energy-volume curves.

The explicit forms of these curves for the wurtzite and rock salt phases (i.e., with and without B_o') can be obtained and are presented in equations A8 and A9.

$$E_{WZ}(V) = -\int_{P_B}^{P_T} P \cdot dV_{wz}$$
$$= \frac{B_{0,WZ}}{B_0'} \cdot V_{WZ} \cdot \left\{ 1 + \left[\frac{(V_{0,WZ}/V_{WZ})^{B_0'}}{(B_0' - 1)} \right] \right\} \Bigg|_{P_B}^{P_T}, \qquad \text{(A8)}$$

$$E_{RS}(V) = -\int_{P_B}^{P_T} P \cdot dV_{RS} \qquad \text{(A9)}$$
$$= B_{0,RS} \cdot V_{RS} - \left[B_{0,RS} \cdot V_{0,RS} \cdot \ln(V_{RS}) \right]_{P_B}^{P_T}.$$

The nanocrystal size dependence in these equations stems both from the direct dependence on P_T and from the size dependence of the volume.

The final term in equation A3 depends only upon the nanocrystal surface area and the surface tension. The surface area in each phase is calculated from the volume assuming spherical crystallites. The best form for the surface tension (γ) is discussed at some length in section 4.4.1.1 and thus will not be repeated here.

This combination of approximations and substitutions, in combination with the constants in table 4.1, allows for numerical evaluation of all of the terms in equation A3 except the rock salt phase surface energy. This is used in section 4.4.1.2 to compare this thermodynamic model to the size dependent phase transition data collected on a variety of nanocrystals.

4.7 Notes and References:

1. This type of behavior has been observed in a variety of very different clusters. Examples of novel bonding geometries in covalent, metallic, and ionic clusters include: H. W. Kroto, J. R. Heath, S. C. O'Brien, R. F. Curl, and R. E. Smalley, *Nature* **318**, 162

(1985); B. K. Teo, X. Shi, and H. Zhang, *J. Am. Chem. Soc.* **113**, 4329 (1991); J. Deifenbach and T.P. Martin, *J. Chem. Phys.* **83**, 4585 (1985).

2. A. N. Goldstein, C. M. Echer, and A. P. Alivisatos, *Science* **256**, 1425 (1992).

3. C. J. Coombes, *J. Phys.* **2**, 441 (1972); P. Buffat and J.-P. Borel, *Phys. Rev. A* **13**, 2287 (1976).

4. S.H. Tolbert and A.P. Alivisatos, *Science*, **265**, 373 (1994).

5. C. B. Murray, D. J. Norris, and M. G. Bawendi, *J. Am. Chem. Soc.* **115**, 8706 (1993).

6. J. E. Bowen Katari, V. L. Colvin, A. P. Alivisatos, *J. Phys. Chem.* **98**, 4109 (1994).

7. For the these experiments we have defined the thermodynamic phase transition pressure as the mid-point of the hysteresis curve, or equivalently the average of the upstroke and downstroke transition pressures. This produces a bulk CdSe transition pressure of 2 GPa, in comparison to the upstroke value of 3 GPa. Experiments on bulk CdSe which show full hysteresis data include: (a) A.L. Edwards, and H. G. Drickamer, *Phys. Rev.* **122**, 3196 (1962); (b) A. Onodera, *Rev. Phys. Chem Japan* **39**, 65 (1969); (c) W. C. Yu and P. J. Gielisse, *Mat. Res. Bull.* **6**, 621 (1971).

8. A. P. Alivisatos, T. D. Harris, L. E. Brus, and A. Jayaraman, *J. Chem. Phys.* **89**, 5979 (1988).

9. S. H. Tolbert and A. P. Alivisatos, *Z. Phys. D* **26**, 56 (1993).

10. M. Haase and A. P. Alivisatos, *J. Phys. Chem.* **96**, 6756 (1992).

11. X. S. Zhao, J. Schroeder, P. D. Persans, and T. G. Bilodeau, *Phys. Rev. B* **43**, 12580 (1991).

12. L. J. Cui, U. D. Venkateswaran, B. A. Weinstein, and F. A. Chambers, *Phys. Rev. B* **45**, 9248 (1992).

13. S. H. Tolbert and A. P. Alivisatos in NATO ASI Proceeding on *Nanophase Materials: Synthesis-Properties-Applications*, G. C. Hadjipanayis and R. W. Siegel, Eds. (Kluwer Academic Publishers, Dordrecht, 1993), pp. 471-482.

14. J.J. Shiang, A.V. Kadavanich, R.K. Grubbs, and A.P. Alivisatos, submitted to *J. Phys. Chem.*

15. L.R. Becerra, C.B. Murray, R.G. Griffin, and M.G. Bawendi, *J. Chem. Phys.* **100**, 3297 (1994).

16. S. H. Tolbert and A. P. Alivisatos, unpublished data.

17. JCPDS-ICDD powder pattern card # 8-459, (c) 1989.

18. JCPDS-ICDD powder pattern card # 21-829, (c) 1989; J. Osugi, K. Shimizu, T. Nakamura, and A. Onodera, *Rev. Phys. Chem. Jpn.*, **36**, 59 (1966).

19. A. N. Mariano and E. P. Warekois, *Science* **142**, 672, (1963).

20. JCPDS-ICDD powder pattern card # 19-191, (c) 1989.

21. R. A. Montalvo and D. W. Langer, *J. Appl. Phys.* **41**, 4101, (1970); C. F. Cline and D. R. Stephens, *J. Appl. Phys.* **36**, 2869 (1965).

22. S. H. Tolbert, A. B. Herhold, C. S. Johnson, and A. P. Alivisatos, *Phys. Rev. Lett.* **73**, 3266 (1994).

23. J. A. Corll, *J. Appl. Phys.* **35**, 3032 (1964).

24. Throughout this document we use term "surface tension" to refer to the force per unit area associated with a nanocrystal surface. The nanocrystal surface is not, however, in contact with the vacuum, so the more appropriate term is actually "interfacial tension." The relevant interface is that between the nanocrystal surface and the organic passivating groups. The term "surface tension" is used only to emphasize the difference between a solid-solid interface, and the nanocrystal solid/ligand interface.

25. I. Szleifer, D. Kramer, A. Ben-Shaul, W. M. Gelbart, and S. A. Safran, *J. Chem. Phys.* **92**, 6800, (1990).

26. For a review of these ideas see: R. S. Berry, S. A. Rice, and J. Ross, *Physical Chemistry*, New York, Wiley, c1980, pp. 875 - 883.

27. C. Solliard, and M. Flueli, *Surface Science* **156**, 487 (1985).

28. F. Grieser, G. Mills, and D. Meisel, *J. Colloid Interface Sci.* **120**, 540 (1987).

29. B. F. Ordmont, *Dokl. Akad. Nauk. SSSR* **124**, 132 (1959); S. N. Sadumkin, *Fiz. Tverd. Tela* **2**, 880 (1960).

30. X. Li and R. Jeanloz, *Phys. Rev. B* **36**, 474 (1987); R. Jeanloz, *J. Geophys. Res.* **79**, 10352 (1987).

31. B. N. Oshcherin, *Phys. Stat. Sol. (a)* **34**, K181 (1976).

32. R. E. Hanneman, M. D. Banus, and H. C. Gatos, *J. Phys. Chem. Solids* **25**, 293 (1964).

33. U. D. Venkateswaran, L. J. Cui, B. A. Weinstein, and F. A. Chambers, *Phys. Rev. B* **45**, 9237 (1992).

34. J. K. Burdett and T. J. McLarnan, *J. Chem. Phys.* **75**, 5765 (1981); J. K. Burdett, *Prog. Solid St. Chem.* **15**, 173 (1984).

35. J. Ma, J. E. Fischer, Y. Cao, and A. J. Heeger, *Solid State Comm.*, **83**, 395 (1992).

36. D. Moses, A. Feldblum, E. Ehrenfreund, A. J. Heeger, T.-C. Chung, and A. G. MacDiarmid, *Phys. Rev. B* **26**, 3361 (1982); A. Brillante, M. Hanfland, K. Syassen, and J. Hocker, *Physica B & C* **139 & 140**, 533 (1986).

37. J. K. Burdett, and S. Lee, *J. Am. Chem. Soc.* **105**, 1079 (1983).

38. B.A Weinstein, in *High Pressure Science and Technology*, K.D. Timmerhaus and M.S. Barber, eds., (Plenum, New York, 1979), Vol. 1, p. 141.

39. D.J. Chadi and R.M. Martin, *Solid State Comm.*, **19**, 643 (1976).

40. S.-K. Chan, *Mat. Sci. Forum*, **56-58**, 101 (1990).

41. T.P. Dougherty, G.P. Wiederrecht, K.A. Nelson, M.H. Garrett, H.P. Jensen, and C. Warde, *Science*, **258**, 770 (1992).

42. N. Nakanishi, A. Nagasawa, and Y. Murakami, *J. Physique*, **43**, C4-35 (1982).

43. P. Wollants, J. R. Roos, and L. Delaey, *Prog. Mat. Sci.* **37**, 227 (1993).

44. D. Turnbull, *Solid State Phys.* **3**, 225 (1956).

45. D. Turnbull, *J. Chem. Phys.* **20**, 411 (1952); D. Trunbull, *J. Appl. Phys.* **21**, 1022 (1950); D. Trunbull, *J. Appl. Phys.* **20**, 817 (1949).

46. J. B. newkirk and D. Turnbull, *J. Appl. Phys.* **26**, 579 (1955).

47. J. Lin, E. Cates, and P.A. Bianconi, *J. Am. Chem. Soc.* **116**, 4738 (1994).

48. A. Onodera, *Rev. Phys. Chem. Japan* **39**, 65 (1969); M. Bockowski, S. Krukowski, and B. Lucznik, *Semiconductor Sci. Tech.* **7**, 994 (1992).

49. F. D. Murnaghan, *Proc. Natl. Acad. Sci. USA* **30**, 224 (1944).

50. It has recently been brought to our attention that the Murnaghan equations of state can over-estimate the value of B_o'. A better approximation of this value can be obtained using the Birch-Murnaghan Equations of State.

Chapter 5: High Pressure Studies on Si Nanocrystals

5.0 Abstract:

The kinetics of solid-solid phase transitions are explored using pressure induced structural phase transformations in Si nanocrystals. In agreement with the predictions of soft mode theories, large elevations in phase transition pressure are observed in nanocrystals as compared to bulk Si, and high pressure X-ray diffraction peak widths indicate an overall change in nanocrystal shape upon transformation. Additionally, unlike the BC8 phase recovered from bulk Si, amorphous Si nanocrystals are recovered upon release of pressure providing an example of kinetic size control over solid phases.

5.1 Introduction:

Recent progress in the preparation of finite-sized semiconductor crystallites has created an opportunity to better understand first order solid-solid phase transitions. Pressure induced solid-solid phase transitions in extended semiconductors are generally highly hysteretic, and typically involve multiple nucleations and domain fracture.[1] The space groups of the two phases frequently have a group-subgroup relationship.[2] This has led to the conclusion that these phase transitions must involve specific motions that carry the solid from one structure to another. Formally, this motion belongs to a specific irreducible representation of the higher symmetry group.[2] Convincing evidence for this model lies in the observation of soft modes, or vibrations of the crystal that tend towards zero frequency as the transition pressure is approached.[3] In this Chapter we demonstrate that studies of pressure induced transformations in nanocrystals provide another route for observing the pathway of solid-solid phase transitions, as well as a means of explaining the hysteresis and fragmentation observed in bulk transformations.

Nanocrystals are smaller than the fragment domains that result when a single crystal undergoes a solid-solid phase transition. Thus, nanocrystals of CdSe have been

observed to transform from wurtzite to rock salt structures as single domains, with only one nucleation event per crystallite.[4] Further, these CdSe studies[4] demonstrated that the smaller the nanocrystallite, the higher the transformation pressure. These observations led to a hypothesis, consistent with a soft-mode transformation mechanism, in which the nanocrystals change shape upon structural transformation. If the nanocrystals have dominantly low index surfaces as synthesized in the low pressure phase, then the shape change must result in high index, high energy surfaces in the high pressure phase. These newly created high energy surfaces destabilize the high pressure phase and explain the elevation in transformation pressure with reduction of nanocrystal size. The soft mode hypothesis therefore requires that nanocrystals change shape upon undergoing pressure induced solid-solid transitions. Observing this change in shape, however, is not a simple matter.[5] At atmospheric pressure, the shape of a nanocrystal can readily be observed using transmission electron microscopy.[6] The pressure induced transitions observed to date, although hysteretic, are reversible, so that back transformation prevents simple analysis of shape in recovered samples. The shape must therefore be determined at high pressure. In this chapter we demonstrate that X-ray diffraction line widths can be used to observe the change in shape that occurs when Si nanocrystals are converted under pressure from the diamond to the primitive hexagonal structure.

Beyond access to the microscopic nature of phase transitions, another primary goal of nanocrystal research is the search for non-standard bonding geometries in finite size. In very small clusters, these unusual geometries are sometimes found to be thermodynamically stable. In larger nanocrystals, however, the effect of size is not sufficient to stabilize these novel bonding geometries. In dynamic processes such as crystal growth and structural transformations, however, the possibility exists to use smaller variations in thermodynamic stability to trap *metastable* structures in larger crystallites. This effect is seen in the growth of kinetically trapped rock salt phase CdS

nanocrystals in a highly ionic polymer matrix.[7] In this work, we demonstrate the kinetic trapping of amorphous Si (a-Si) nanocrystals upon release of pressure from the β-Sn phase.

In this Chapter, high pressure X-ray diffraction and optical absorption are used to examine the phase stability of SiO_2 coated Si nanocrystals.[8] The Si/SiO_2 interface has an extremely low dangling bond density and is considered to be a well passivated surface.[9] This stable diamond phase interface should emphasize phase transition path induced changes in surface structure by producing a significant increase in the total energy of the nanocrystals upon transformation. In addition, this covalent semiconductor contrasts well with previous high pressure studies on ionic semiconductor nanocrystals.[4,10]

Another advantage to studying Si is its extremely rich phase stability: Bulk Si has been observed in as many as 10 different solid structures between atmospheric pressure and 45 GPa. Extensive theoretical and experimental work has gone into understanding the many stable phases of bulk Si. Bulk Si transforms from the diamond structure to the β-Sn phase at approximately 11 GPa.[11] The β-Sn phase undergoes a second order transformation to the closely related Imma structure.[12] The Imma phase then converts via a second order transformation to a primitive hexagonal (PH) structure near 16 GPa.[12,13,14] By 40 GPa, bulk Si is found in a hexagonal close packed structure (HCP).[13] Upon partial release of pressure from 40 GPa, the PH and β-Sn phases are again observed.[14] Bulk Si does not, however, transform back to the diamond phase upon full release of pressure. Instead, a number of metastable crystalline[15] and amorphous[16] phases are observed. The most common of these, known as BC8, is a slightly distorted tetrahedral structure.[17]

5.2 Experimental:

The nanocrystal samples used in these experiments consist of diamond phase Si crystallites coated with an approximately 15 Å thick layer of SiO_2.[8] The nanocrystals

were synthesized by gas pyrolysis[8] of Si_2H_6 and O_2 and characterized using Transmission Electron Microscopy (TEM), electron diffraction, X-ray diffraction, luminescence, and optical absorption. Nanocrystal sizes ranged from 100 to 500 Å in diameter with size dispersions varying from 20% for small samples to 35% for larger samples. Samples were observed to be highly crystalline, both by TEM and by agreement of TEM sizes and sizes calculated form X-ray diffraction peak widths.

High pressure experiments were carried out using piston-cylinder style diamond anvil cells; pressures were determined using standard ruby fluorescence techniques. The Si nanocrystal samples were dissolved in ethylene glycol (EG). Under pressure, EG forms a glass which deforms in a quasi-hydrostatic manner up to about 10 GPa. Above this pressure, EG will support significant pressure gradients. Well dissolved samples, however, remained optically clear at all pressures reached in these experiments. High pressure optical absorption data was obtained using a scanning Cary model 118 UV/visible spectrometer. High pressure X-ray diffraction experiments were carried out on wiggler beam line 10-2 at the Stanford Synchrotron Radiation Laboratory (SSRL). Focused monochromatic 20 KeV X-rays were utilized in an angle dispersive geometry. Debye-Scherrer rings were angle integrated to produce the data presented here. Diffraction peak widths were deconvoluted for both the instrument function and broadening due to pressure gradients; a gaussian distribution of pressures around the measured pressures was assumed. Domain sizes were calculated from the peak widths using the Debye-Scherrer formula.

5.3 Results:

Like bulk Si, Si nanocrystals are indirect gap semiconductors. Optical absorption thus shows only a featureless rising edge in the diamond phase.[18] Despite the lack of discrete features, the onset of structural transformation can be easily seen in the absorption

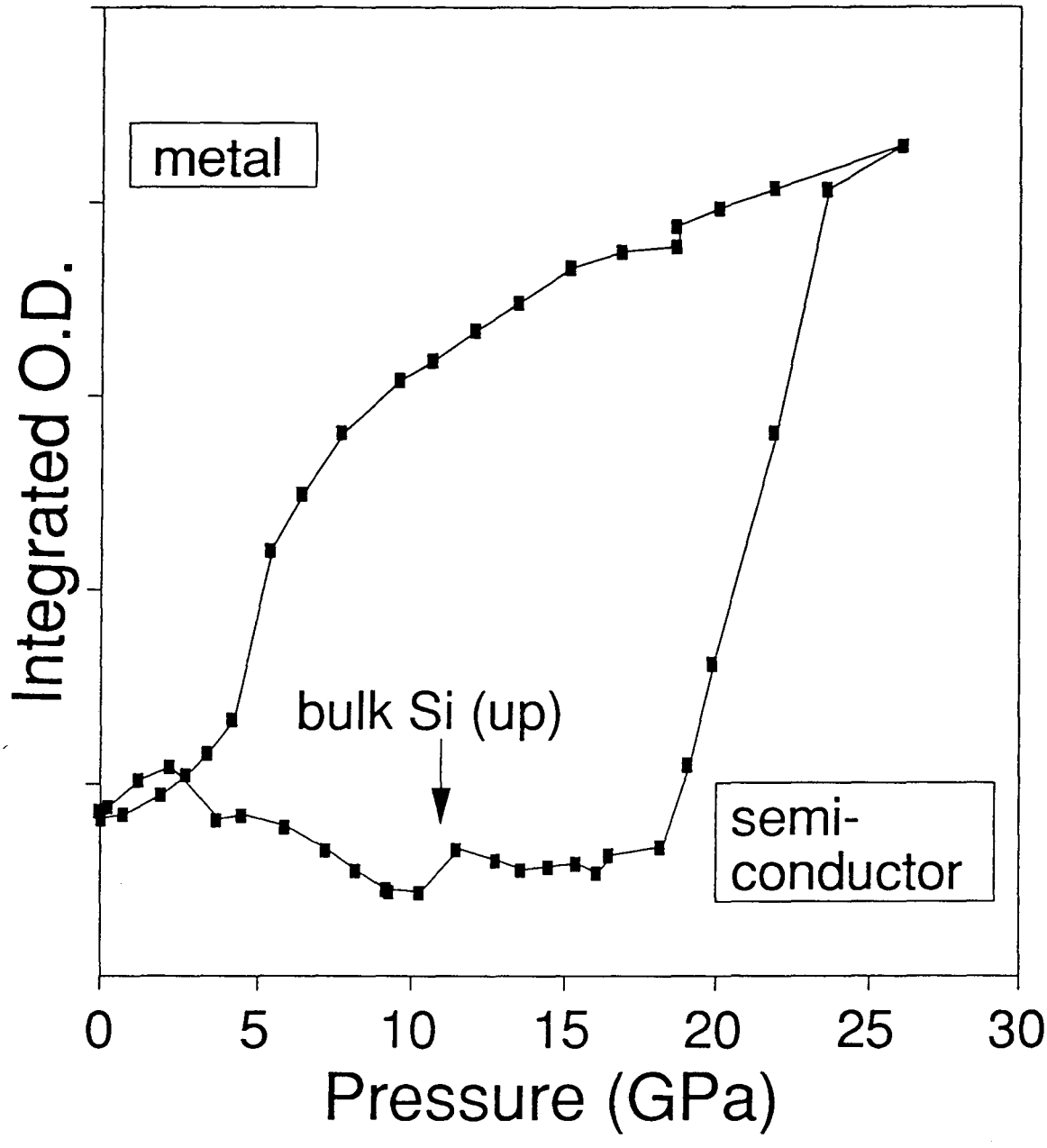

Figure 5.1: Phase behavior for 9.6 nm diameter Si crystallites coated with SiO_2 measured by optical absorption. The increase in optical density at about 22 GPa marks the semiconductor to metal transformation. The decrease in optical density at 5 GPa marks the β-Sn to amorphous Si transformation. The arrow marks the bulk Si upstroke diamond to β-Sn phase transition pressure.

spectra as a large increase in optical density (O.D.)[19] and the loss of the $\sqrt{O.D.}$ versus energy dependence in the spectrum. Figure 5.1 shows the change in absorbance observed in 96 Å diameter crystallites. These hysteresis data are constructed by integration of the absorption intensity between 1.95 and 2.05 eV. Similar results are obtained by integration at any other comparable visible wavelengths. The upstroke semiconductor-to-metal transformation in figure 5.1 appears at approximately 22 GPa, in sharp contrast to the bulk Si diamond to β-Sn transition which takes place around 11 GPa.[11] Also in contrast to bulk Si, nanocrystals appear to recover to a semiconducting phase, while the metastable BC8 phase most commonly observed in recovered bulk Si is a semi-metal.[17]

Since optical absorption cannot distinguish the many metallic high pressure phases of Si, diffraction experiments are required to determine the actual structures involved. High pressure X-ray diffraction powder patterns obtained on 492 Å Si nanocrystals are presented in figure 5.2. Nanocrystals are initially in the diamond phase[20] ① and are seen to be stable to well above the bulk Si diamond to β-Sn phase transition pressure of 11 GPa.[11] With application of sufficient pressure, however, the system can be converted to the PH structure[13] ②. Upon partial release of pressure, an Imma phase is observed ③ as well as a β-Sn phase (not shown).[12] Upon full release of pressure, instead of recovering the metastable BC8 phase[17] observed in bulk silicon, the sample appears to form a-Si ④. Note the change in the amorphous scattering background between the Imma and amorphous Si patterns. In the crystalline phases, this background is probably dominated by SiO_2. In the a-Si phase, the back ground is altered because it is now a combination of SiO_2 and a-Si.

5.4 Discussion:

The most striking feature of the high pressure behavior observed in Si nanocrystals is the extreme elevation in upstroke phase transformation pressure observed in crystallites as large as 500 Å in diameter. These nanocrystals contain ~10^6 atoms per crystallite, so

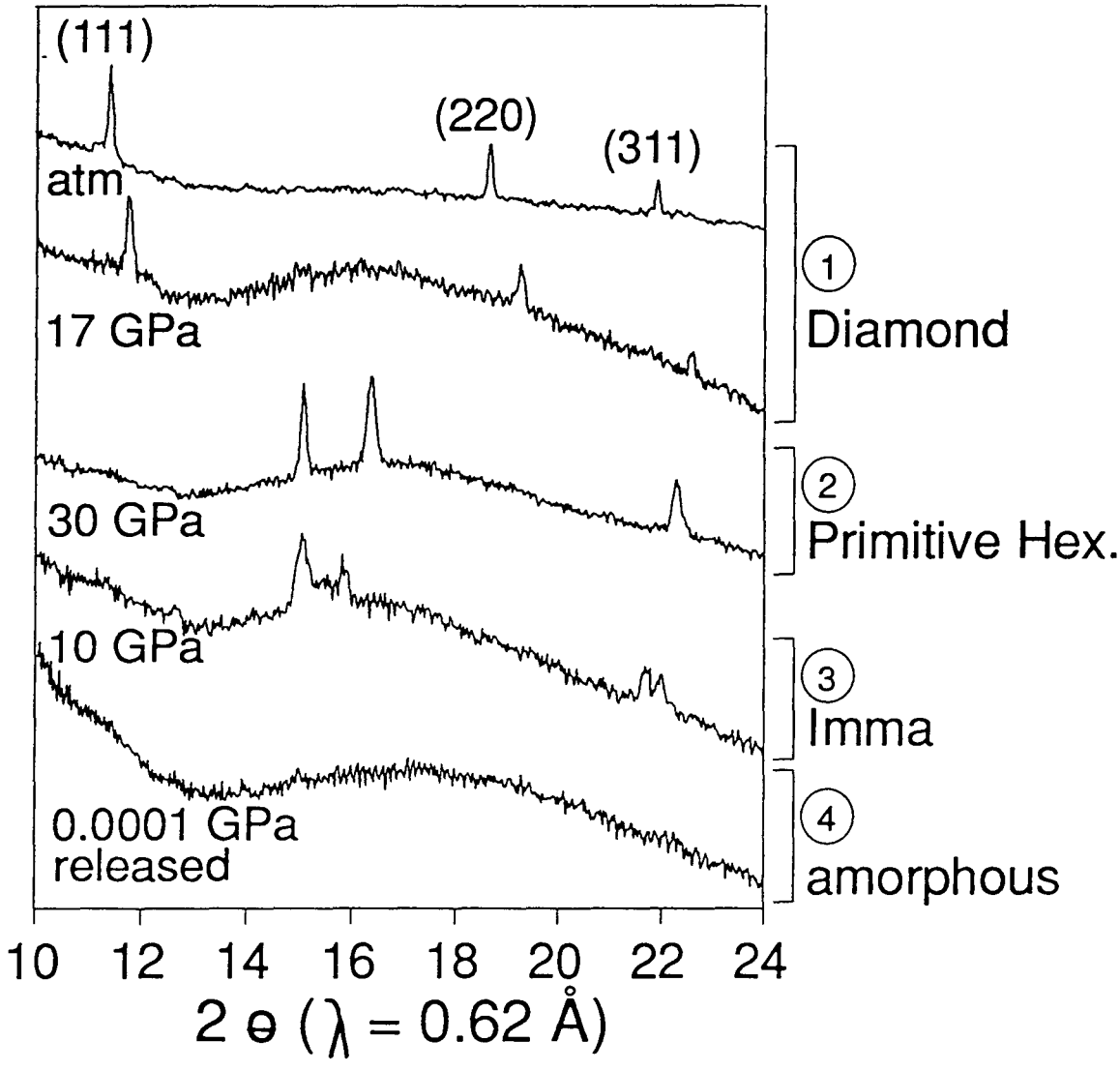

Figure 5.2: High pressure X-ray diffraction data obtained on 49 nm diameter Si nanocrystals coated with SiO_2. Pressures, indexing, and structures are indicated on the figure.

the vast majority of atoms are in an almost completely bulk-like interior environment. CdS and CdSe nanocrystals in this size range show bulk-like phase behavior.[4] Insight gained from studies on CdS and CdSe nanocrystals, however, can be used to postulate that transition path induced changes in surface structure destabilize the high pressure phase and cause an increase in transition pressure. It is highly unlikely that the stable Si/SiO_2 interface can survive intact when the interior Si atoms, but not the exterior SiO_2 atoms, move along the transition path. The result is the destruction of the low energy Si/SiO_2 interface upon structural transition. Analogous results have been observed in GaAs/AlAs superlattices.[21] This large change in interfacial energy at the Si nanocrystal transformation point necessitates a great deal of additional work to make the system change phase. This explains the observed significant deviations from bulk behavior, even for very large crystallites, and provides important confirmation of the postulate that surface energy controls the phase stability in nanocrystalline solids.

Because of the symmetry of the structures involved, Si nanocrystals can also be used to seek evidence for a path driven change in the shape of a nanocrystal upon transformation, providing direct confirmation of the theory of soft mode transitions in solids.[3] Propagating atoms of a diamond phase crystallite along the proposed transition path produces a crystallite with a long axis in the (001) direction, and shorter axes in the degenerate (100) and (010) directions.[22] By examining the widths of the (100) and (001) diffraction peaks, evidence for overall changes in nanocrystal shape upon transformation can be obtained.[23]

Figure 5.3 shows an enlargement of the Si nanocrystal PH diffraction pattern at 21 GPa. The peak widths in the (100) and (001) directions are clearly different. When deconvoluted for the instrument function and pressure gradients and averaged over multiple diffraction patterns between 20 and 30 GPa, these peak widths correspond to domain sizes of 549 ± 68 Å in the (001) direction and 267 ± 10 Å in the (100) direction. This results in an aspect ratio of ~2.05, in good agreement with a value of ~1.9 expected

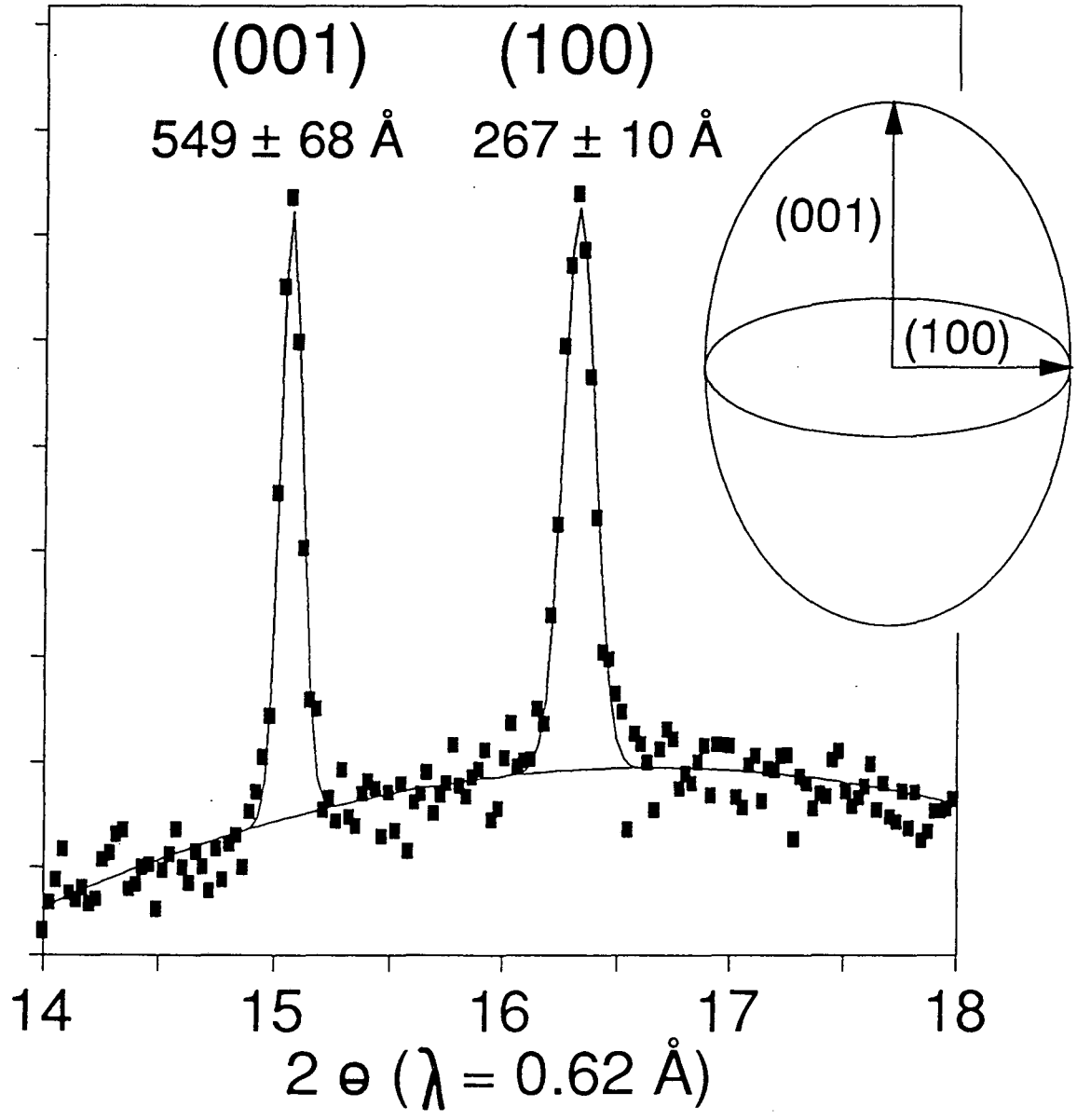

Figure 5.3: Expanded view of figure 5.2 ② shows that the (001) and (100) diffraction peak widths differ. The difference in domain size is due to a shape change in the crystallites.

from the change in unit cell shape along the most probable transition path.[22] The domain size in the (101) direction is in reasonable agreement with the geometric average of these two domains. These results strongly suggest an overall change in nanocrystal shape upon transformation. Note that the alternative explanation, that the nanocrystals fragment upon transformation, can be ruled out from the data: At 17 GPa, a pressure where the nanocrystals are still clearly in the diamond phase, some broadening of the diffraction peaks in comparison to atmospheric pressure is seen due to pressure inhomogeneity. While the peak widths in the PH (100) direction are significantly broader than the 17 GPa diamond phase lines, the peak widths in the PH (001) direction are actually narrower than the 17 GPa diamond phase lines. This effect can not result from fragmentation. The difference in peak widths thus provides direct evidence for an overall change in nanocrystal shape. The results are a confirmation of the soft mode theory of phase transformations.

Another observation of key interest is the recovery of a-Si upon release of pressure in nanocrystals, in contrast to the recovery of the metastable BC8 phase in bulk Si. Amorphous Si is a metastable phase of Si which can be kinetically trapped upon release of high pressure under certain circumstances.[16] Under the conditions of this experiment, a-Si is not kinetically favored in the bulk. A wide variety of experimental and theoretical work, however, has suggested that a-Si is more stable than diamond phase Si in very small size nanocrystals (below ~30 Å in diameter),[24] which is reasonable as long range bonding is not required to stabilize the amorphous phase. While a-Si is not predicted to be thermodynamically stable over the diamond phase in larger sizes, it is likely that some stabilization of the amorphous phase persists even for 500 Å nanocrystals. These ideas can be combined to gain an understanding of our room temperature recovery of a-Si nanoclusters. The amorphous phase, while not the thermodynamic ground state, is stabilized in finite size, and as a consequence, the barrier for the β-Sn to a-Si reaction is

reduced in finite size in comparison to the β-Sn to BC8 reaction channel. An additional kinetic factor favoring the dynamic formation of a-Si in finite size systems can also be found: As the β-Sn to a-Si transition is diffusive (that is, it has no symmetry prescribed transition path), no change in the nanocrystal shape is required upon transition so there are no symmetry dictated changes in the surface structure. All of this points to an important general phenomenon for nanocrystal studies: While "novel" bonding geometries do not generally appear to be thermodynamically stable in large crystallites, it is possible to use kinetics in combination with the slightly altered stability of higher lying states to trap metastable structures. This general phenomenon is worth further exploration.

5.5 Conclusions:

In summary, high pressure optical absorption and X-ray diffraction studies show large elevations in the semiconductor to metal structural transformation in SiO_2 coated Si nanocrystals. The elevation can be attributed to destruction of the low energy Si/SiO_2 interface at the structural transformation. Recovery of a-Si clusters upon release of pressure shows further how the observed phase stability in nanocrystals can be controlled by kinetics: Formation of a-Si clusters is demonstrated to be a kinetically, rather than a thermodynamically controlled process. Finally, overall changes in the shape of a nanocrystal upon transformation are observed by X-ray diffraction in Si crystallites. These changes, induced by motion of interior atoms along a transition path, are the root of kinetic control of phase stability in nanometer scale systems. Further, the observed changes in nanocrystal shape provide direct confirmation of soft-mode theories of phase transitions in solids.

5.6 Notes and References:

1. R. E. Hanneman, M. D. Banus, and H. C. Gatos, *J. Phys. Chem. Solids* **25**, 293 (1964); U. D. Venkateswaran, L. J. Cui, B. A. Weinstein, and F. A. Chambers, *Phys. Rev. B* **45**, 9237 (1992).

2. F. Falk, *J. Physique*, **43**, C4-3 (1982), and references therein.

3. D. J. Chadi, R. M. Martin, *Sol. St. Comm.*, **19**, 643 (1976); B. A. Weinstein, in *High Pressure Sci. & Tech.*, K. D. Timmerhaus, M. S. Barber, eds., (Plenum, N.Y., 1979), V. 1, p. 141; S.-K. Chan, *Mat. Sci. Forum*, **56-58**, 101 (1990); T. P. Dougherty, *et al.*, Science **258**, 770 (1992).

4. S. H. Tolbert and A. P. Alivisatos, *Science*, **265**, 373 (1994); S. H. Tolbert and A. P. Alivisatos, *J. Chem. Phys.* **102**, 4642 (1995).

5. Observation of macroscopic changes in crystal shape upon structural transformation have been made in some temperature induced transformation molecular crystals: W. L. Fraser and S. W. Kennedy, *Acta Cryst.* **B28**, 3101 (1972); S. W. Kennedy, J. H. Patterson, R. P. Chaplin, and A. L. Mackay, *J. Sol. State Chem.* **10**, 102 (1974).

6. J. J. Shiang, A. V. Kadavanich, R. K. Grubbs, and A. P. Alivisatos, submitted to *J. Phys. Chem.*

7. J. Lin, E. Cates, and P. A. Bianconi, *J. Am. Chem. Soc.* **116**, 4738 (1994).

8. K. A. Littau, P. J. Szajowski, A. J. Muller, A. R. Kortan, and L. E. Brus, *J. Phys. Chem.* **97**, 1224 (1993); W. L. Wilson, P. F. Szajowski, and L. E. Brus, *Science* **262**, 1242 (1993).

9. E. Yablonovitch, *Science* **246**, 347 (1989).

10. A. P. Alivisatos, T. D. Harris, L. E. Brus, and A. Jayaraman, *J. Chem. Phys.* **89**, 5979 (1988); X. S. Zhao, J. Schroeder, P. D. Persans, and T. G. Bilodeau, *Phys. Rev. B* **43**, 12580 (1991); M. Haase and A. P. Alivisatos, *J. Phys. Chem.* **96**, 6756 (1992); S. H.

Tolbert and A. P. Alivisatos in NATO ASI Proc. on *Nanophase Materials,* G. C. Hadjipanayis and R. W. Siegel, Eds. (Kluwer Academic, Dordrecht, 1993) p. 471.

11. J. C. Jamieson, *Science* **139**, 762 (1963); B. A. Weinstein and G. J. Piermarini, *Phys. Rev. B* **12**, 1172 (1975).

12. M. I. McMahon, R. J. Nelmes, *Phys. Rev. B* **47**, 8337 (1993).

13. H. Olijnyk, S. K. Sikka, and W. B. Holzapfel, *Phys. Lett.* **103A**, 137 (1984).

14. J. Z. Hu and I. L. Spain, *Sol. St. Comm.* **51**, 263 (1984).

15. Y.-X. Zhao, F. Buehler, F. R. Sites, and I. L. Spain, *Sol. St. Comm.* **59**, 679 (1986).

16. M. Imai, K. Yaoita, Y. Katayama, J.-Q. Chen, K. Tsuji, *J. Non-Cryst. Sol.* **150**, 49 (1992).

17. R. H. Wentorf, Jr. and J. S. Kasper, *Science* **139**, 338 (1963); F. P. Bundy, *J. Chem. Phys.* **41**, 3809 (1964).

18. S. H. Tolbert, A. B. Herhold, C. S. Johnson, and A. P. Alivisatos, *Phys. Rev. Lett.* **73**, 3266 (1994).

19. B. Welber, C. K. Kim, M. Cardona, and S. Rodriguez, *Solid State Com.* **17**, 1021 (1975).

20. JCPDS-ICDD powder pattern card #27-1402, (c) 1989.

21. L. J. Cui, U. D. Venkateswaran, B. A. Weinstein, and F. A. Chambers, *Phys. Rev. B* **45**, 9248 (1992).

22. M. T. Yin, M. L. Cohen, *Phys. Rev. B* **26**, 5668 (1982); R. J. Needs, R. M. Martin, *Phys. Rev. B* **30**, 5390 (1984); K. J. Chang, M. L. Cohen, *Phys. Rev. B* **31**, 7819 (1985); S. P. Lewis, M. L. Cohen, *Phys. Rev. B* **48**, 16144 (1993).

23. A. Guinier, *X-Ray Diffraction in Crystal* (W. H. Freeman and Co., U.S.A., 1963) p. 137.

24. S. Veprek, Z. Iqbal, and F.-A. Sarott, *Phil. Mag. B* **45**, 137 (1982); U. Röthlisberger, W. Andreoni, and M. Parrinello, *Phys. Rev. Lett.* **72**, 665 (1994).

Chapter 6: Conclusions Thus Far

6.1 From Phase Transition to Molecular Isomerization:

Cluster research has led to a general question: can crystal size be added as a new axis to the phase diagrams of materials? In the case of melting, it appears that the answer is yes. A 1/radius axis that varies from 0 to 1 can be added to the bulk phase diagram, extending it into a new dimension. Only at the very smallest sizes, below 50 atoms, is there any remaining uncertainty on this point. The complete bulk phase diagram, however, occupies the P, T plane. The results presented here suggest that a great deal of caution is required before the size dimension can be added to the complete P, T phase diagram. Indeed, the solid-solid phase transitions studied here appear to evolve smoothly into kinetically controlled molecular isomerizations in finite size.

The dependence of the phase transition pressure on the transition path exemplifies a fundamental difference between the surface tension induced change in nanocrystal melting temperature and the surface tension induced change in nanocrystal solid-solid phase transition pressure. In melting, the transition temperature is reduced because the liquid phase has a thermodynamically lower surface energy than the solid phase. In solid-solid phase transitions, in contrast, the surfaces formed in the high pressure phases are path driven and thus are *non-equilibrium surfaces*. If the high pressure experiments were performed at sufficiently high temperatures to allow for rapid reorganization of the crystallite surface structure, the uniform elevation in phase transition pressure that has just been described would not be observed. Instead, a decrease in phase transition pressure would be observed in most cases. While these high temperature/high pressure experiments should still extrapolate to the bulk limit at infinite size, they should extrapolate from the opposite direction; that is, from depressed transition pressures.

Given the potential for such profound kinetic control of the transformations, these transformations cannot be described as true solid-solid phase transitions. Kinetically

controlled molecular isomerizations between metastable phases are common. In fact, almost all molecular isomerizations take place between thermodynamically metastable states. More importantly dependence on the path specified by P, T, or other intensive thermodynamic variables is common in molecular isomerizations. Theoretically, phase transitions are thermodynamic path independent. For a true thermodynamic phase transition, the following two T, P paths should produce the same final product: 1) The temperature is raised at atmospheric pressure, and then lowered at atmospheric pressure. The pressure is then raised above the bulk phase transition pressure, but below the nanocrystal transition pressure. The result: low pressure phase nanocrystals. 2) The temperature is raised at atmospheric pressure. The pressure is then raised above the bulk phase transition pressure; at high temperature, this pressure should be sufficient to induce a transformation. Finally, the temperature is lowered. The result: metastable high pressure phase nanocrystals. These two paths obviously produce completely different final products.

It should be noted that residual signatures of these path effects are present in bulk transformations as well. In bulk systems, however, the crystalline domains are sufficiently large that path induced changes in surface structure do not have a controlling effect on the total energy of the system. Thus, the widths of the hysteresis curves reflect the shape changes and path effects we have described; however, the midpoints of the curves do not. The midpoint of the bulk hysteresis curve properly belongs on the phase diagram. Note that many existing phase diagrams of solids report the upstroke transition pressure on the phase diagram, which is clearly in error. In addition, when bulk solids undergo multiple cycles through these phase changes, nucleation induced decreases in the domain size are often observed, with nanometer-sized domains produced in many cases.[1,2,3] As soon as the number of surface atoms approaches the number of interior atoms, these systems cease to undergo true solid-solid phase transitions.

The discussion presented above emphasizes the point that nanocrystals present a unique regime in structural transformations. As the understanding of these unusual structural changes improves, insight into the nature of true molecular isomerizations and true solid-solid phase transitions should improve as well. The need to extend the present measurements to high temperature and to ever smaller sizes is apparent.

6.2 Summary and Conclusions:

In chapters 3-5 of this thesis, we have presented a number of methods which can be used for studying structural transformations in semiconductor nanocrystals. High pressure EXAFS can be used to learn about structural changes in both low and high pressure phases of nanocrystals, and to measure linear compressibilities. EXAFS is limited to certain materials, however, as not all elements have a core absorption energy appropriate for work in the diamond cell: low energy X-rays can not penetrate the diamonds, and high energy X-rays can not be focused. Additionally, EXAFS can not provide information about the degree of crystallinity in the transformed phases. High pressure X-ray diffraction can provide a great deal of information about phase transitions in nanocrystals. Diffraction peak positions and intensities can provide an absolute measure of structure as a function of pressure, and diffraction peak widths can be correlated with the crystallinity of a nanoparticle. Diffraction experiments on nanocrystals are time consuming, however, and require synchrotron radiation. With a knowledge of the structure and crystallinity from diffraction experiments, high pressure optical absorption can be routinely used to determine phase transition pressures and hysteresis curves for nanocrystals of many sizes. By combining all of these experiments, a real understanding of the pressure induced structural changes in semiconductor nanocrystals can be obtained.

Using melting in nanocrystals as a model, the changes in phase transition pressure resulting from changes in nanocrystal size can be related to the difference in surface energies between the low and high pressure phases. As a reduction in surface tension in

the liquid phase causes a decrease in melting temperature in finite systems, the increase in solid-solid phase transition pressure must be caused by an increase in surface tension in high pressure phases of semiconductor nanocrystals. The compact high pressure phase structures, however, are usually predicted to have fairly low surface energies. The apparent contradiction can be understood in terms of phase transition paths. Because the basic connectivity of atoms does not change in a solid-solid phase transition, symmetry allowed motions of the interior atoms (related to Peierls distortions) control the motions of all atoms in a nanocrystal during a transformation. This results in the formation of high energy surfaces in the transformed phases. This elevated surface energy disfavors the formation of the high pressure phase crystallites and caused the observed elevations in transition pressure.

In a nanocrystal, where the surface energy makes a dominant contribution to the total energy of the system, the surface structure can actually control the phase stability of the crystallites. Despite this fact, the interior geometry appears to control the surface structure: Upon phase transformation at room temperature, the motion of interior atoms along the phase transition path moves surface atoms from low energy environments, formed during high temperature synthesis of the nanocrystals, to high energy environments. A real understanding of this effect is limited, however, by the fact that the potential in which atoms (particularly surface atoms) move during a transformation is not well understood. In contrast to the wealth of simulations of melting in nanocrystals,[4,5] no detailed calculations have been performed for solid-solid transformations in nanocrystals. There is great potential to further understanding by simulations of the experiments described here. In particular, molecular dynamics could provide real insight into understanding the hysteresis in these transformations.

While the structural transformations described here appear to be non-equilibrium events, the basic conclusions drawn from them are still very general. As more nanocrystal systems are studied under high pressure and simulations are performed, these effects of the

transition path on the surface structure and the phase transition pressure should become increasingly well understood. In addition, these results provide one more link in understanding the relationship between the phenomena observed in bulk and in molecular systems. The findings clarify a wide variety of existing data as well as predicting results for future studies.

6.3 Notes and References:

1. J. M. Besson, J. P. Itié, A. Polian, and G. Weill, *Phys. Rev. B* **44**, 4214 (1991).

2. U. D. Venkateswaran, L. J. Cui, B. A. Weinstein, and F. A. Chambers, *Phys. Rev. B* **45**, 9237 (1992).

3. S. H. Tolbert and A. P. Alivisatos, *Science*, **265**, 373 (1994); S. H. Tolbert and A. P. Alivisatos, *J. Chem. Phys.* **102**, 4642 (1995).

4. J. Broughton, *Phys. Rev. Lett.* **67**, 2990 (1991).

5. F. Ercolessi, W. Andreoni, and E. Tosatti, *Phys. Rev. Lett.* **66**, 911 (1991).

Chapter 7: C_{60} Single Crystals at High Pressure and Variable Temperature

7.0 Abstract:

Vibrational Raman studies on C_{60} up to 18.0 GPa and between 4 and 360 K are presented. No significant changes are observed up to 10 GPa; mode-Grüneisen parameters are calculated. The low pressure, temperature dependent Raman spectrum shows a sharp shift in peak position and width at 240 K. This is near the point were C_{60} molecules are reported to begin rotating freely.[1] The data can be explained in terms of rotational-vibrational coupling. Comparison of high pressure and low temperature data suggests the formation of a rotational glass at high pressures.

7.1 Introduction:

The recent discovery of a method of producing C_{60} in macroscopic quantities[2] has spurred intense investigation in many branches of physics and chemistry. One such area is the structure of solid C_{60} and the way it is affected by extremes in temperature and pressure. Powder diffraction studies on C_{60} at high pressure suggest that it behaves like most molecular solids, having a large decrease in intermolecular spacing, and a small change in bond length with pressure.[3] Low temperature diffraction studies also show a small decrease in intermolecular spacing with decreasing temperature; in addition, they show a first order phase transition at 249 K from a low temperature rotationally ordered phase, to a high temperature phase where individual molecules are rotationally disordered.[1a] The situation has been further illuminated by a recent low temperature NMR study which confirms that C_{60} molecules are freely rotating on the NMR time scale above 260 K, and which also suggests that between about 190 K and 260 K, molecules are undergoing large amplitude hops between symmetry related sites.[1b]

In this chapter, we present Raman data on C_{60} at high pressures and low temperatures. Our data can be modeled in terms of dephasing of high frequency vibrations

by low frequency librations, and is consistent with the data obtained by others which is summarized above. Further, by comparison of high pressure and low temperature data, we can hypothesize about the rotational state of C_{60} at high pressure.

7.2 Experimental:

C_{60} samples were prepared by the method of Hawkins, et. al., and included separation of C_{60} from C_{70} on a Prikle phenylglycine-based HPLC column.[4] Crystals were grow by heating C_{60} powder in a temperature gradient in a sealed quartz tube under moderate vacuum (10^{-6} torr). The tubes were heated to approximately 560 °C for 36 hours, followed by slow cooling over 4 days. Samples were heated to about 200 °C before sealing the quartz tubes to drive off bound surface gasses. Shiny, black, faceted crystals were found at the cool end of the tubes, approximately 14 cm from the original sample. All samples were stored in a desiccator under nitrogen.

High pressure studies were performed using a Mao and Bell type diamond anvil cell. A sample consisted of two or three pieces of C_{60}, approximately 20 to 40 μm in diameter, and some ruby dust. Spring steel or rhenium gaskets with holes ranging from 0.15mm to 0.25mm in diameter were used with either a 16:3:1 mixture of methanol:ethanol:water, liquid nitrogen, or liquid argon as the pressure medium. None of these variables seemed to affect the data. In all experiments the pressure was determined by ruby R_1/R_2 fluorescence. Pressure gradients never exceeded 5% in any experiment.

Low temperature samples were prepared by attaching crystals to a sapphire window with low temperature, conducting silver epoxy. Samples were cooled with liquid He or liquid N_2.

Raman studies were carried out using the 514.532 nm line of an Ar^+ laser. For the diamond cell studies, 30 to 60 mWatt of incident power were used and both 45 degree and back scattering geometries were employed. The detection system consisted of a Spex triplemate monochromator with a Photometrics series 200 nitrogen cooled CCD detector.

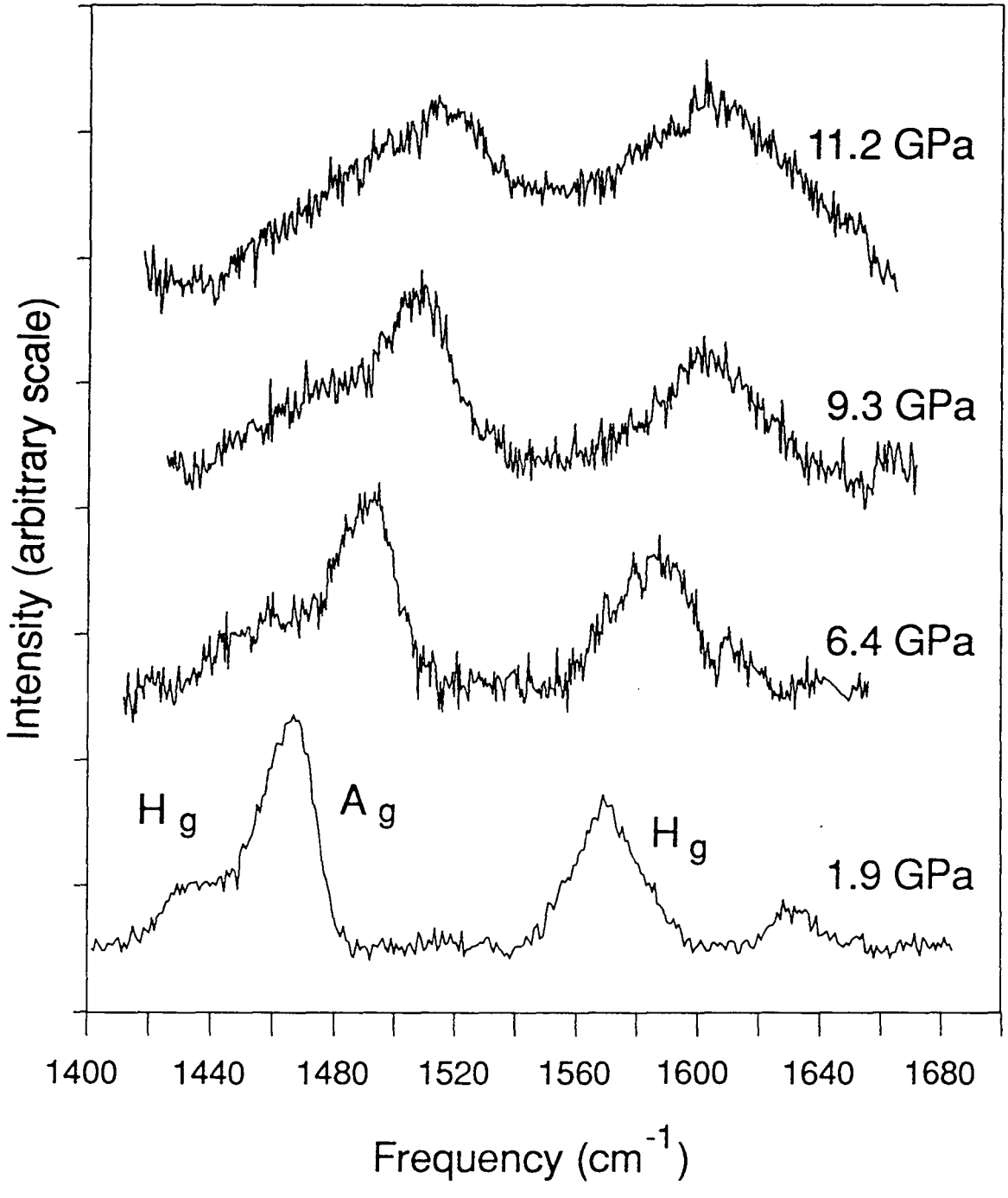

Figure 7.1: Raman spectra of the three high frequency C_{60} modes at pressures from 1.9 GPa to 11.2 GPa. Spectra are offset vertically for clarity.

In the low temperature experiments, 1 mWatt incident power was used with a flow-through cryostat in a back-scattering geometry.

7.3 Results:

Raman spectra of three C_{60} modes are shown in Figure 7.1 as a function of pressure. Peak assignments are consistent with the work of Bethune, et. al.[5] Spectra up to 9.2 GPa are qualitatively similar. The width of the non-degenerate A_g mode peak does not change significantly, though the 5-fold degenerate H_g mode peaks do appear to broaden slightly. This can easily be explained by breaking of the H_g mode degeneracy due to the lower site symmetry of the crystal environment. By 11.0 GPa the lower frequency A_g and H_g modes have completely merged. This pattern continues at higher pressures so that by 16.0 GPa the spectrum has decreased to the point that it can not be distinguished from the background. Signal does not return as pressure is increased to 18.0 GPa, the maximum value for the present experiments. Signal was recovered upon lowering the pressure. We were unable to obtain Raman data on other C_{60} modes in the diamond cell because of the low intensity of those modes.

Figure 7.2 show dν/dP for the three high frequency C_{60} modes. Values are consistent with those presented by Butler, et. al. for the high frequency C_{60} IR active mode.[6] Different symbols indicate different experiments; linear fits to the data and mode-Grüneisen parameters are also presented. Mode-Grüneisen parameters (γ_i) are dimensionless quantities which relate the fractional change in volume to the fractional change in frequency for a given mode (i),

$$\frac{\Delta\nu_i}{\nu_i} = \gamma_i \cdot \frac{\Delta V}{V}. \qquad (1)$$

Values of γ_i can thus be calculated from dν/dP and the atmospheric isothermal bulk modulus (K_o). The value of Duclos, et. al. (K_o=18.1 GPa) was used.[3a] The mode-Grüneisen parameters describes how the frequency of a given mode scales with the

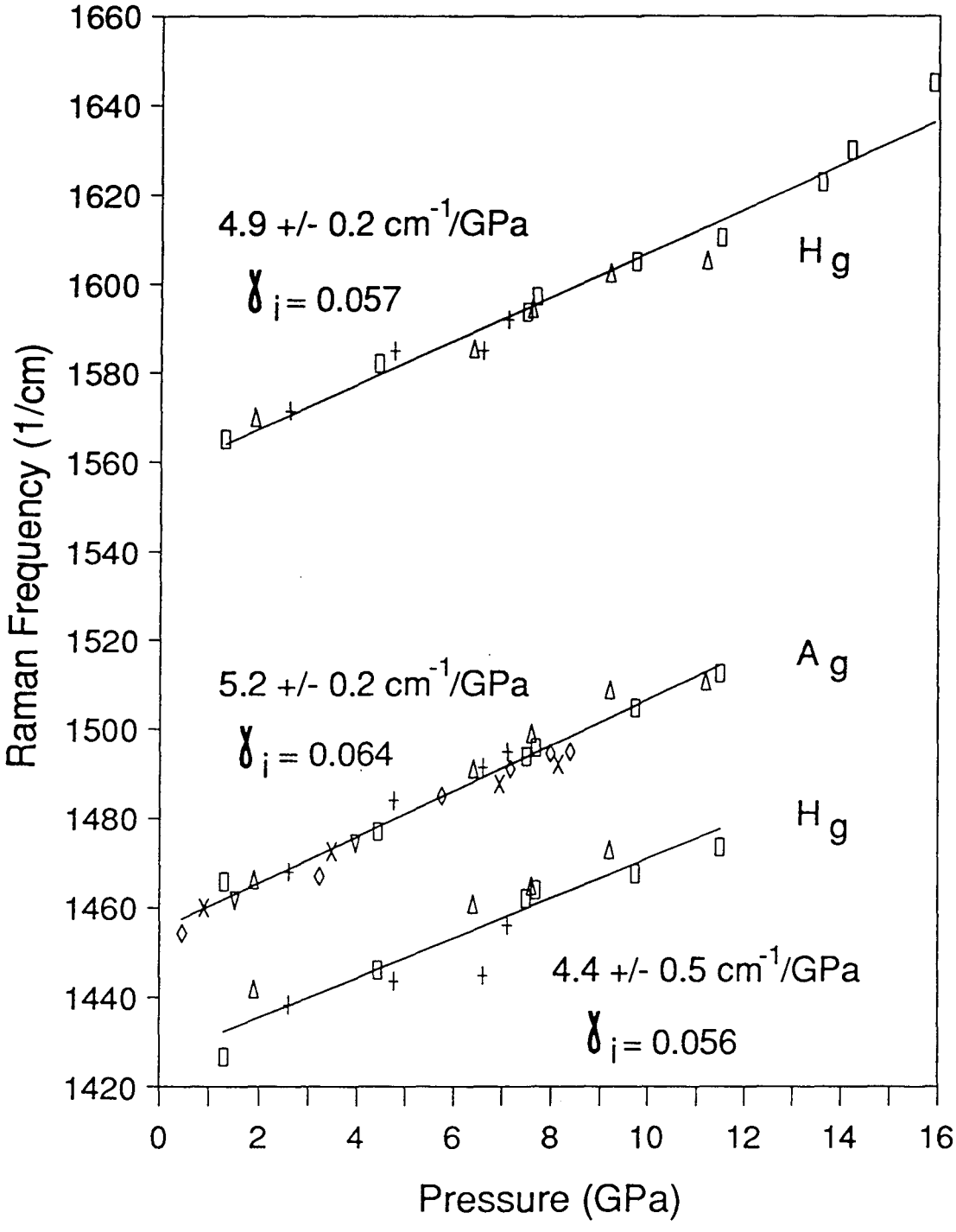

Figure 7.2: Raman peak position plotted versus pressure for the three high frequency C_{60} modes. Different symbols denote different experimental runs. Lines are fits to the data with slopes ($d\nu/dP$) as shown. Values of mode-Grüneisen parameters (γ_i) are calculated from the frequency shift with pressure.

volume. The very small values of γ_i are compatible with there being little change in intramolecular bond length for a given change in intermolecular spacing. The values of γ_i presented here are typical of high frequency modes in molecular crystals.[7]

The shift in Raman frequency with temperature for the totally symmetric A_g mode is shown in Figure 7.3. Again, different symbols denote different experimental runs. The most distinctive feature is the sharp break at approximately 240 K. This corresponds reasonably well with the temperatures reported by Heiney, et. al.[1a] and Tycho, et. al.[1b] for the first order phase transition to a rotationally disordered state. A plot of full width at half maximum height (FWHM) versus temperature (Figure 7.4) also shows a sharp discontinuity at 240 K with an approximately two fold increase in width at this point. The fact that our shift is seen at slightly lower temperature than previous studies could be explained by a slight heating of the sample by the laser.

7.4 Discussion:

The shift in vibrational frequency with temperature can be described in terms of two effects: thermal or population effects, and density or lattice expansion effects. This can be summarized by

$$\left(\frac{d\nu}{dT}\right)_P = \left(\frac{\partial \nu}{\partial T}\right)_V - K_0\alpha \cdot \left(\frac{\partial \nu}{\partial P}\right)_T, \qquad (2)$$

where the first term describes population effects and the second density effects. K_o is the bulk modulus, and α is the isobaric thermal expansion coefficient, calculated from the paper of Heiney, et. al.,[1a] and having the value of 9.6×10^{-5} K^{-1}. By examining both temperature and pressure shifts, it is possible to determine the fractional shift due to density effects, given by

$$\eta = -K_0\alpha \cdot \frac{(\partial \nu/\partial P)_T}{(\partial \nu/\partial T)_P}. \qquad (3)$$

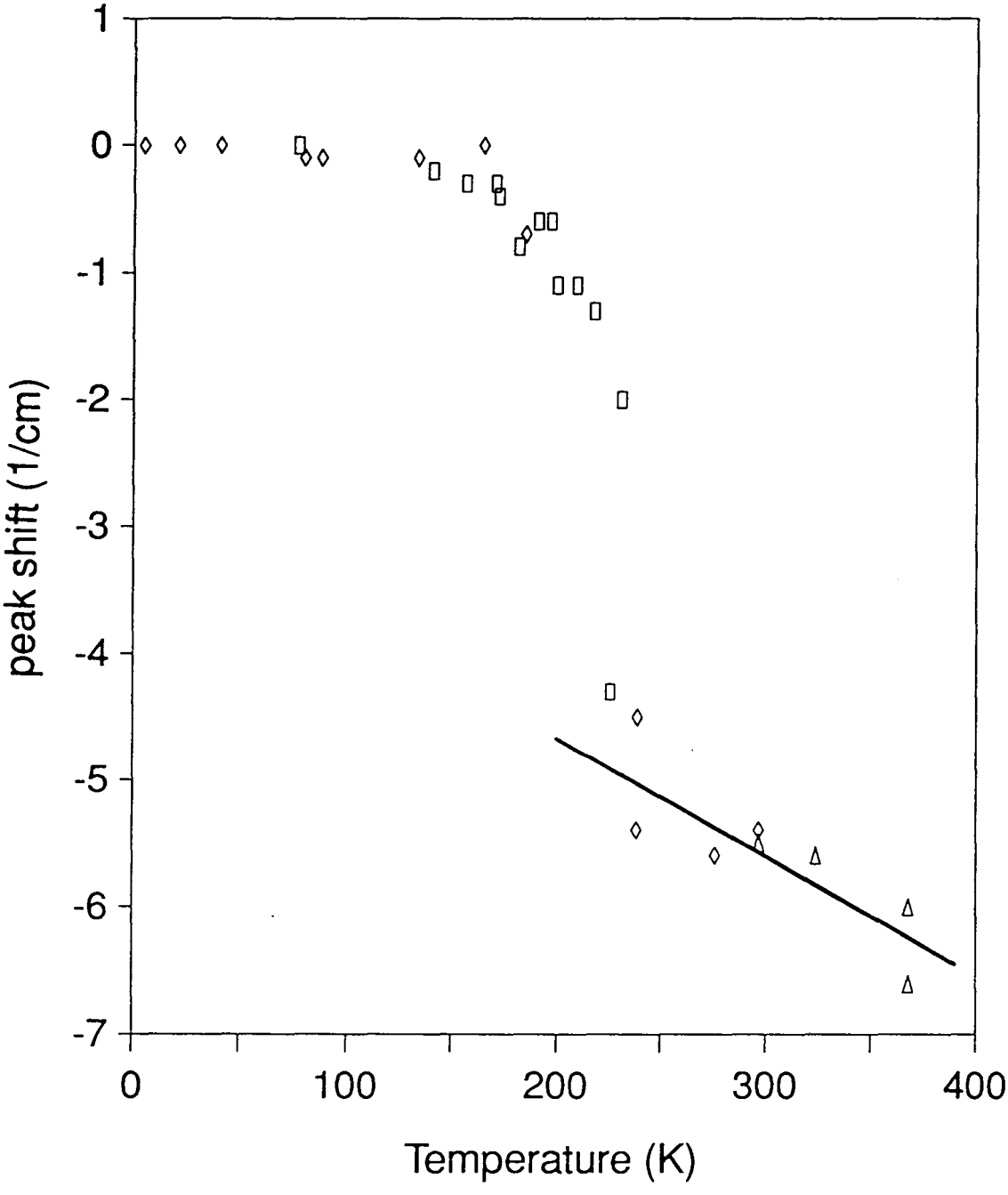

Figure 7.3: Raman peak shift plotted versus temperature for the C_{60} high frequency A_g mode. The peak position in the low temperature limit is 1466 cm^{-1}. Different symbols denote different experimental runs. The line has a slope of η=1 and represents pure density effects. The discontinuous change in peak position at about 240 K correlates well with the rotational ordering phase transition reported by Fischer, et. al.[1a]

A value of η=1 corresponds to pure density effects; $\eta \approx 0$ to pure population effects.[8] In the region below 240 K, the peak position is shifting very rapidly with temperature, and thus $\eta << 1$. This means that population effects dominate and the observed shift is largely due to coupling between the observed vibration and some other low frequency mode that is being thermally populated as the temperature changes. For the case of C_{60}, a likely low frequency mode is a libration.

To model coupling between vibrational and rotational motion, it is necessary to consider the time scale of the rotation. In the region from 190 K to 240 K, Tycho, et. al.[1b] obtained values of τ_c the rotational autocorrolation times, on the order of 60ns. Although these correlation times are fast on the NMR time scale, and correspond to significant narrowing of NMR lines through large amplitude molecular motions, they are approximately 3 orders of magnitude slower than the vibrational time scale.[9] In this temperature region then, we can assume that on the time scale of a vibration, C_{60} molecules move only small amounts, and that rotational motion can be modeled as librations within a single potential minimum. This prediction is confirmed by the molecular dynamics simulations of Goddard, et. al.[10]

There are a number of papers that model the dephasing of a high frequency mode by a lower frequency mode.[9,11,12] The coupling of a vibration and a libration is given by perturbation theory as

$$H = H_V + H_L + H_{VL}, \tag{4}$$

where H_{VL} is the perturbing hamiltonian and is usually considered to be of the form

$$H_{VL} \propto \theta^2 q^2, \tag{5}$$

with q the vibrational coordinate and θ is the librational coordinate.[11,12] The temperature dependence of the vibrational frequency shift thus depends only on $\langle \bar{\theta}^2 \rangle$, which is a function of the librational frequency, and can usually be calculated explicitly for a harmonic oscillator in thermal equilibrium. For the case of C_{60} though, the situation is complicated by the fact that as the temperature changes, the lattice spacing and thus the

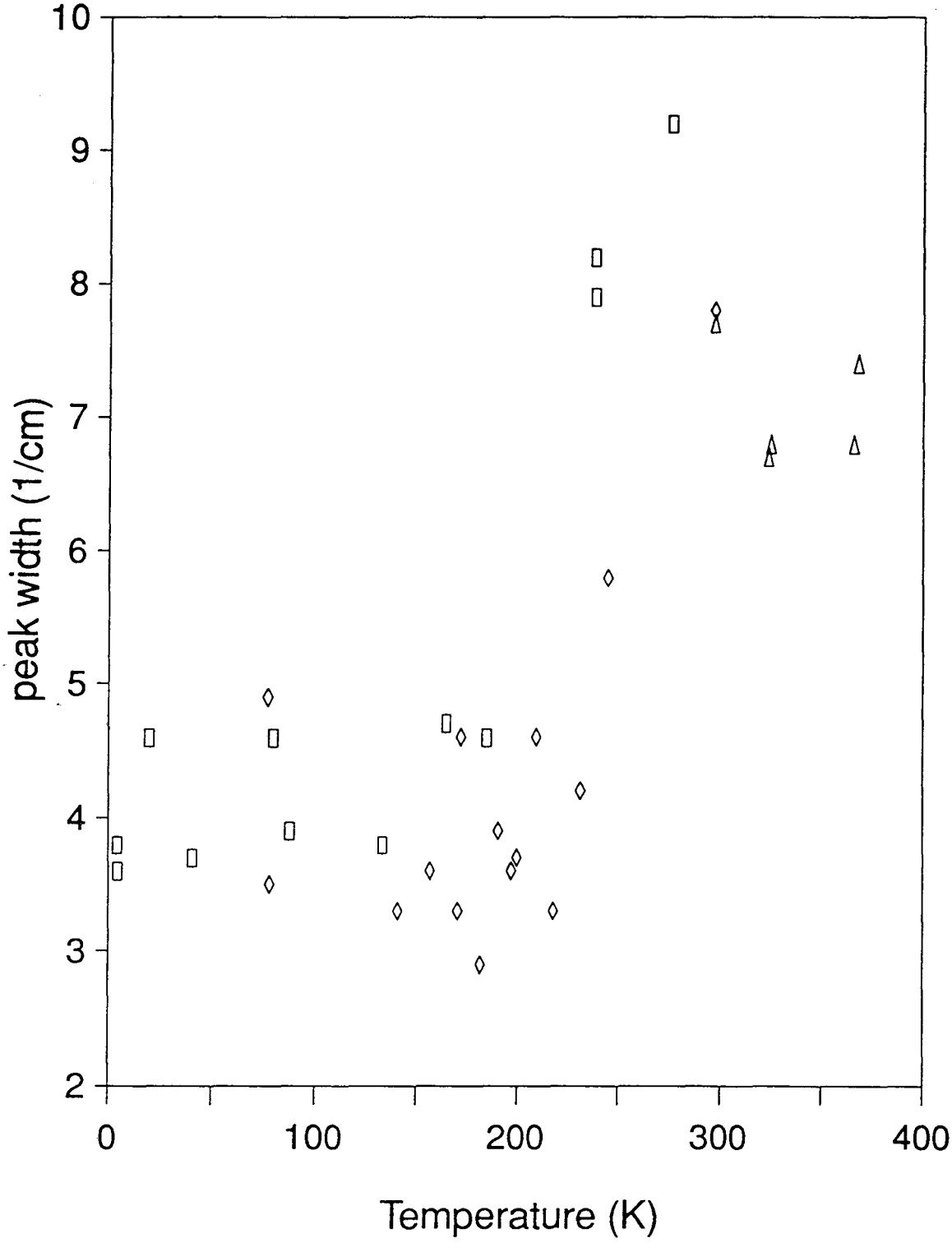

Figure 7.4: Raman peak width plotted versus temperature for the C_{60} high frequency A_g mode. Again a discontinuous change can be seen at about 240 K.

rotational barrier height (V) and the librational frequency should change. It is not possible to fit the change in position and width of the Raman line using a single barrier height to rotation; the theoretical shift in peak position due solely to the thermal population of a low frequency libration is nearly linear as opposed to the strongly nonlinear temperature dependence observed in Fig. 3. As classical potentials for the C_{60}-C_{60} interaction are developed, a critical test will be their ability to predict the change in barrier height with intermolecular separation. Since vibrational-librational coupling in the fixed barrier limit is well documented and understood, the present data will be useful in determining the change in barrier height with intermolecular spacing.

In the limit of free rotation (above ≈250 K), $<\bar{\theta}^2>$ is no longer a meaningful quantity and dν/dT can not be explained in terms of rotational-vibrational coupling. Examination of Figure 7.3 though, shows that the data is well approximated by a line of slope $\eta=1$ in this high-temperature regime. In other words, in the free rotation limit, the rotational motion can no longer be modeled as a simple thermally populated libration, and the entire frequency shift with temperature is instead accounted for by density effects. The fact that the coupling changes dramatically when the rotational motion changes emphasizes that the frequency shifts in excess of pure density effects are due to rotational-vibrational coupling.

The final picture is then one in which a high frequency vibration is coupling to a low frequency libration at low temperatures. As the libration is thermally populated and shifts in frequency with temperature, the effect on the high frequency mode changes. Near 250 K, the coupling undergoes a dramatic change as the rotational barrier decreases to the point that free rotation is possible. Above this temperature the coupling between the rotational and vibrational modes no longer changes significantly with temperature. Using this model and assuming that the phase transition is solely a function of the crystal density, we can calculate from our Raman data the pressure at which the C_{60} rotations should order and freeze: 0.1 GPa. In practice the transition pressure should be somewhat higher

than this because molecules in the diamond cell at room temperate have higher kinetic energy than molecules cooled to 250 K and thus should be able to reorient despite a higher potential barrier. Further, the entropy is higher at room temperature than at 250 K.

Assuming these effects are relatively small, we conclude that the C_{60} is rotationally frozen in all of our high-pressure measurements. If C_{60} molecules order as they freeze, as they do in the low temperature case, one would expect that peak widths obtained in the diamond cell would be narrow, and that the intercept of the dv/dP line would correspond to the peak position in the low temperature limit (1466 cm^{-1}). Experimentally, we observe peak widths up to 9.3 GPa that are approximately equal to the atmospheric pressure room temperature value. Also the intercept of the dv/dP line corresponds to the high temperature limit (high T=1459 cm^{-1}, intercept=1455 $\pm$ 3 cm^{-1}). This suggests that as pressure is increased, molecules are not able to order into the same structure as that observed at low temperatures and low pressures. We speculate that they freeze but do not order forming a rotational glass at high pressure. The conclusion is reasonable in light of the extremely short time required to change the pressure in a diamond cell compared to the time required to grow highly ordered crystals.

7.5 Notes and References:

1. a) P. A. Heiney, J. E. Fischer, A. R. Ghie, W. J. Romanow, A. M. Denenstein, J. P. McCauley, and A. B. Smith, Phys. Rev. Lett. 66 (1991) 2911.

b) R. Tycko, G. Dabbagh, R. M. Fleming, R. C. Haddon, A. V. Makhija, and S. M. Zahurak, Phys. Rev. Lett. 67 (1991) 1886.

2. W. Krätschmer, L. D. Lamb, K. Fostiropoulos, and D. R. Huffman, Nature 347 (1990) 354.

3. a) S. J. Duclos, K. Brister, R. C. Haddon, A. R. Kortan, and F. A. Thiel, Nature 351 (1991) 380.

b) J. E. Fischer, P. A. Heiney, A. R. McGhie, W. J. Romanow, A. M. Denenstein, J. P. McCauley, A. B. Smith, Science 252 (1991) 1288.

4. J. M. Hawkins, T. A. Lewis, S. D. Loren, A. Meyer, J. R. Heath, Y. Shibato, and R. J. Saykally, J. Org. Chem. 55 (1990) 6250.

5. a) D. S. Bethune, G. Meijer, W. C. Tang, H. J. Rosen, W. G. Golden, H. Seki, C. A. Brown, and M. S. de Vries, Chem. Phys. Lett. 179 (1991) 181.

b) D. S. Bethune, G. Meijer, W. C. Tang and H. J. Rosen, Chem. Phys. Lett. 174 (1990) 219.

6. Y. Huang, D. F. R. Gilson, and I. S. Butler, J. Phys. Chem. 95 (1991) 5723.

7. R. Zallen and M. L. Slade, Phys. Rev. B. 18 (1978) 5775.

8. R. Zallen, E. M. Conwell, Solid State Commun. 31 (1979) 557.

9. a) H. L Strauss, J. Am. Chem. Soc. 114 (1992) 905.

b) K. A. Wood and H. L. Strauss, J. Phys. Chem. 94 (1990) 5677.

10. Y. Guo, N. Karasawa, and W. A. Goddard, Nature, 351 (1991) 464.

11. a) R. M. Corn, V. L. Shannon, R. G. Snyder, and H. L. Strauss, J. Chem. Phys. 81 (1984) 5231.

b) R. A. MacPhail, R. G. Snyder, H. L Strauss, J. Chem. Phys. 77 (1982) 1118.

12. a) C. B. Harris, R. M. Shelby, and P. A. Cornelius, Phys. Rev. Lett. 39 (1977) 1415.

b) R. M. Shelby, C. B. Harris, and P. A. Cornelius, J. Chem. Phys. 70 (1979) 34.

Chapter 8: Optical Properties of CdSe Nanocrystals in the Rock Salt Phase

8.0 Abstract:

The size dependent electronic absorption spectra of CdSe nanocrystals have been measured in a diamond anvil cell. Under pressure, these nanocrystals are reversibly converted from a direct gap wurtzite structure to a rock salt structure which has an indirect gap in the bulk. It is thus possible to compare the influence of quantum confinement on direct and indirect transitions in nanocrystals of the same size. The ratio of oscillator strength between direct and indirect structures does not change with size, indicating that zero-phonon transitions are not occurring in the indirect nanocrystals.

8.1 Introduction:

In semiconductors of finite size, there are pronounced quantum confinement effects on the electronic absorption spectra. Nanocrystals of the prototypical direct gap semiconductor, CdSe, exhibit the following effects: shifts to higher energy of the onset of absorption on the order 0.5 eV,[1] and the concentration of oscillator strength into just a few optical transitions,[2] as the size of the nanocrystals is decreased. There is less knowledge of what happens to the optical spectra of indirect gap semiconductors in finite size, which in the bulk require phonon assistance and have much lower oscillator strengths. These issues have been brought to the fore by the observation of intense photo-luminescence in porous Si [3] and Si nanocrystals.[4] Much speculation has been made about the exact nature of this luminescence, which is not observed in bulk samples of this indirect gap semiconductor.[5] The relative oscillator strength of direct and indirect gap semiconductor nanocrystals is not experimentally known. Simple confinement models,[6] which should apply to both types of transitions, predict comparable shifts in energy levels derived from any highly curved region of the band structure. These same models predict concentration of oscillator strength for both zero phonon direct gap transitions and

phonon assisted (vibronically allowed) indirect gap transitions. However, zero phonon transitions may become allowed in finite size indirect gap semiconductors due to mixing of momentum states, yielding a further enhancement in the oscillator strength of indirect versus direct gap semiconductors.[7,8] CdSe nanocrystals can be converted under pressure from direct (wurtzite) to indirect gap (rock salt) structures, providing an absolute comparison of the quantum confinement under the different selection rules.

We have chosen to study the effects of quantum confinement on the electronic absorption spectra. While luminescence is frequently used as a measure of oscillator strength in these types of systems, the results are complicated by the fact that luminescence can involve one or more highly localized states. In the case of nanocrystals, these localized states tend to originate in the crystallite surface, which can contain a large fraction of the total number of atoms in the nanocrystal. Extremely fast trapping to the surface has been observed in semiconductor nanocrystals,[9] and thus surface dominated luminescence is expected. This is confirmed by the observation that chemical modification of nanocrystal surfaces can change the luminescence. Absorption, in contrast, automatically probes the interior states of the nanocrystal. Support of this conclusion comes from the fact that the relative spacings of the multiple absorption features follow simple confinement rules, and the fact that chemical modification of nanocrystal surfaces is not observed to change the absorption.

8.2 Experimental

CdSe nanocrystals in the wurtzite structure were synthesized chemically by a modification of the method of Murray and Bawendi.[9,10] Samples have been characterized by TEM, X-ray diffraction, small angle X-ray scattering (SAXS), Raman, and XPS, and have been shown to be highly crystalline with narrow size distributions (σ = 5%). Figure 8.1a (bottom) shows diffraction data obtained on an ensemble of randomly oriented 4 nm diameter wurtzite phase CdSe nanocrystals in a high pressure diamond anvil cell (DAC).

The diffraction peaks are broadened only by the finite size of the nanocrystals and are consistent with nanocrystals containing less than one stacking fault per crystallite. The optical absorption spectrum of these same nanocrystals (figure 8.1b, bottom) consists of a sharp absorption onset with multiple discrete features and is consistent with quantum confined direct gap absorption. For all high pressure diffraction and optical absorption data presented here, nanocrystal samples were homogeneously dissolved in a soft organic solvent (4-ethyl-pyridine) which has been shown to be a reasonable quasi-hydrostatic pressure medium to pressures in excess of 10 GPa. In all cases, pressure was determined using standard ruby fluorescence techniques. Diffraction data was obtained at the Stanford Synchrotron Radiation Laboratory in an angle dispersive geometry using a Merrill-Bassett style diamond anvil cell. High pressure electronic absorption data was collected in a modified Mao-Bell style diamond cell. Visible absorption was obtained using a scanning Cary model 118 spectrometer. Extension of this data to the near IR (figure 8.2) was accomplished using a chopped tungsten lamp, lock-in detection, and either two germanium or two silicon diodes.

8.3 Results and Discussion

The X-ray diffraction data in figure 8.1a (middle) shows that under pressure, the nanocrystals undergo a solid-solid phase transition. The new diffraction pattern at 9.7 GPa indexes cleanly to rock salt structure CdSe. Furthermore, the diffraction line widths do not broaden, indicating no introduction of defects into the sample upon phase transition. Electronic absorption data obtained on rock salt phase nanocrystals at 8.5 GPa (figure 8.1b, middle) show no discrete features in the IR or visible regions, and are thus consistent with a vibronically allowed transition. The strength of the absorption near threshold is much weaker in this phase. Upon release of pressure, recovery of a direct gap, tetrahedral structure is observed in diffraction (figure 8.1a, top). The recovered diffraction data is consistent with a mixture of the closely related direct gap structures,

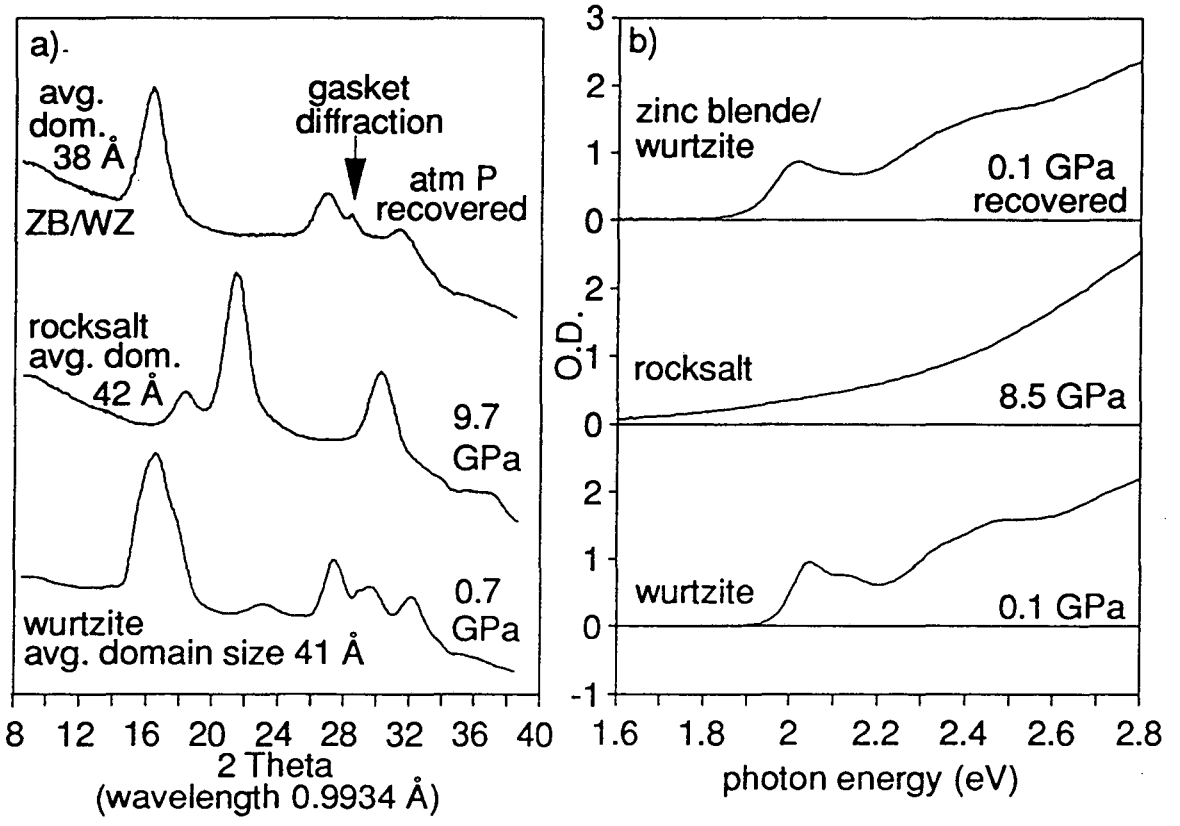

Figure 8.1: (a) High pressure X-ray diffraction data obtained on 4 nm diameter CdSe nanocrystals showing forward and reverse pressure induced structural transformations. (b) High pressure optical absorption of the same 4 nm CdSe nanocrystals.

zinc blende and wurtzite. The electronic spectrum also recovers its full intensity, and many of the discrete features, albeit with some broadening. The recovery of discrete features upon release of pressure supports our assumption that lack of structure in the rock salt phase absorption spectrum is intrinsic and not due to inhomogeneity: shape and surface structure variation resulting from one solid-solid phase transition should only be increased after two such transitions. Additionally, because the rock salt structure has higher symmetry than the wurtzite, the number of possible transition paths, and thus the potential for induced inhomogeneity, in going from wurtzite to rock salt is much lower than that in recovering from rock salt to zinc blende or wurtzite.[11] These effects combine to show that crystalline, homogeneous, rock salt CdSe nanocrystals can be created at high pressure, and that the spectra of these nanocrystals do not exhibit discrete states.

Rock salt structure CdS and CdSe are indirect gap semiconductors in the bulk. This conclusion is supported by local density approximation calculations of the bulk CdSe rock salt band structure[12] which predict that this material should be an indirect gap semiconductor with an absorption onset in the near IR. Previous calculations on the related semiconductor, CdS, also show that it is indirect in the rock salt structure.[13] Two possible transitions are suggested by these calculations, from either the L or Σ point in the valence band to the X point in the conduction band. Previous experimental work[14] on bulk CdSe further substantiates the conclusion that rock salt phase CdSe has an indirect gap, and place the absorption onset at 0.76 eV at 3 GPa. Finally, the absorption near threshold in rock salt CdS measured by Batlogg, et al.[15] shows a weak, featureless indirect gap spectrum arising from a far red band gap of 1.7 eV.

"Direct" and "indirect" gap absorption spectra for three sizes of nanocrystals are shown in figure 8.2. While the wurtzite to rock salt structural transformation pressure is observed to vary with nanocrystal size, these size effects are the topic of another chapter.[16] For this experiment, all rock salt phase data were collected at pressures well above the highest transition pressure, and all data were collected at approximately the

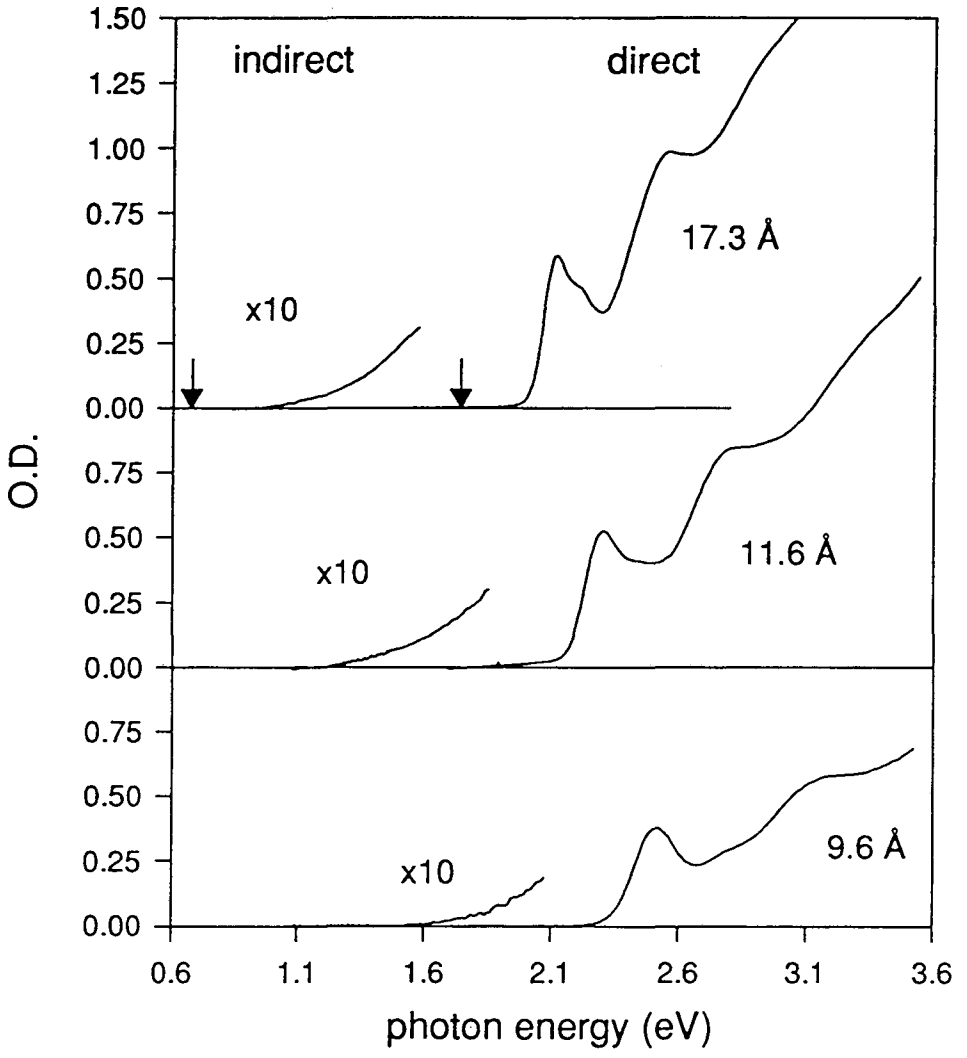

Figure 8.2: Electronic absorption of 17.3, 11.6, and 9.6 Å CdSe nanocrystals in the wurtzite (atmospheric pressure) and rock salt phases (9.3±5 GPa). The spectra have been normalized so that the concentration and path length in the direct and indirect gap phases are the same. Additionally, spectra have been scaled so that the integrated area under the first two absorption features in the direct gap phase are the same. Indirect gap spectra have been multiplied by 10 to improve clarity. The bulk CdSe rock salt band gap at 9 GPa and the bulk wurtzite band gap at atmospheric pressure are indicated with arrows.

same pressure (9.3 ± 0.5 GPa). We have previously established that the compressibility of the nanocrystals in both phases is the same as the bulk and does not depend on size within the present range of sizes.[11,17] This ensures that all the rock salt spectra were collected on nanocrystals with the same bond length. We also note that the shift in the bulk indirect gap absorption with pressure is very small, ≈ -15 meV/GPa.[14]

The effect of confinement on the energy of the absorption threshold in each phase in figure 8.2 can be clearly seen. More precise indirect absorption onsets were determined by extrapolating O.D.$^{1/2}$ versus energy to the energy intercept. These data, obtained on a wide variety of sizes, are presented in figure 8.3 plotted as confinement energy versus inverse radius squared, with the direct gap absorption data included for comparison. The data are plotted this way because the crudest model of quantum confinement predicts that the shifts will vary in proportion to the increased kinetic energy of the carriers as the "box" size is reduced. In nanocrystals, the translational momentum, k, is not well defined. Simple confinement theories model the electronic energy levels of a nanocrystal as superpositions of bulk electronic energy levels of differing momentum. For a given size of nanocrystal, the degree of mixing, Δk, is fixed. One hypothesis is that the intrinsic matrix element for absorption is unchanged in a nanocrystal, but that the density of electronic states is altered by quantum confinement. In that case, the shift in energy, ΔE, and the concentration of oscillator strength are *both* determined by the curvature of the bulk bands. The fact that ΔE versus size is so similar for the wurtzite and rock salt structure of CdSe (figure 8.3) means that the ratio of oscillator strength should not change as a function of size, provided the oscillator strength dependence on size arises only from this collapse of momentum states. This hypothesis is supported by the observation that the curvature at valence and conduction band extrema is similar in the wurtzite and rock salt structures.[12,18] Any additional oscillator strength changes with size, observed in the ratio of wurtzite and rock salt absorption spectra, can be assigned to changes in the matrix element for absorption, for instance, zero phonon processes.

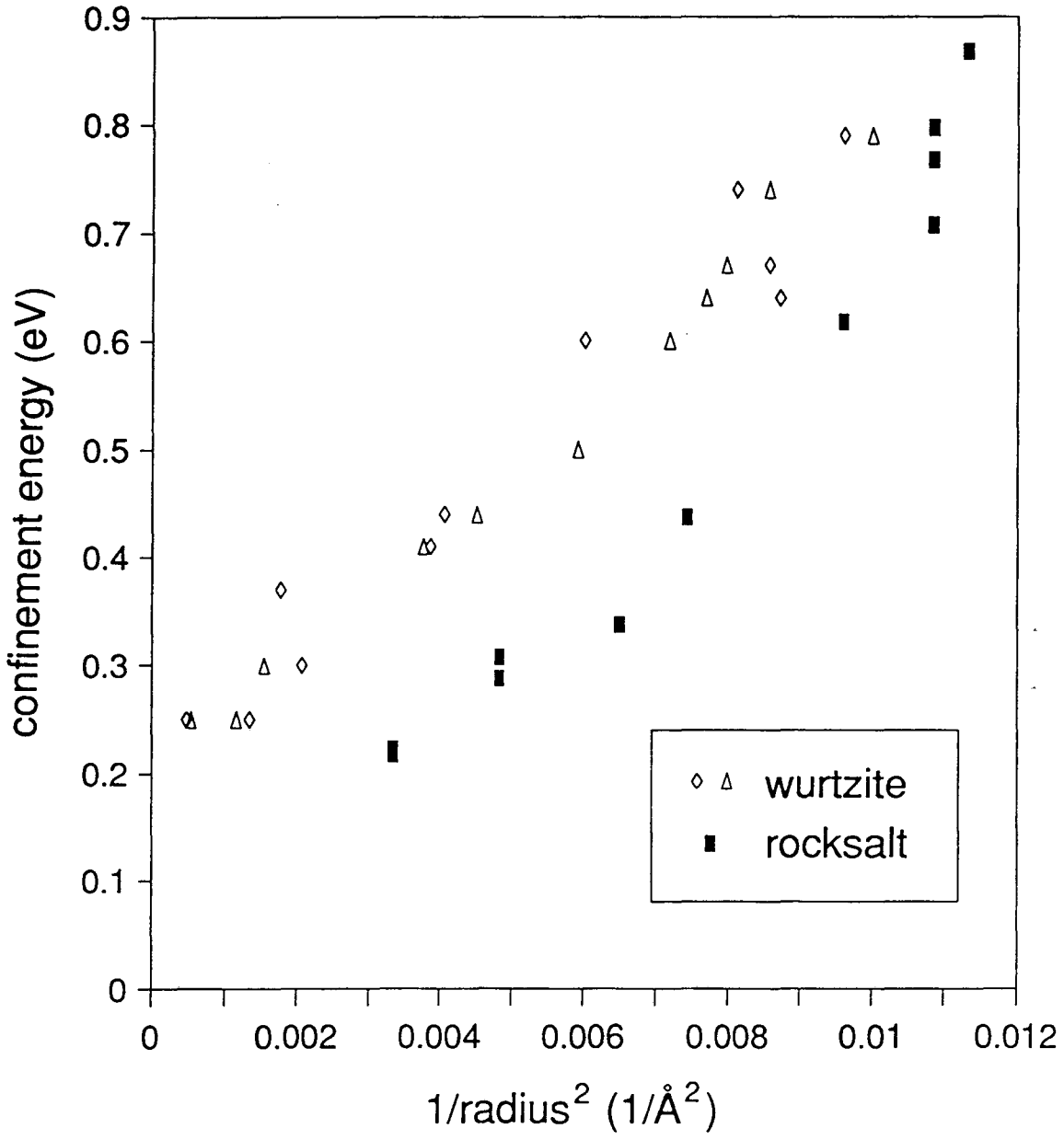

Figure 8.3: Confinement energy versus 1/radius^2 for wurtzite and rock salt phase CdSe nanocrystals. Rock salt phase absorption onsets (■) are plotted relative to a bulk value of 0.67 eV at 9 GPa and room temperature.[14] Wurtzite phase nanocrystals are included for comparison. These crystallites were sized by both TEM (✧) and SAXS (△) and are plotted relative to a bulk room temperature absorption onset of 1.74 eV.[19] For the wurtzite phase, the absorption onset is assigned to the peak of the first excited state.

Figure 8.4 shows rock salt absorption data for five sizes of CdSe nanocrystals. These data have been ratioed to the integrated area of their recovered direct gap absorption spectra. Normalization in this way allows for determination of changes in indirect gap absorption intensity relative to the direct gap intensity, and accounts for gasket deformation with increasing pressure which can change the optical path length. Gasket deformation upon release of pressure is found to be small. The results show clearly that within the precision of this experiment (± 5%), no change in relative absorption intensity between the two phases is observed for nanocrystals ranging from 9.6 Å to 17.3 Å in radius. To the degree that quantum confinement influences oscillator strength, it has the same effect on both wurtzite and rock salt electronic transitions.

The featureless nature of the absorption spectrum and its weak intensity relative to the direct gap phase allow us to conclude that in rock salt phase CdSe nanocrystals down to 9.6 Å in radius, the material is still fundamentally an indirect gap semiconductor. Further, despite the finite size, the terms "direct" and "indirect" appear to still apply, in the sense that vibrational assistance is still required in the "indirect" case. Increases in absorption intensity with size in the indirect gap phase due to concentration of oscillator strength can be accounted for by normalization against the direct gap phase. The possibility of a further increase in oscillator strength in these small nanocrystals of rock salt CdSe due to zero phonon processes can be ruled out by our observations.

These experimental results are readily generalizable to nanocrystals of other indirect gap semiconductors. In most indirect materials, for example Si, GaP, and AgBr, as well as rock salt CdSe and rock salt CdS, the change in crystal momentum required for the lowest energy transition is nearly the length of the Brillouin zone. For nanocrystals containing more than about 100 atoms, the crystal momentum mixing induced by finite size is relatively small in comparison to the change in crystal momentum required for the indirect transition and thus does not give rise to significant absorption from zero phonon processes, as is observed in our rock salt CdSe nanocrystals. Since the amount of crystal

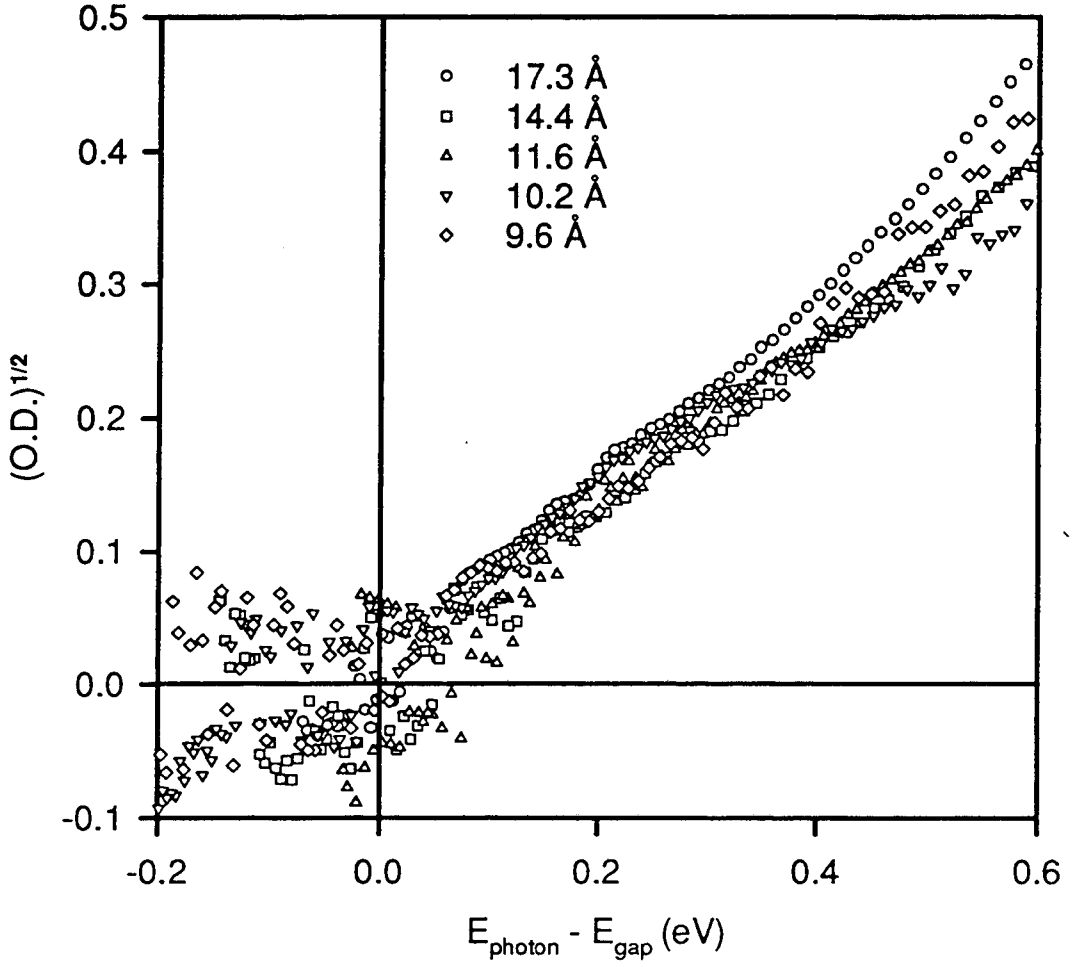

Figure 8.4: Electronic absorption spectra of 5 sizes of rock salt phase CdSe nanocrystals at 9 GPa. The spectra are plotted as $O.D.^{1/2}$ versus energy relative to the absorption onset. All spectra have been scaled such that the integrated area under the first two absorption peaks in the recovered direct gap absorption is the same. Within the experimental error, no variation in the ratio of direct to indirect gap absorption intensity can be observed in sizes ranging from 17.3 to 9.6 Å in radius.

momentum mixing depends only on the crystallite size and not the material, this result should also be true for other indirect gap nanocrystals with valence and conduction band extrema that are well separated in k space. This conclusion is shared by Wilson *et al.*[4] who used radiative rate measurements to show that zero phonon processes do not significantly affect oscillator strength in Si nanocrystals. Experiments by Chen *et al.*[20] on AgBr nanocrystals, and calculations by Hybertsen[7] and Wang *et al.*[21] on Si nanocrystals also find slow radiative rates, indicating that phonon assisted processes dominate. Further, these results show that despite the increased oscillator strength in indirect gap nanocrystals compared to the bulk, direct gap nanocrystals retain their advantage over indirect ones for optical applications where fast radiative rates are important.[22]

8.4 Notes and References:

1. R. Rossetti, R. Hull, J. M. Gibson, and L. E. Brus, J. Chem. Phys. **82**, 552 (1984); M. L. Steigerwald, A. P. Alivisatos, J. M. Gibson, T. D. Harris, R. Kortan, A. J. Muller, A. M. Thayer, T. M. Duncan, D. C. Douglass, and L. E. Brus, J. Am. Chem. Soc. **110**, 3046 (1988).

2. C. B. Murray, D. J. Norris, M. G. Bawendi, J. Am. Chem. Soc. **115**, 8706 (1993).

3. C. Pickering, M. I. J. Beale, D. J. Robbins, P. J. Pearson, R. Greef, J. Phys. C **17**, 6535 (1984); L. T. Canham, Appl. Phys. Lett. **57**, 1046 (1990).

4. K. A. Littau, P. J. Szajowski, A. J. Muller, A. R. Kortan, and L. E. Brus, J. Phys. Chem. **97**, 1224 (1993); W. L. Wilson, P. F. Szajowski, and L. E. Brus, Science **262**, 1242 (1993).

5. F. Koch, Mat. Res. Soc. Symp. Proc. **298**, 319 (1993) and references there in.

6. L. E. Brus, J. Chem. Phys. **80**, 4403 (1984); R. Rossetti, R. Hull, J. M. Gibson, and L. E. Brus, J. Chem. Phys. **83**, 1406 (1985); L. E. Brus, J. Phys. Chem. **90**, 2555 (1986).

7. M. S. Hybertsen, Phys. Rev. Let. **72**, 1514 (1994).

8. T. Takagahara and K. Takeda, Phys. Rev. B **46**, 15,578 (1992).

9. R. W. Schoenlein, D. M. Mittleman, J. J. Shiang, A. P. Alivisatos, and C. V. Shank, Phys. Rev. Let. **70**, 1014 (1993).

10. J. E. Bowen Katari, V. L. Colvin, and A. P. Alivisatos, J. Phys. Chem., **98**, 4109 (1994).

11. S. H. Tolbert and A. P. Alivisatos, J. Chem. Phys. **102**, 4642 (1995).

12. A. Rubio, O. Zakharov, and M. L. Cohen, Dept. of Physics, Univ. of California, Berkeley (private communication).

13. S. W. Liu and S. Rabii, Phys. Rev. B **13**, 1675 (1976).

14. A. L. Edwards and H. G. Drickamer, Phys. Rev. **122**, 1149 (1961).

15. B. Batlogg, A. Jayaraman, J. E. Cleve, and R. G. Maines, Phys. Rev. B **27**, 3920 (1983).

16. S. H. Tolbert and A. P. Alivisatos, Science **265**, 373 (1994).

17. S. H. Tolbert and A. P. Alivisatos, in NATO ASI Proceedings on *Nanophase Materials: Synthesis-Properties-Applications*, G. C. Hadjipanayis and R. W. Siegel, Eds. (Klewer Academic Publishers, Dordrecht, 1993) pp. 471-482.

18. A. Kobayashi, O. F. Sankey, S. M. Volz and J. D. Dow, Phys. Rev. B **28**, 935 (1983); P. Schröer, P. Krüger, and J. Pollmann, Phys. Rev. B **48**, 18264 (1993).

19. V. V. Sobolev, V. I. Donetskina, and E. F. Zagainov, Sov. Phys. Solid State (English Transl.) **21**, 646 (1978).

20. W. Chen, G. McLendon, A. Marchetti, J. M. Rehm, M. I. Freedhoff, and C. Myers, J. Am. Chem. Soc. **116**, 1585 (1994).

21. L.-W. Wang and A. Zunger, J. Phys. Chem. **98**, 2158 (1994).

22. V. L. Colvin, M. C. Schlamp, and A. P. Alivisatos, Nature **370**, 354 (1994).

LAWRENCE BERKELEY LABORATORY
UNIVERSITY OF CALIFORNIA
TECHNICAL INFORMATION DEPARTMENT
BERKELEY, CALIFORNIA 94720